Development of an Empirical Force Field and Molecular Dynamics Simulation of N,N'-dialkylimidazolium Ionic Liquids

by

Siraj Musanur Abrar

Thesis

Submitted in fulfilment of the requirements for the degree

Magister Scientiae

in

Chemistry

in the

Faculty of Science

at the

University of Stellenbosch

Supervisors: Prof J.L.M. Dillen and Dr. C. Esterhuysen

April 2004

Declaration

I, the undersigned, hereby declare that the work contained in this thesis is my own original work and that I have not previously in its entirety or in part submitted it at any university for a degree.

Signature :

Date :

Summary

In an ongoing study an empirical force field that can correctly model N,N'-dialkylimidazolium halide ionic liquids, the Imidazolium Ionic Liquid Force Field – IILFF, was developed based on experimental data obtained from the Cambridge Structural Database (CSD) and data calculated using *Gaussian98*.

Different conformations of the isolated cations were optimised at the Hartree-Fock level using the 6-31G(d) basis set. Structural, vibrational and partial atomic charge data of the lowest energy conformation of each cation were taken as observables during optimisation of the force field parameters. Initial parameters of the IILFF were taken from existing force fields and were optimised using the above mentioned data.

The IILFF was used to minimise isolated cations as well as crystals. These results were successfully tested against isolated cations minimised using *Gaussian98* and the experimental crystals.

Finally, the melting process of the 1,3-dimethylimidazolium chloride crystal was studied using an NPT ensemble starting from an ordered crystal cell and increasing the simulation temperature beyond the experimental melting temperature. The IILFF was then used to calculate the potential energy of the system.

Opsomming

In 'n voortgaande studie om 'n empiriese kragveld te bou wat N,N'-dialkielimidasoliumhalied ioniese vloeistowwe korrek kan modelleer is die Imidasolium Ioniese Vloeistof Kragveld (IIVK) ontwikkel. Die kragveld is ontwikkel gebasseer op eksperimentele data verkry uit die Cambridge Strukturele Databasis (CSD) asook uit data vanaf *Gaussian98* berekeninge.

Verskillende konformasies van die geïsoleerde katione is geoptimiseer deur middel van *Hartree Fock* 6-31G(d) berekeninge. Strukturele data, asook vibrasies en gedeeltelike atoom ladings van die laagste energie konformasie van elke katioon is gebruik as waarneembare veranderlikes vir die bepaling van die optimale kragveld parameters. Beginwaardes vir die IIVK is geneem uit bestaande kragvelde en geoptimiseer met behulp van bogenoemde data.

Die IIVK is gebruik om geïsoleerde katione asook kristalle te minimiseer. Die resultate is suksesvol getoets teen geïsoleerde katione wat met behulp van *Gaussian98* geminimiseer is en eksperimenteel bepaalde kristalle.

Laastens is die smeltproses van die 1,3-dimetielimidasolium chloried kristal bestudeer met behulp van 'n NPT ensemble. Daar is begin by 'n geordende kristal en die simulasie temperatuur is verhoog tot meer as die eksperimentele smeltpunt. Die IIVK is dan gebruik om die potensiële energie van die sisteem te bepaal.

Acknowledgements

First of all I would like to thank, Allah the Almighty, for giving such opportunity and finish it successfully.

I would like to thank the following people and institutions, without whom this work would not have been possible.

- ★ Prof. J. L. M. Dillen, my promoter, for his encouragement and willingness to help throughout this study
- ★ Dr. C Esterhuysen, my co-promoter, for her encouragement, advice and assistance in giving constructive feedback when writing up my thesis
- ★ The Eritrean Human Resource Development Project for funding my study
- ★ The International office of the University of Stellenbosch for their financial support to finish my work
- ★ All members of my family especially my father and mother, my brother Abdulhamid and lovely fiancé Merdia as they were my main source of encouragement during my study.
- ★ Gerhard Venter and Mengistu G. Woldu for their willingness to discuss problems and for their valuable friendship
- ★ My brother, Abdulhamid Musanur, for his assistance in analysing my data.
- ★ Gerhard Venter for translating the English version of my summary to Africans and for his numerous cooperation when writing up my thesis.
- ★ All those persons who in some way or another contributed towards this study.

List of Figures

Chapter 1

Chapter 2

Chapter 3

Chapter 4

List of Tables

Chapter 2

Chapter 3

Table 4.3 : Selected torsions of the imidazolium cation and their variation during the simulation.

Table of Contents

Abbreviations

CSD:	Cambridge Structural Database
DMEIM :	1,2-dimethyl-3-ethylimidazolium
DMIM:	1,3-dimethyl-imidazolium
DMIMCl :	1,3-dimethylimidazolium chloride
DMPIM :	1,2-dimethyl-3-propylimidazolium
EMIM :	1-ethyl-3-methyl-imidazolium
EMIMCl :	1-ethyl-3-methylimidazolium chloride
G98:	*Gaussian98*
HF :	Hartree-Fock
IILFF:	Imidazolium Ionic Liquid Force Fields
MM2 :	the class 1 Allinger molecular mechanics program
NBMIMCl :	1-n-butyl-3-methylimidazolium chloride
PEFF:	a Program for the Development of Empirical Force Field
RMS :	Root Mean Square
UFF :	Universal Force Field

Chapter 1 : Introduction and Objectives

In recent years, a new class of solvents, generally referred to as room temperature molten salts or ionic liquids has attracted remarkable scientific activities (Welten, 1999). Ionic liquids are described as those comprising organic cations and weakly coordinating anions. In particular, those ionic liquids containing cationic imidazolium derivatives represent good solvents for a broad range of both organic and inorganic materials, since they exhibit a high stability against strong reaction media, are immiscible with water and have a very low vapour pressure.

Historically, the first ionic liquids, with chloroaluminate ions, were developed in 1948 by Hurley and Wier at the Rice Institute in Texas as bath solutions for aluminium electroplating. However, they were not studied further until the group of Osteryoung and Wilkes rediscovered them in late 1970, when they prepared room temperature liquid chloroaluminate melts (Wasserscheid & Keim, 2000).

The characteristic properties of ionic liquids can be significantly varied by the choice of anions and cations. The size, shape and distribution of charge in the respective ions can also be considered as the origin of many of these properties in the ionic liquid. To further understand the structure-property relationship it is important to look beyond the local structure of the ions to the structural organisation in the bulk liquid.

Understanding the structure-property relationship of ionic liquids and the forces that give rise to a specific property allows the possibility of designing ionic liquids with tailored structures and properties. Molecular dynamics is one way to study these properties where the property of ionic liquids can be studied as a function of temperature.

The aim of this study is to develop a force field that can correctly model imidazole based ionic liquids based on experimental data obtained from the Cambridge Structural Database (Allen and Kennard, 1993) and from calculations using *Gaussian98* (Frisch et al., 1998). This force field will then be used to study the dynamics simulation of the melting process of 1,3-dimethylimidazolium chloride ionic liquid starting from an ordered crystal. For a computational study, studying a melting process is more preferable than crystallisation.

The general structure of the ionic liquids that will be modelled here are indicated in Fig 1.1, where X indicates a methyl group, Y indicates a methyl group or hydrogen and Z can be a methyl, ethyl or propyl group. The remaining two aromatic carbons will always have hydrogen atom constituents.

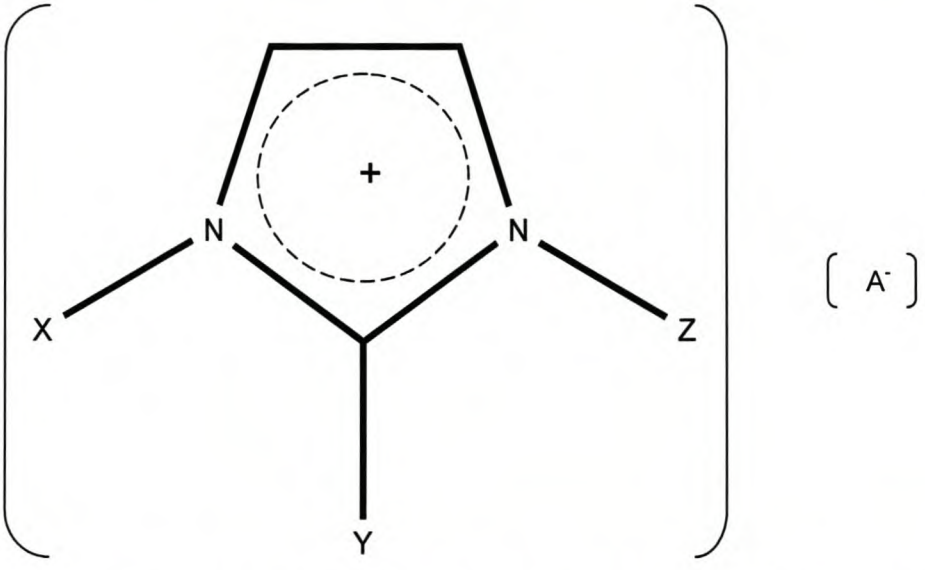

Fig 1.1 : General structure of the ionic liquids that will be modelled, where A^- is any of the halides.

In chapter 2 a general introduction to the important concepts utilised in this study is given. In particular the methods used when developing a force field, as well as general principles of the molecular dynamics simulations are discussed, with particular attention to those algorithms used in Cerius^2. Also mentioned in this chapter is a summary of some selected articles related to the work. Details of the force field development are discussed in chapter 3. The two sources of data, the CSD and *Gaussian98* calculations, are also discussed. The performance of the developed force field for isolated cations and crystals is analysed, by comparison with structures obtained experimentally or minimised using other force fields. Chapter 4 will discuss the general principles used when simulating the melting process of ionic liquids. In this work the dynamics simulations of both a perfect and a defective crystal of 1,3-dimethylimidazolium chloride is discussed. A summary of the important aspects from each chapter will be given in chapter 5.

Chapter 2 : Theoretical Background and Review of Selected Subjects

2.1. Introduction

In this study an attempt is made to comprehensively discuss principles considered when developing a force field for modelling ionic liquids. A brief discussion of the concept of molecular dynamics simulation is also included.

A brief introduction to ionic liquids is given in section 2.2. This section describes the properties of ionic liquids, as compared to organic solvents, and some characteristic properties of ionic liquids. Section 2.3 contains details and comparisons between the three molecular modelling techniques used in this study. In section 2.4 energy minimisation is discussed with particular attention being paid to minimisation algorithms used by PEFF (Program for the Development of Empirical Force Fields), which is used for the force field development. Derivative and non-derivative minimisation methods are mentioned.

Principles of molecular dynamics are discussed in section 2.5. This section also includes a description of the algorithms used in Cerius^2 (Molecular Simulations Inc., 1998). Monte Carlo simulation methods are also discussed and compared with molecular dynamics methods. This chapter is concluded by section 2.6, in which a summary of some computational studies related to the current work is given.

2.2. Ionic liquids

Since the early 1980s room temperature ionic liquids have attracted great interest due to the commercial and environmental advantages they offer over existing organic solvents (Bruce, 2000). Ambient temperature ionic liquids can be defined in broad terms as molten salts which are fluid at room temperature. In general, salts melting below 100°C are considered as ionic liquids.

The melting of ionic compounds is usually a high temperature process since they most often comprise two very small ions with opposite electrical charges. The similar size and shape of

these ions ensure that the electrical attraction between them is so strong that it requires an enormous amount of energy to overcome the ionic attraction. NaCl, which melts at around 800^0 C, is a good example of such a compound. Due to their high melting points, high temperature molten salts would be unsuitable solvents for heat sensitive organic molecules. The melting points of ionic compounds can however be lowered dramatically by introducing bulky and asymmetrical ions that fit together loosely in a crystal lattice. Due to their ill-fitting nature less of the ions' attractive forces are utilised in binding them to each other in the crystal lattice.

There are roughly 300 organic solvents that are used widely throughout the chemical industry whereas it is possible to have more than one trillion possible ionic liquids (Bruce, 2002). Organic solvents are used in a variety of industrial applications that include synthesis of chemicals, manufacturing of electronic components, processing of polymers, production of pharmaceuticals, etc. As a result of their volatile nature, organic solvents readily evaporate into the environment. The use of these volatile organic compounds poses a risk to people working in or living close to such processing facilities.

It is from this background that the pioneering work on ionic liquids was commenced. Ionic liquids have the potential to make environmentally friendly solvents as they can be recycled and they have a negligible vapour pressure and thus do not evaporate into the atmosphere. This makes them more environmentally responsible materials than traditional organic solvents. Different combinations of ions results in ionic liquids that can dissolve a large range of substances, including coal, plastics, metals etc. Furthermore, ionic liquids are relatively undemanding and inexpensive to manufacture.

Ambient temperature ionic liquids typically consist of a heterocyclic cation based on substituted imidazole or pyridine and an inorganic anion such as Cl^-, Br^-, I^-, $[PF_6]^-$ etc. By changing the anion or an alkyl chain of the cation, one can vary the hydrophobicity, viscosity, density, and solvation of the ionic liquid system. Acidity and basicity of ionic liquids can also be adjusted by controlling the combination of the anions and cations. As mentioned above, ionic liquids are composed of poorly coordinating ions. This gives them the potential to be highly polar coordinating solvents that can be useful in transition metal based catalytic systems.

The constituents of ionic liquids are constrained by coulombic forces and exert practically no vapour pressure above the surface of the liquid. This may allow the development of novel recovery schemes for certain organic species in which the product recovery can be affected by distillation. The liquid range of ionic liquids can be as large as 300^0 C, which is higher than that of water and offers the potential for considerable kinetic control of extractive processes.

Despite their obvious superiority over conventional organic solvents, ionic liquids have not been widely employed in industry because of lack of raw physical property data for engineers to use when designing new processes. For efficient design of any new industrial process incorporating ionic liquid technology a complete understanding of the behaviour of the solvent during operation is necessary. Physical properties such as viscosity, density, heat capacity and surface tension are some of the important considerations here.

With the advent of modern computers chemists have been able to use powerful simulation software packages to estimate how a particular process will behave under certain operating conditions. For this purpose there are software packages that predict physical properties of any solvents by using a number of empirical and semi-empirical equations. Unfortunately, these equations were developed for molecular compounds and tend to require critical temperature and pressure data, information which doesn't apply to ionic liquids. This lack of predictive power and overall lack of physical property data in the literature will inevitably slow the transfer of ionic liquid technology into industrial processes (Ercolessi, 1997).

2.2.1. Characteristic properties of ionic liquids

The physical and chemical properties of ionic liquids can be varied over a wide range by the selection of suitable cations and anions. The ionic reaction medium can thus be optimised for a specific application by a stepwise "tuning" of the relevant solvent properties. For this reason ionic liquids have been referred to as "designer solvents". In the following discussion the relationship between the structural features and important physical and chemical properties will be illustrated.

A. Melting point

The melting point of a pure compound is a familiar property because it is often used as evidence when identifying compounds and also serves as an indicator of purity. For ionic liquids this is a key criterion as they are usually identified by their melting point. In comparing the melting points of different chloride salts, it is clear that high melting points are characteristic for alkali metal chlorides, whereas chloride salts with suitable organic cations are observed to melt at temperatures below 150°C, as shown in Table 2.1 (Wasserscheid & Keim, 2000). There are a variety of reasons associated with this, the main ones being low symmetry, weak intermolecular interactions and good distribution of charges throughout the cation.

Table 2.1. Melting points of different chloride salts.

Salt	Melting Point (^{0}C)
NaCl	803
KCl	772
DMIMCl *	125
EMIMCl #	87
NBMIMCl &	65

* = 1,3-dimethylimidazolium chloride

= 1-ethyl-3-methylimidazolium chloride

& = 1-nbutyl-3-methylimidazolium chloride

Anions also influence the melting point of ionic compounds. A comparison of the melting points of different salts containing the same imidazole based cation, 1-ethyl-3-methyl-imidazole (EMIM), is shown in Table 2.2 below (Wasserscheid & Keim, 2000). It is clear that increasing the size of the anion while retaining the same charge leads to a decrease in the melting points.

Table 2.2. Melting points of different EMIM cation salts*

Imidazolium Salt	Melting Point (^{0}C)
[EMIM]Cl	87
[EMIM]NO_2	55
[EMIM]NO_3	38
[EMIM]$AlCl_4$	7
[EMIM]BF_4	6
[EMIM]CF_3SO_3	-9
[EMIM]CF_3CO_2	-16

* = 1-ethyl-3-methyl-imidazolium

In ionic liquids prepared by reaction of a $[cation]^+X^-$ with a Lewis acid MX_y, the molar ratio of the two reactants influences the melting points. For such systems a local maximum in melting temperature is observed at exactly 1:1 mixtures of the system $[cation]^+X^- / MX_y$. This indicates that the presence of several anions in the ionic liquid has the effect of decreasing the melting point.

B. Density

The densities of comparable ionic liquids decreases as the bulkiness of the organic cation increases. The dependence of the density of ionic liquids on the size of the cation was studied by Wasserscheid & Keim (2000) and their results are illustrated clearly in Table 2.3. The anion in all cases is $[AlCl_4]^-$ and cation is $[RMIM]^+$, where R is an alkyl chain. They showed the existence of a linear dependence between the density of an ionic liquid and the length of the alkyl chain on the cation. This is because a slight change in the structure of the cation causes an observable change in the structure of the whole crystal and hence in the density. Wasserscheid & Keim also obtained the same effect when varying the anion.

Table 2.3 :- Effect of size of R on the density of $[RMIM]^+[AlCl_4]^-$ *ionic liquids*

R	Density (g/cm^3)
Methyl	1.31
Ethyl	1.25
n-Propyl	1.23
n-Butyl	1.20

C. Vapour pressure and thermal stability

Ionic liquids have no measurable vapour pressure. This is a real advantage from a process-engineering point of view, since separation by distillation of a reaction mixture becomes more effective as a method of product isolation from the ionic liquid solvent. The thermal stability of ionic liquids is limited by the strength of their heteroatom to carbon and heteroatom to hydrogen bonds. Ionic liquids synthesised by direct protonation of an amine show significantly restricted thermal stability, while imidazole based ionic liquids show acceptable thermal stability (Rooney and Seddon, 2001).

2.3. Molecular modelling

Molecular modelling uses the structures of molecules to aid in the prediction of their physical or chemical properties. Low-energy conformations of compounds, reactivity of molecules, dynamic properties of molecules (or ions), chemical pathways between reactants and products, etc. are typical properties that can be calculated.

In molecular modelling many different techniques can be employed. These are generally classified within three different approaches, namely quantum mechanical, semi-empirical and force field methods. These three main techniques will be discussed in the following sections.

2.3.1. Quantum mechanical methods

Quantum mechanical methods are based on the exact mathematical description of the behaviour of electrons in a molecule and thus give an accurate description of the chemistry of that molecule. Theoretically, quantum mechanics can predict any property of an individual atom or molecule exactly. However, in practice, quantum mechanical equations can only be solved exactly for one electron systems, such as the hydrogen atom. A highly accurate solution can nevertheless be obtained for relatively small systems by using advanced mathematical approximations. Unfortunately as soon as complex molecules are studied the problem becomes difficult and very computationally intensive.

In quantum mechanical calculations particles are described using the Schrödinger equation:

$$H\Psi = E\Psi \qquad \text{--- 2.1}$$

where H is the Hamiltonian operator, Ψ is a wave function (eigenfunction) and E the energy (eigenvalue). The Hamiltonian operator is composed of kinetic and potential energy parts. It takes into account five contributions to the total energy of a system. These are the kinetic energies of the electrons and nuclei, the attraction of the electrons to the nuclei and the inter-electronic and inter-nuclear repulsions. The Hamiltonian operator when expressed in mathematical terms is as follows:

$$H = -\sum_i \frac{\hbar^2}{2m_e}\nabla_i^2 - \sum_k \frac{\hbar^2}{2m_k}\nabla_k^2 - \sum_i \sum_k \frac{e^2 Z_k}{r_{ik}} + \sum_i \sum_{i<j} \frac{e^2}{r_{ij}} + \sum_l \sum_{l<k} \frac{e^2 Z_k Z_l}{r_{kl}} \qquad \text{--- 2.2}$$

where i and j run over electrons, k and l run over nuclei, $\hbar$ is Planck's constant ($(h)/2\pi$), m_e is the mass of the electron, m_k is the mass of nucleus k, ∇^2 is the Laplacian operator, e is the charge on the electron, Z is an atomic number and r_{kl} is the distance between particles k and l. In equation 2.2, the last three potential energy terms appear exactly as they do in classical mechanics. The kinetic energy for a quantum mechanical

particle, however is not expressed as $\frac{p^2}{2m}$, but rather as the eigenvalue of the kinetic energy operator, $T = -\frac{\hbar^2}{2m}\nabla^2$.

The wave function, Ψ, is a function of the electron and nucleus positions. It describes the electron as a wave and can thus yield the probability of the electron being in a certain location but cannot predict its exact location. In order to get physically relevant solutions to the Schrödinger equation, the wave function Ψ must be continuous, single valued, normalisable and anti-symmetric with respect to the interchange of electrons. The wave function itself does not have a direct meaning, whereas the square of the wave function yields the probability of finding the electron. Quantum mechanical methods are characterised by their various mathematical methods used to get the solution. Here a short discussion of typical quantum mechanical method, *ab initio,* is given.

Ab initio is a Latin word meaning "from the beginning". This method is solely based on the laws of quantum mechanics. In this method no experimental parameters are used which means that a calculation using such an approach would require as an input only physical constants such as the speed of light, Planck's constant, mass of elementary particles and so on. An *ab initio* method usually refers to a calculation that uses the full Hartree-Fock equations (Foresman and Frisch, 1993), without ignoring or approximating any of the integrals or any of the terms in the Hamiltonian.

Hartree-Fock is the least expensive *ab initio* method because it includes the effect of electron correlation only in an average sense. This neglect of electron correlation results in over or under estimation of some measurements. For example, frequencies calculated at Hartree-Fock level are over-estimated by 10 or 12%.

Other methods that include electron correlation, like density functional methods (DFT), account for the instantaneous interactions of pairs of electrons with opposite spin. The electron approximation made in the Hartree-Fock method makes it less expensive when compared to DFT.

2.3.2. Force field methods

Organic chemists often build ball and stick or space filling models of their molecules to examine their shapes. Force field methods are in a sense a generalization of these models, with the added features that the atoms and bonds are not fixed at one size and length. Furthermore, force field calculations enable predictions of relative energies and barriers for inter-conversion of different conformations.

In force field methods, molecules are modelled as balls held together by springs. The atoms may have different sizes and softness and the bonds may be more or less stiff. Unlike quantum mechanics, the interactions between the atoms in force field methods are treated by classical mechanics, i.e. Newton's second law.

Force field methods, also referred to as molecular mechanics methods, are used to calculate the structures and energies of molecules based on nuclear motions. In force field methods electrons are not considered explicitly, but rather it is assumed that they will find their optimum distribution once the positions of the nuclei are known. This assumption is based on the Born-Oppenheimer approximation of the Schrödinger equation. The Born-Oppenheimer approximation states that nuclei are much heavier and move much more slowly than electrons (Jensen, 1999). Thus, nuclear motions, vibrations and rotations can be studied separately from electrons; the electrons are assumed to move fast enough to adjust to any movement of the nuclei.

The foundation of force field methods is the observation that molecules tend to be composed of units that are structurally similar in different molecules. For example, all C-H bond lengths and C-H stretch vibrations are roughly constant in all molecules. This implies that the C-H parameters are also comparable.

2.3.2.1. General features of a molecular mechanics force field

To define a force field one must specify the energy functions that are used to describe how energies penalties are associated with the deviation of bonds or angles from their reference values. In addition to this it is also necessary to specify various parameters, such as for

stretching, bending, torsional, van der Waals hardness, van der Waals radius etc. Two molecular mechanics force fields may use identical functional forms yet have different parameters, while two force fields having different functional forms may give comparable results.

The force fields used in molecular modelling are primarily designed to reproduce structural properties or to predict other properties such as vibrational spectra. Generally, a force field is designed to predict specific properties and will be parameterised accordingly. This does not mean that a force field cannot predict other quantities that have not been included in the parameterisation process. It can always be tried but failure of the force field to successfully model one aspect does not necessarily mean failure of the force field as a whole.

Force fields are empirical and hence a variety of them can be modelled for the same set of molecules. The decision as to which one to use is always based on their performance in predicting the properties required, as well as computational efficiency.

Transferability of the functional form and parameters is an important feature of a force field. This means that the same set of parameters should be used to model a series of related molecules, rather than having to define a new set of parameters for each individual molecule. Transferability is important when using the force field to make predictions for other compounds not involved in the training set of the force field. For example, it should be possible to use a force field parameterised for methane and ethane to predict properties of any straight chain alkane.

The functional forms employed in molecular mechanics force fields are often a compromise between accuracy and computational time. The most accurate functional form may not be satisfactory for efficient computation. In addition to this, in order to use techniques such as energy minimisation and molecular dynamics, it is usually desirable to be able to calculate the first and second derivatives of the energy with respect to the atomic co-ordinates.

The idea of molecules being composed of atoms that are structurally similar in different molecules, is implemented in force field methods as atom types. The atom types depend on the atomic number and the type of chemical bonding the atom is involved in. An atom type

may be denoted either by a number or by a simple letter code depending on the force field author.

In a force field there is a possibility that a given element may have several atom types. For example, the 1-ethyl-3-methyl imidazolium cation contains both sp^3 and sp^2-hybridised carbons. Sp^3-hybridised carbons have a tetrahedral bonding geometry, while sp^2-hybridised carbons have a trigonal planar bonding geometry. Hence the assignment of different atom types is necessary depending on the environment in which the atoms are involved. Such details should be clearly specified when developing the force field.

2.3.2.2. Force field energy

The total force field energy of a molecule is divided into several terms called force potentials, or potential energy equations, which define the potential energy surface of a molecule. Force potentials are calculated independently and summed to give the total energy of the molecule. Examples of force potentials are the equations for the energies associated with bond stretching, bond bending, torsional strain and van der Waals interactions:

$$E_{FF} = \sum E_{str} + \sum E_{bend} + \sum E_{tors} + \sum E_{oop} + \sum E_{vdw} + \sum E_{coul} + \sum E_{cross} \quad \text{---} \quad 2.3$$

E_{FF} is the potential energy which is a function of the position (r) of the particle, E_{str} is the energy function for stretching a bond between two atoms, E_{bend} represents the energy required for bending an angle, E_{tors} is the torsional energy for rotation around a bond, E_{vdw} and E_{coul} describe the non-bonded atom-atom interactions and finally E_{cross} describes coupling between the first three terms.

Given such energy functions, the relative energy and geometry of a molecule can be calculated and the most stable conformations can be obtained by minimizing E_{FF} as a function of atomic coordinates.

In the following discussion, details of the first five energy functions will be given. The information mentioned in this section can be found in many computational chemistry text-

books, but they are nevertheless included here due to their importance when developing the force field.

a. Bond stretching energy

The stretch energy, E_{str}, is the energy function for stretching a bond between two atom types, A and B. The simplest way to model this is to treat atoms as balls of mass *m* and the bond as a spring having a spring constant of *k*. The easiest way to mathematically describe the energy of such a system is to use Hooke's law; which is stated as a constant multiplied by the square of the displacement from the equilibrium position (Goodman, 1998):

$$E_{str} = \frac{1}{2} k_{str} (l - l_o)^2 \qquad \text{--- 2.4}$$

where l_o is the reference bond length and k_{str} is the stretch force constant.

This bond stretching energy formula indicates that the energy of the system goes up whether the bond is stretched or compressed. This however is not true with real molecules for the simple reason that a bond breaks when stretched far from the equilibrium position, a concept that cannot be explained by Hooke's law. Therefore, the harmonic approximation to the true energy profile is not sufficiently accurate for systems far from the equilibrium bond length. The stretch energy equation can be improved by introducing more terms in the Taylor expansion:

$$E_{str} = k_2(\Delta l)^2 + k_3(\Delta l)^3 + k_4(\Delta l)^4 \qquad \text{--- 2.5}$$

There are, however, a number of problems associated with the above formula. Firstly, many parameters have to be optimised. The second problem is that this formula does not give good results when a bond is stretched to infinity. Using such a formula for energy minimisation in those circumstances can cause a molecule to fly apart. The correct limiting behaviour for a bond stretched to infinity is that the energy converges towards the dissociation energy. A simple function which satisfies this criterion is the Morse potential:

$$E_{morse}(l) = D(1 - e^{-\alpha\Delta l})^2 \quad \text{--- 2.6}$$

where D is the dissociation energy and α is related to the force constant by $\alpha = \sqrt{k/2D}$. This function reproduces the actual behaviour quite accurately over a wide range of distances. There are nevertheless some difficulties involved with using the Morse potential in actual applications. Firstly, it is not suitable for efficient computation since it requires three parameters to be specified for each bond. Secondly, for long bond lengths the restoring force is quite small. In addition, distorted structures, which may either occur due to a poor starting geometry or develop during simulation, will display a slow convergence towards the equilibrium bond length.

Since it is rare in molecular mechanics calculations for a bond to deviate significantly from its equilibrium value, for minimisation purposes and simulations at ambient temperatures it is sufficient to employ the simple Hooke's law expression mentioned above.

b. Angle bending energy

Bending energy is the energy required for bending an angle formed by three atoms A-B-C, where there is a bond between A and B and between B and C. The deviation of an angle from its reference value is usually described using a harmonic approximation:

$$E_{bend} = \frac{1}{2} k_{bend} (\theta - \theta_o)^2 \quad \text{--- 2.7}$$

where the contribution of each angle is described by a constant value (k_{bend}), which is dependant on the type of the three atoms forming the bond and the reference value (θ_o). This equation is realistic only for small displacements from equilibrium and it works well to about $\pm 30^o$ from the equilibrium geometry. If a more accurate value is required the above expression should be modified by including higher order terms.

In comparison to the energy required for stretching and compression, the energy required to distort an angle from its equilibrium value is very low. This can be shown clearly from the

values of the force constants. For example, Table 2.4 compares some stretch (k_{str}) and bend (k_{bend}) force constants in the MM2 force field (Allinger, 1977).

Table 2.4 :- comparison between stretch and bend force constants

Bond	$k_{str}(kcal.mol^{-1}\text{Å}^{-2})$	Angle	$k_{bend}(kcal.mol^{-1}\,\text{deg}^{-1})$
$C_{sp^3}-C_{sp^3}$	634	$C_{sp^3}-C_{sp^3}-C_{sp^3}$	0.0099
$C_{sp^3}-C_{sp^2}$	634	$C_{sp^3}-C_{sp^2}-C_{sp^3}$	0.0099
$C_{sp^2}=O$	1,554	$C_{sp^3}-C_{sp^2}=O$	0.0101

c. Torsion energy

Assuming there exist bonds between A-B, B-C and C-D, the torsion angle is defined as the angle between bonds AB and CD when they are projected into the plane bisecting BC. Mathematically, torsional potentials are always expressed as a cosine series expansion. One function is:

$$E_{tors}(\omega) = \sum_{n=1}^{N} \frac{V_n}{2}\left[1 + \cos(n\omega - \gamma_n)\right] \qquad \text{--- 2.8}$$

where V_n refers to the barrier height and its value gives a qualitative indication of the relative barriers to rotation. For example, the value of V_n for a double bond is significantly larger than for a single bond. Practically speaking, there are also some other terms in the force field equation that can contribute to the barrier height as a bond is rotated; particularly, the non-bonded interaction between atoms A and D (1,4 atoms). n in the above equation gives the number of minima as the bond rotates 360° and N takes a value of 3 or 6. The phase factor γ_n determines where the torsion angle passes through its minimum value and ω is the torsion angle.

Bond stretching and angle bending terms are often regarded as hard energies, in that quite a substantial energy is required to cause a significant deformation from their reference values. On the other hand a relatively small amount of energy is required to make a major torsional

change. Hence most of the variation in structure and relative energy is due to the complex interplay between the torsional and non-bonded contributions.

This term is particularly important for the simulation of the melting process of crystals because the collapse of a crystal starts with the rotation of some bonds leading to the removal of non-bonded interactions and ultimately to melting.

d. Out-of-plane bending energy

Incorporating an out-of-plane interaction in a force field is usually important because it is used to ensure certain geometries, for example, the planarity of imidazole rings or benzene. There are several ways in which out-of-plane bending terms can be incorporated into a force field. One approach is to treat the four atoms as an improper torsion angle, i.e., a torsion angle in which the four atoms are not bonded in the sequence A-B-C-D. This improper torsion angle is represented by δ in equation 2.9.

$$E_{oop}(\delta) = k(1 - \cos 2\delta) \qquad \text{--- 2.9}$$

This is the most widely used method as it can easily be included with the proper torsional term discussed above. In some force fields a very similar formula to equation 2.9 is used to define an out-of-plane bending term, except that the angle δ is defined as an angle between a bond from the central atom and the plane defined by the central atom and the other two atoms.

Other methods involving calculating the height of the central atom above a plane defined by the three atoms attached to this central atom can also be used to incorporate an out-of-plane bending term.

e. Non-bonded interactions

Non-bonded interactions also play an important role in determining the structure of individual molecular species. They do not depend upon a specific bonding relationship but rather on their separation in space. Non-bonded interactions are usually modelled as a function of some inverse power of distance. The non-bonded terms in a force field are usually considered in

two groups, one consisting of van der Waals interactions and the other, electrostatic interactions.

i. Electrostatic energy

Electrostatic interactions are a part of the non-bonded interactions that are created due to the internal distribution of the electrons in a molecule. Electrostatic interactions between two molecules or between different atoms of the same molecule are calculated as a sum of the interactions between point charges, using Coulomb's law (Leach, 2001):

$$E_{coul} = \sum_{i=1}^{N-1} \sum_{j=i+1}^{N} \frac{q_i q_j}{4\pi\varepsilon_o r_{ij}} \qquad \text{--- 2.10}$$

Where N is the number of atoms, ε_o is the permittivity of free space and r_{ij} is the distance between two point charges, q_i and q_j.

In a molecular mechanics force field this could be modelled in two ways. Firstly, by directly assigning a charge to each atom and hence using Coulomb's law to calculate the interaction. Secondly by assigning a bond increment to each bond in the molecule, which is used to calculate the partial atomic charges of the atoms in the molecule. These two descriptions give similar results. In this work the second method is used.

ii. Van der Waals Energy

Electrostatic interactions cannot account for all of the non-bonded interactions in a system. This can be illustrated by the noble gases, which exhibit solid and liquid phases and deviate from ideal gas behaviour, thus indicating some kind of non-bonded interaction. Since the multipole moments of noble gases are zero, the non-bonded interactions cannot be electrostatic and must therefore be explained by van der Waals interactions. Investigation of the interaction between any two isolated noble gas atoms shows that their interaction energy varies with distance in the manner illustrated in Figure 2.1.

An important feature of this curve is that the interaction energy is zero at infinite distance. Another feature is that, as the separation is reduced, the energy decreases, passing through a shallow minimum at a certain distance, the van der Waals radius. The energy then increases rapidly as the separation decreases further.

In a force field such interactions need to be accurately modelled, which requires a simple empirical expression that can be rapidly calculated since the number of van der Waals interactions that must be determined is often very large, especially when dealing with complex systems.

The best known of the van der Waals potential functions is the Lennard-Jones function, which was originally formulated as:

$$E_{vdw}(r) = k\varepsilon\left[\left(\frac{\sigma}{r}\right)^{n} - \left(\frac{\sigma}{r}\right)^{m}\right] \qquad \text{--- 2.11}$$

where $k = \frac{n}{n-m}\left(\frac{n}{m}\right)^{\frac{m}{n-m}}$ and σ is the collision parameter (or the separation for which energy is zero) and ε is the well depth. These parameters are illustrated graphically in Figure 2.1.

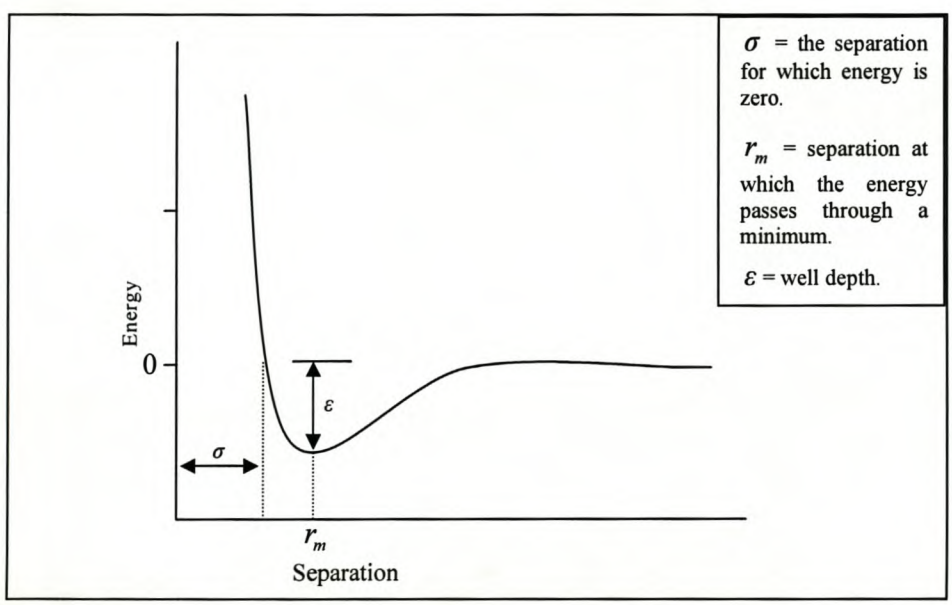

Fig. 2.1: Lennard-Jones potential

The above Lennard-Jones equation contains only two adjustable parameters that can be optimised relatively easily. The Lennard-Jones potential is characterized by an attractive part that varies as r^{-m} and a repulsive part that varies as r^{-n}. In practical terms the values of n and m should be pre-evaluated. m is usually taken to be 6 whereas n can vary, usually being taken as 10, 12 or 9. The 12-6 Lennard-Jones potential is used for calculating large systems, where the value of n is taken to be 12, since r^{-12} can rapidly be calculated by squaring the r^{-6} term.

$$E_{vdw}(r) = 4\varepsilon\left[\left(\frac{\sigma}{r}\right)^{12} - \left(\frac{\sigma}{r}\right)^{6}\right] \qquad \text{--- 2.12}$$

For the purpose of easy parameter optimisation the above equation can be expressed in terms of the separation at which the energy passes through a minimum, r_m. At this separation, the first derivative of the energy with respect to the inter-nuclear distance is zero $\frac{\partial E_{vdw}}{\partial r} = 0$, and from this it can be shown that the relation between σ and r_m is $r_m = 2^{\frac{1}{6}}\sigma$. The Lennard-Jones potential can thus be rewritten in a simple form with two relatively easily adjustable parameters.

$$E_{vdw}(r) = \varepsilon\left[\left(\frac{r_m}{r}\right)^{12} - 2\left(\frac{r_m}{r}\right)^{6}\right] \qquad \text{--- 2.13}$$

f. Cross terms

It is common to observe bond stretching or compression in a molecule as a result of a decrease or increase in a bond angle. This clearly shows that coupling occurs between the stretching of the bond and an angle closing or vice versa. When developing a molecular mechanics force field for a specific purpose, like predicting vibrational spectra, including such terms is very important to achieve optimal performance of a force field.

Most cross terms are functions of two internal coordinates, like stretch-stretch, stretch-bend, stretch-torsion terms etc. But it is not unusual to see cross terms involving more than two internal coordinates, such as bend-bend-torsion. One example of a stretch-stretch cross term is given below:

$$E_{cross}(l_1,l_2) = \frac{k_{l_1,l_2}}{2}\left[(l_1 - l_{1,0})(l_2 - l_{2,0})\right] \quad \text{--- 2.14}$$

where $l_{1,0}$ is the reference bond length between atoms 0 and 1 and $l_{2,0}$ is between atoms 0 and 2. In this discussion no further details of these terms are given, as they are not used in our force field development.

2.3.3. Semi-empirical methods

Semi-empirical methods have a similar general structure to quantum mechanical calculations. They use a Hamiltonian and a wave function; however, within these methods certain pieces of information are approximated.

These methods are a compromise between the accuracy of quantum mechanical methods and the speed of force field methods. This means that semi-empirical calculations are faster than quantum mechanical calculations and the results obtained are more reliable than those results computed using force field methods. However, sometimes the results can be erratic and fewer properties can be computed reliably. To correct such errors the method is parameterised by fitting the results to the experimental results or results obtained with *ab initio* methods.

With this method quite acceptable results can be obtained if the molecule being computed is similar to the molecules in the database used to parameterise the method. On the other hand, if the molecules are significantly different from anything in the parameterisation set the results may be poor.

A typical semi-empirical method is the parameterisation method 3 (PM3) (Stewart; 1989), this method is very popular for modelling organic systems.

2.3.4. Hybrid Force Field – Electronic Structure Methods (QM-MM)

Force field methods are inherently unable to describe the details of bond breaking or forming reactions, since there is an extensive rearrangement of the electrons during these steps and hence the motion of electrons is neglected in the classical model. If the system of interest is

too large to treat entirely by quantum mechanical methods, there are two possible approximation methods that can be used. In some cases, the system can be reduced in size by replacing unimportant parts of the molecule by smaller model groups, for example, substitution of a hydrogen or methyl group for a phenyl ring. However, for studying large biological molecules like enzymes it is usually assumed that the whole system is important for holding the active site in the proper arrangement, while the backbone conformation may change during the reaction.

Hybrid methods have been designed for modelling such cases, where the active site is calculated by quantum mechanical methods (usually *ab initio* or DFT methods), whereas the backbone is calculated by a force field method. Such methods are often denoted "Quantum Mechanics–Molecular Mechanics" (QM-MM).

The main problem with the QM-MM scheme is deciding how the two parts should be connected. Partial charges on the MM atoms can be incorporated into the electronic Hartree-Fock equations, analogously to nuclear charges and the QM atoms thus feel the electronic potential due to all the MM atoms.

2.4. Energy minimisation

In molecular modelling the local and global minimum energy points on the energy surface are of particular interest. Minimum energy arrangements of the atoms correspond to stable states of the system, while any structural change away from a minimum gives a configuration with a higher energy. To identify those geometries of the system that correspond to minima on the energy surface a minimisation algorithm is used. Energy minimisation is the process of making small adjustments to a molecule's geometry in order to reduce the energy of the conformation until any change made leads to an increase in energy.

A minimum can be mathematically described as a point where the first derivative of the function with respect to each of the variables is zero and the second derivatives are all positive (Hinchliffe, 1996).

$$\frac{\partial f}{\partial x_i} = 0 \quad \text{and} \quad \frac{\partial^2 f}{\partial x_i^2} > 0 \qquad \text{--- 2.15}$$

Molecular mechanics minimisations are mostly performed in Cartesian coordinates, where the energy is a function of 3N variables, while internal coordinates are commonly used with quantum mechanics.

There are many factors that must be taken into account when choosing the most appropriate algorithm (or combination of algorithms) for a given problem. The ideal minimisation algorithm is the one that provides the answer as quickly as possible, using the least amount of computational effort. However, most software packages offer a choice of methods because no single minimization method has yet proved to be ideal for all molecular modelling problems. For instance, a method that works well with quantum mechanics may not be the most suitable for use for molecular mechanics. This is partly because quantum mechanics is usually used to model systems with fewer atoms than molecular mechanics. Quantum mechanics and molecular mechanics require different amounts of computational effort to calculate the energies and derivatives of the various configurations. Thus an algorithm that takes many steps may be appropriate for molecular mechanics but inappropriate for quantum mechanics.

Most minimisation algorithms only follow downhill paths on the energy surface, so they can only locate the minimum that is nearest to the starting point. Locating more than one minimum or the global minimum usually requires a way of generating different starting points, each of which is then minimised. Some specialised minimisation methods can follow an uphill path in order to seek out minima lower in energy than the nearest one, but no algorithm has yet proved capable of locating the global energy minimum from an arbitrary starting position.

The input for a minimisation program consists of a set of initial coordinates for the system, which may come from a variety of sources, experimental techniques, like X-ray crystallography or NMR or from a theoretical method such as a conformational search algorithm.

There are a variety of minimisation methods available, but in this study we will concentrate on those approaches that are most commonly used in molecular modelling. Minimisation algorithms can be classified into two groups, those which use derivatives of the energy with respect to the coordinates and those which do not.

2.4.1. Non-derivative minimisation methods

Non-derivative minimisation methods do not require the calculation of the derivative of the potential energy surface. The most commonly used non-derivative method is the simplex method.

Simplex method

The simplex method is a systematic way of trying larger and smaller values for the coordinates and keeping the change that results in a lower energy. For a one dimensional system this method can be done very easily, but it becomes more complex as the number of dimensions increase.

Mathematically this process is done as follows: first, a starting point, x_o is chosen and the potential energy U is calculated at that point, $U(x_o)$. Then x_o is incremented by Δx and the energy at $x_o + \Delta x$ is calculated, $U(x_o + \Delta x)$. If $U(x_o + \Delta x) < U(x_o)$, then this process is repeated for $x_o + 2\Delta x$, $x_o + 3\Delta x$ etc... until the potential energy starts to increase. At that point the exact minimum can be obtained by decreasing the value of Δx. If $U(x_o + \Delta x) > U(x_o)$, then x_o is decremented by Δx and the energy at $x_o - \Delta x$ is calculated, $U(x_o - \Delta x)$, and the process continues as above (Leach, 2002).

This method is used very rarely for two reasons. First, it can only find the minimum nearest to the trial point and it cannot guarantee that this is a global minimum. Second, it requires a great amount of CPU time.

2.4.2. Derivative minimisation methods

Most popular minimisation methods use derivatives, as they provide certain useful information. For instance, the direction of the first derivative of the energy indicates where

the minimum lies and the magnitude of the gradient indicates the steepness of the local slope. The second derivative indicates the curvature of the function, information that can be used to predict where the function will change direction (i.e., pass through the minimum).

The derivative methods can be classified according to the highest order derivative used. First order methods use the first derivative (i.e., the gradients) whereas second order methods use both first and second derivatives.

2.4.2.1. First order minimisation methods

First order minimisation methods change the coordinates of the atoms as they move the system closer and closer to the minimum point. The starting point for each iteration is the molecular configuration obtained from the previous step. The first derivative minimisation algorithm that is most frequently used in molecular modelling is the steepest descent method.

Steepest descent method

In the steepest descent minimisation technique the gradient is calculated and then a step size is chosen in order to progress towards the bottom of the potential energy curve. This is equivalent to walking down a hill using the steepest path. In this method the step size is very important and can create a problem when using this method, because a large step size can lead to the possibility of missing the minimum. On the other hand when a small step size is used then the calculation will be extremely slow. Experience shows that the first few steps in a calculation progresses rapidly towards the minimum, but it slows down when the molecular conformation reaches a flatter part of the potential energy curve. Since this method has a large convergence radius it can be used successfully for very large molecules or for molecules with a very uncertain starting conformation.

2.4.2.2. Second derivative methods

The second derivative method uses not only the first derivative (i.e., the gradient) but also the second derivatives to locate a minimum. Second derivatives provide information about the curvature of the function. This method has a small convergence radius, which means that it

can only work for structures close to the minimum geometry. A typical second order method is the Newton-Raphson method.

Newton-Raphson

The Newton-Raphson method is the simplest second derivative method. The search for a minimum using this method involves the second derivative to be evaluated and the inversion of the Hessian matrix. This makes Newton-Raphson computationally expensive. Especially for large systems the calculation and inversion of the Hessian matrix may be very impractical.

In this method it is very important that the Hessian matrix of the second derivative be positive definite. If it happens that the Hessian matrix is not positive definite then the Newton-Raphson method breaks down and stops. Also, if the system is far from minimum then the minimisation process might become unstable. So it is always advisable to use simpler methods, such as steepest descent, until the structure nears the minimum before applying the Newton-Raphson method.

2.5. Molecular dynamics simulation

2.5.1. Introduction

Molecular dynamics is a computer simulation technique mostly utilising force field methods, where the time evolution of a set of interacting atoms is followed by integrating their equations of motion according to Newton's laws (Leach, 2001). The result is a trajectory that specifies how the positions and velocities of the particles in the system vary with time.

The trajectory is obtained by solving the differential equations embodied in Newton's second law:

$$F = ma \quad ; \quad \frac{d^2 x_i}{dt^2} = \frac{F_{xi}}{m_i} \qquad \text{--- 2.16}$$

This equation describes the motion of a particle of mass, m_i, along the x coordinate due to a force of F_{xi} acting along that direction. In order for the calculation to work, a force field must be designed that describes inter-molecular forces, not only at the equilibrium position but also away from equilibrium.

In order to be a realistic model of intermolecular interactions, the force on each particle changes its position whenever any of the other particles with which it interacts changes position. Under the influence of a continuous potential the motions of all the particles are coupled together, giving rise to a many-body problem that cannot be solved analytically. Under such circumstances the equations of motion are integrated using a technique called the finite difference method.

Finite difference techniques are used to generate molecular dynamics trajectories with continuous potential models. The idea is that the integration is broken down into many small stages, each separated by a fixed time, δt. The total force on each particle in the configuration at a time t is calculated as the vector sum of its interaction with other particles. From the forces the accelerations of the particles can be determined, which are then combined with the positions and velocities at a time t to calculate the position and velocities at a time $t + \delta t$. The force is assumed to be constant during the time step. The forces on the particles in their new positions are then determined, leading to new positions and velocities at time $t + 2\delta t$.

The heart of a molecular dynamics program is its time integration algorithm, required to integrate the equation of motion of the interacting particles and follow their trajectory. The general concept of a finite difference method is that given atomic positions, velocities, etc. at time t, one can obtain the position, velocity, etc. at time $t + \Delta t$ to a sufficient degree of accuracy. By iterating the procedure, the time evolution of the system can be followed for a long time.

There are several algorithms available for performing the numerical integration of the equations of motion that are commonly used in molecular dynamics calculations. Some of these are the Verlet algorithm, the velocity Verlet algorithm, the leap-frog algorithm, Beeman's algorithm and the predictor corrector.

The one concept that is common to all these integration algorithms is that they all assume that the positions and dynamic properties (velocities, accelerations) can be approximated by a Taylor series expansion:

$$r(t+\delta t) = r(t) + v(t).\delta t + \frac{1}{2}a(t).\delta t^2 + \frac{1}{6}b(t).\delta t^3 + \frac{1}{24}c(t).\delta t^4 + \ldots$$

$$v(t+\delta t) = v(t) + a(t).\delta t + \frac{1}{2}b(t).\delta t^2 + \frac{1}{6}c(t).\delta t^3 + \ldots$$

$$a(t+\delta t) = a(t) + b(t).\delta t + \frac{1}{2}c(t).\delta t^2 + \ldots \quad \text{--- 2.17}$$

where v is the velocity (first derivative of the positions with respect to time) and a is the acceleration (second derivative of the position with respect to time).

2.5.2. Molecular dynamics integration algorithms

Several time-integration algorithms are mentioned above, but in this work only those that are used by Cerius^2, the program with which the dynamics calculations were performed, will be discussed.

2.5.2.1. The Verlet algorithm

The Verlet algorithm (Verlet, 1967) is the most widely used method for integrating the equations of motion in a molecular dynamics simulation. The Verlet algorithm uses the positions and accelerations at time t, and the positions from the previous step, $r(t-\delta t)$, to calculate the new positions at $t+\delta t$, $r(t+\delta t)$. The following relationships between these quantities and the velocities at time t exist:

$$r(t+\delta t) = r(t) + v(t).\delta t + \frac{1}{2}a(t).\delta t^2 \quad \text{--- 2.18}$$

$$r(t-\delta t) = r(t) - v(t).\delta t + \frac{1}{2}a(t).\delta t^2 \quad \text{--- 2.19}$$

The new positions are calculated by adding these two equations:

$$r(t+\delta t) = 2r(t) - r(t-\delta t) + a(t).\delta t^2 \qquad \text{---} \quad 2.20$$

The velocities are calculated by taking the difference between equations 2.18 and 2.19,

$$v(t) = \frac{[r(t+\delta t) - r(t-\delta t)]}{2\delta t} \qquad \text{---} \quad 2.21$$

Implementing this algorithm is straight-forward and it works well for longer time steps. The only drawback is that the positions $r(t+\delta t)$ are obtained by adding a small term $a(t).\delta t^2$ to the difference between two much larger terms, $2r(t)$ and $r(t-\delta t)$. This may lead to a loss of precision. The other disadvantage is the lack of an explicit velocity term in the equations, which makes it difficult to obtain the velocities, and indeed the velocities are not available until the positions have been computed at the next step. In addition it is not a self-starting algorithm; meaning the new positions, $r(t+\delta t)$, are obtained from the current positions $r(t)$ and the positions from the previous step, $r(t-\delta t)$, which obviously doesn't exist at the beginning of the dynamics.

2.5.2.2. Velocity Verlet algorithm

The velocity Verlet algorithm (Swope et al., 1982) gives positions, velocities and accelerations at the same time, but does not compromise precision:

$$r(t+\delta t) = r(t) + v(t).\delta t + \frac{1}{2}a(t).\delta t^2 \qquad \text{---} \quad 2.22$$

$$v(t+\delta t) = v(t) + \frac{1}{2}[a(t) + a(t+\delta t)].\delta t \qquad \text{---} \quad 2.23$$

To calculate the new velocity in the velocity Verlet algorithm requires the acceleration at both t and $t+\delta t$. Thus in the first step the positions at $t+\delta t$ are calculated according to equation 2.22 using the velocities and acceleration at time t. The velocities at time $t+\frac{1}{2}\delta t$ are then determined using

$$v(t+\frac{1}{2}\delta t) = v(t) + \frac{1}{2}a(t).\delta t \qquad \text{--- 2.24}$$

New forces are computed from the positions, thus giving $a(t+\delta t)$. In the final step, the velocities at time $t+\delta t$ are determined using

$$v(t+\delta t) = v(t+\frac{1}{2}\delta t) + \frac{1}{2}a(t+\delta t).\delta t \qquad \text{--- 2.25}$$

Unlike Verlet algorithm velocity Verlet algorithm is selfstaring.

2.5.2.3. Leap-frog algorithm

The leap-frog algorithm (Hockney, 1970) uses the following relationship to calculate the velocity and position of an atom.

$$v(t+\frac{1}{2}\delta t) = v(t-\frac{1}{2}\delta t) + a(t).\delta t \qquad \text{--- 2.26}$$

$$r(t+\delta t) = r(t) + v(t+\frac{1}{2}\delta t).\delta t \qquad \text{--- 2.27}$$

The leap-frog algorithm is implemented by first calculating the velocities $v(t+1/2.\delta t)$ from the velocities at time $t-1/2.\delta t$ and the accelerations at time t. The positions $r(t+\delta t)$ are then deduced from the velocities just calculated, together with the positions at time t, using equation 2.26. The velocity at time t can be calculated from

$$v(t) = \frac{1}{2}\left[v(t+\frac{1}{2}\delta t) + v(t-\frac{1}{2}\delta t) \right] \qquad \text{--- 2.28}$$

As its name indicates, the velocities leap-frog over the positions to give their values at time $t+1/2t$ and the positions then leap over the velocities to give their new values at $t+\delta t$.

This method has two advantages over the standard Verlet algorithm: it explicitly includes the velocity and does not require the calculation of the differences between large numbers. However, it has the obvious disadvantage that the position and acceleration are not

synchronised. This means that it is not possible to calculate the kinetic energy contribution to the total energy at the same time as the positions are defined.

Cerius[2] uses a combination of velocity Verlet and leap-frog algorithms for the time integration algorithms for Dynamics simulation.

2.5.3. Molecular dynamics at constant temperature

Temperature plays an important role in molecular dynamics simulations, not only when dealing with a constant temperature ensemble, but also when simulating constant volume and energy (NVE) dynamics. The main reason for this is that in a dynamics simulation the aim is to determine how the behaviour of the system changes with temperature, such as the breaking or formation of non-bonded interactions, rotation of bonds, etc.

It is therefore interesting to see how this process is performed computationally. The relationship between the temperature of the system and the kinetic energy can be expressed mathematically as follows:

$$\langle K \rangle_{NVT} = \frac{3}{2} N K_B T \qquad \text{--- 2.29}$$

where $\langle K \rangle_{NVT}$ is an average kinetic energy for an ensemble where the volume, number of particles and temperature are all constant. An obvious way of altering the temperature of the system is to scale the velocity. Hence the velocity and the temperature in the above equation can be changed proportionally. Therefore, multiplying the velocity by a factor λ, the associated temperature change $(\Delta T = T_{req} - T_{Curr})$ can be calculated as follows:

$$\sum_{i=1}^{N} \frac{1}{2} m_i (\lambda v_i)^2 - \sum_{i=1}^{N} \frac{1}{2} m_i v_i^2 = \frac{3}{2} N K_B \Delta T$$

Solving for ΔT

$$\Delta T = \frac{1}{2} \sum_{i=1}^{N} \frac{2}{3} \frac{m_i (\lambda v_i)^2}{N K_B} - \frac{1}{2} \sum_{i=1}^{N} \frac{2}{3} \frac{m_i v_i^2}{N K_B}$$

$$\Delta T = \frac{1}{2}\sum_{i=1}^{N}\frac{2}{3}\frac{m_i v_i^{\,2}}{NK_B}\left[\lambda^2 - 1\right]$$

$$\Delta T = T_{curr}\left[\lambda^2 - 1\right] \qquad \text{--- 2.30}$$

The simplest way to control the temperature is thus to multiply the velocity at each time step by the factor $\lambda = \sqrt{\frac{T_{req}}{T_{curr}}}$, where T_{Curr} is the current temperature of the system as calculated from the kinetic energy and T_{req} is the desired temperature.

Coupling the system to an "external heat bath" fixed at the desired temperature is an alternative way of maintaining the temperature. The "bath" acts as a source of thermal energy, supplying or removing heat from the system as appropriate. The velocities are scaled at each step, such that the rate of change of temperature is proportional to the difference in temperature between the "bath" and the system:

$$\frac{dT_{curr}}{dt} = \frac{1}{\tau}\left(T_{bath} - T_{curr}\right) \qquad \text{--- 2.31}$$

τ is a coupling parameter whose magnitude determines how tight the bath and the system are coupled together. This method gives an exponential decay of the system towards the desired temperature. The change in temperature between successive time steps is

$$\Delta T = \frac{\delta t}{\tau}\left(T_{bath} - T_{curr}\right)$$

Rearranging and substituting for $\frac{\Delta T}{T_{curr}}$ from equation 2.30

$$\lambda^2 = 1 + \frac{\delta t}{\tau}\left(\frac{T_{bath}}{T_{curr}} - 1\right) \qquad \text{--- 2.32}$$

If τ is large, then the coupling will be weak. If τ is small, the coupling will be strong and when the coupling parameter equals the time step ($\tau = \Delta t$) then the algorithm is equivalent to

the simple velocity scaling method mentioned previously. The advantage of this approach is that it does permit the system to fluctuate around the desired temperature.

These two relatively simple temperature-scaling methods do not generate rigorous canonical averages. Velocity scaling artificially prolongs any temperature difference among the components of the system, which can lead to the phenomenon of "hot solvent-cold solute", in which the temperature of the solute is lower than that of the solvent, even though the overall temperature of the system is at the desired value. One solution to this problem is to apply temperature coupling separately to the solute and the solvent, but the problem of unequal distribution of energy between the various components (and between the various modes of motion) may still remain.

2.5.4. Parameters for molecular dynamics

A molecular dynamics experiment needs several parameters to be specified. The most important of these are discussed here:

1. ***Starting structure***:- a molecular dynamics simulation must begin with a reasonable geometry of the structure of interest. For this an approximate model can be built using experimental data, such as that available from a crystal structure database. This is then minimised (almost certainly to a local minimum rather than the global minimum) so that all the bond lengths and bond angles have reasonable values. It is not necessary to start with the global minimum or a structure close to the global minimum, but if the structure is too strained (or far from the actual structure) errors in the molecular dynamics simulation may accumulate too rapidly and the structure may blow up.

2. ***Temperature or Energy***:- the amount of energy the structure is given depends on the temperature of the system. The energy is divided between kinetic energy and potential energy, which is then divided between the atoms so that each atom gets the same energy. If all the energy were given to one atom, then that atom would probably escape from the rest of the molecules.

It is necessary to check the energy after every step and adjust it so that the system will not deviate irreversibly, due to both errors in the numerical solutions of Newtonian equations or the inability of force fields to predict the properties of distorted structures.

3. ***Step size***:- the calculation of how the molecule will move works by determining what the molecule will be doing a very short time in the future, which has to be much shorter than the shortest time in which anything interesting can happen to the molecule. This is called the characteristic time for the system. The fastest process that can be undergone by a molecule is an electronic transition. However, molecular mechanics ignores electrons, so these need not be considered. Thus, the characteristic time is determined by the fastest mechanical change undergone by the molecule.

The characteristic time for a molecular dynamics simulation may be estimated by considering an ordinary infrared spectrum. The peaks in an infrared spectrum correspond to the vibrations of the atoms in a molecule. The characteristic time has to be substantially shorter than the fastest of these movements. The highest frequency vibrations are due to bond stretches, especially those of bonds to hydrogen atoms. A $C-H$ bond vibrates with a repeat period of approximately 10 fs (which is equivalent to 3300 cm^{-1}). The required time step for a molecular dynamics simulation is one order of magnitude less than the shortest motion, that is 1 fs. This means that the molecular dynamics run calculates many structures for each oscillation of a carbon – hydrogen bond and very many structures for the slower movements in the molecule.

There are various tricks that can be used to speed the calculation up. For example, the fastest process in a molecular dynamics simulation is the vibration of bonds to hydrogen. It is possible to constrain the carbon–hydrogen bond lengths, on the grounds that this is unlikely to affect the movement of the structure very much. This turns out to be a reasonable approximation and as a result the calculation runs faster. It is thus possible to use a slightly larger time step, perhaps 2 fs instead of 1 fs. It would be useful to constrain bond angles in the same way, but this doesn't work as well, because it seriously inhibits torsional rotations.

4. Length of a simulation:- it is usual to ask the question: how long should a molecular dynamics simulation run? Usually it would be desirable to run it for longer than is feasible,

but the choice of a termination time depends on the information required. A 10 ps simulation when interpreted in terms of an infrared spectrum is equivalent to 3.3 cm^{-1}, which is not far from the edge of the spectrum.

5. ***Boundary Conditions:-*** Treatment of the boundary and boundary effects is crucial in a dynamics simulation because it enables many properties to be calculated using a relatively small number of particles. There are two types of boundary conditions, namely periodic and non-periodic boundary conditions. In this work only periodic boundary conditions are used for the dynamics simulation. Periodic boundary conditions enable a simulation to be performed using a relatively small number of particles, in such a way that the particles experience forces as if they were in a bulk system.

Consider a cubic box of particles, which is replicated in all directions to give a periodic array. Then the coordinates of the particles in the boxes can be computed simply by adding or subtracting integral multiples of the box sides. Should a particle leave the box during the simulation then it is replaced by any particle that enters from the opposite side. This implies that the number of particles within the central box remains the same. Cells of different shapes can be used for the simulation, but the simplest periodic system to visualise and program is a cubic cell.

Periodic boundaries are widely used in computer simulations, but they do have some draw-backs. A clear limitation of the periodic cell is that it is not possible to achieve fluctuations that have a wavelength greater than the length of the cell. This can cause problems in certain situations, such as near the liquid-gas critical point. The range of the interactions present in the system is also important; if the cell size is large compared with the range over which the interactions act then there should be no problem. The effect of imposing a periodic boundary can be evaluated empirically by comparing the results of simulations performed using a variety of unit cell shapes and sizes. Periodic boundary conditions may also cause difficulties when simulating inhomogeneous systems or systems that are not at equilibrium. In other cases, use of periodic boundary conditions would require a prohibitive number of atoms to be included in the simulation.

It is not always necessary to use periodic boundary conditions in computer simulations, since some systems, such as liquid droplets or van der Waals clusters, inherently contain a boundary.

6. ***Dynamics methods:-*** there are several possible dynamics methods which can be used, these are dynamics simulation with constant volume and temperature (NVT), constant volume and energy (NVE), constant enthalpy and pressure (NPH), constant pressure and temperature (NPT), annealing dynamics, impulse dynamics etc. The most common dynamics ensembles used are NVE and NPT.

2.5.5. Monte Carlo method

In a Monte Carlo simulation each configuration depends only upon its predecessor and not upon any of the other previous configurations. The Monte Carlo method generates configurations randomly and uses a special set of criteria to decide whether or not to accept each new configuration. These criteria ensure that the probability of obtaining a given configuration is equal to its Boltzmann factor, $e^{-\frac{E(r)}{k_B T}}$ where $E(r)$ is calculated using a potential energy function.

States with a low energy are generated with higher probability than configurations with a higher energy. For each configuration that is accepted the value of the desired properties are calculated and at the end of the calculation the average of these properties is obtained by simply averaging over the number of values calculated.

In a Monte Carlo simulation each new configuration of the system may be generated by randomly moving a single atom or molecule. In some cases new configurations may also be obtained by moving several atoms or molecules or by rotating about one or more bonds. The energy of the new configuration is then calculated using the potential energy function. If the energy of the new configuration is lower than the energy of the predecessor then the new configuration is accepted. If the energy of the new configuration is higher than the energy of its predecessor then the Boltzmann factor of the energy difference is calculated:

$$\exp\left[\frac{E_{new}(r) - E_{old}(r)}{k_B T}\right] \quad \text{--- 2.33}$$

A random number is then generated between 0 and 1, and compared with this Boltzmann factor. If the random number is higher than the Boltzmann factor then the move is rejected and the original configuration is retained for the next iteration; if the random number is lower then the move is accepted and the new configuration becomes the next state.

2.5.6. Molecular dynamics vs Monte Carlo simulation

Many differences exist between molecular dynamics and Monte Carlo simulations. The most obvious differences are:

- Molecular dynamics provides information about the time dependence of the properties of the system, whereas there is no temporal relationship between successive Monte Carlo configurations. In a Monte Carlo configuration the outcome of each trial move depends only upon its predecessor. In molecular dynamics it is possible to predict the configuration of the system at any time in the future or at any time in the past.

- Molecular dynamics has a kinetic energy contribution to the total energy whereas in a Monte Carlo simulation the total energy is determined directly from the potential energy function.

- The two simulation methods sample from different ensembles. Molecular dynamics are traditionally performed under the micro canonical or constant NVE ensemble whereas traditional Monte Carlo simulation samples from the canonical ensemble, constant NVT. Both methods can be modified to sample from other ensembles too.

- Monte Carlo simulations require less computer time to execute each iteration than a molecular dynamics simulation of the same system.

2.6. Review of selected articles

In this section review of some selected articles related to the work will be mentioned and discussed.

Jones, Elvis and Hubert (2002) developed a classical force field for the room temperature molten salt 1-ethyl-3-methylimidazolium tetrachloroaluminate $[EMIM][AlCl_4]$. They tested the developed force field against the data obtained from a molecular dynamics computer simulation performed at 298K.

They used the AMBER force field to derive their force field parameters for the cation and the functional forms for the potential energy. On the other hand, the anion parameters, $AlCl_4^-$, were parameterised using intra-molecular terms with van der Waals parameters taken from the literature. They used partial atomic charges obtained from *ab initio* calculations.

Finally they performed a molecular dynamics simulation of a mixture containing 128 molecules of 1-ethyl-3-methylimidazolium cation and 128 molecules of tetrachloroaluminate anion. The simulation was carried out in the NVT ensemble with Nose-Hoover thermostat maintaining a temperature at 298 K.

Results of their simulation indicate that the $AlCl_4^-$ anion and the imidazolium residue of the $[EMIM]^+$ cation maintain almost rigid structures, with the imidazolium ring maintaining a planar structure. They also observed a short interaction between a hydrogen on the aromatic ring and the chloride of the anion.

In their dynamics calculation, they computed the diffusion constants for the $[EMIM]^+$ cation and $AlCl_4^-$ anion. The calculated diffusion constants were observed to deviate slightly from the experimental diffusion constant.

In 2001, Hanke, Price and Bell developed an inter-molecular potential suitable for molecular dynamics or Monte Carlo simulations of dimethylimidazolium and methyl-ethylimidazolium

ions. They compared the predicted crystal structure with the experimental crystal structures for chloride and PF_6^- salts.

They used simple potential energy functions since the potential need to be evaluated a large number of times during simulation using molecular dynamics or Monto Carlo methods. Their electrostatic interactions were described by partial charges on the atom sites and the repulsion and dispersion terms by Buckingham potentials.

They used a program called DL_POLY with a Berendsen thermostat for their simulations. The long-range electrostatics was treated by Ewald summation. Most of their simulations contained 192 cations and 192 anions and the box size were adjusted to give close to zero pressure in all cases.

Simulation was carried out at three temperatures (400 K, 450 K and 500 K) for dimethylimidazolium chloride and dimethylimidazolium potassium hexafluoride. Initially the system was equilibrated for five runs of 100 ps at each simulation temperature.

The simulation result gave a larger molecular volume for liquids with PF_6^- anions and the potential energy obtained for this liquid was less negative. The magnitude of the coulombic part is less, as the partial charges on each fluorine atom are quite small.

In 1999 Gavezzotti simulated the melting of an acetic acid crystal using an NPT molecular dynamics calculation. He used a molecular mechanics force field called "Optimised potential for liquid simulation" (OPLS) to calculate the potential energy of the system. A perfect crystal box consisting of 192 molecules was constructed by 2 x 6 x 4 repeats of the unit cell. The simulation started from an ordered crystal box and the simulation temperature was increased until the transition to the melt was induced. The system was warmed up from 275 K to 310 K in steps of 5 K running at a 50 ps simulation at each temperature. A crystal collapse was observed at 310 K, which is 25 K above the melting temperature.

He repeated the calculation with a defective crystal that was prepared by removing 5 molecules chosen at random. The crystal was then exposed to the same warm up procedure as

above. The crystal collapse occurred much quicker in this system, with melting at 295 K, which is 5 K higher than the experimental melting temperature.

Kung, Books, Freeman et al, (1996) used a constant pressure molecular dynamics simulation to explore the behaviour of benzene and brominated phenyl at various temperatures. A cell consisting of 32 benzene molecules and another one containing 27 brominated phenyl compound (BPC) molecules were constructed and a periodic condition was applied to mimic an infinite crystal. The simulation was done in two different ways, for BPC it was sufficient to carry out an NPT dynamics run with velocity scaling followed by an NVE calculation for data collection. However for benzene an NVT/NPT/NVE simulation was used. Four heating runs were performed for BPC with different rates of heating. The total simulation times of 100, 220, 770 and 1150 ps were used for heating from room temperature to melting temperature. The heating runs predict a melting temperature that differs from the experimental melting point by 53%, 33%, 25% and 9% respectively. For benzene NVT/NPT/NVE simulations were performed and one heating run of 1 ns was done. The result obtained agreed with experimental melting to within 8%.

Chariclea et al. (1993) studied the presence of hydrogen bonding in a 1,2-dimethyl-3-propylimidazolium chloride molten salt. Their investigation revealed the presence of hydrogen bonds between ring, methyl and methylene hydrogens and the chloride ion. The criteria that they used to identify strong H---Cl^- interactions in the crystal structure is that the H---Cl^- distance must be less than the sum of their van der Waals radii. Also they observed a short H---Cl^- distance between methyl hydrogen and the chloride ion. Their AM1 calculation indicated that the major portion of the positive charge on the organic cation is located on the hydrogen atoms; therefore the hydrogen bond network can be viewed as resulting from attractive electrostatic energies between the positive charge on the hydrogen atoms and negative charge on the chloride ion.

Jindal, Joan and Edward (2002) studied thermodynamic properties of the ionic liquid 1-*n*-butyl-3-methylimidazolium hexafluorophosphate ([BMIM][PF_6]). They carried out a Monte Carlo simulation in the isothermal-isobaric (NPT) ensemble to calculate thermophysical quantities like molar volume, liquid structure, cohesive energy, density and isothermal compressibility as functions of temperature and pressure. A total of 192 cations

and 192 anions were included in their simulation cubic cell and they then applied a periodic boundary condition on the system.

For their work they developed the United Atom force field using a combination of *ab initio* calculations, carried out on isolated cations and anions at the restricted Hartree-Fock (RHF)/6-31G level and literature values. The results of their calculations showed good agreement with experimental values of the molar volume, isothermal compressibility and cubic expansion coefficient. They observed a 5% deviation from the experimental value on molar volume, which is acceptable.

They also examined the three-dimensional probability plot of anions around the cation. Their investigation showed that the highest probability is found around the aromatic carbon bonded to the two aromatic nitrogens. That is, this aromatic carbon is the centre with the largest positive charge on the cation.

CHAPTER 3 :- Force Field Development

3.1. Introduction

In this chapter the development of a force field applicable for modelling imidazole based ionic liquids will be discussed with particular reference to the procedures followed and the data used for the training set.

The ionic liquids that will be modelled here are those containing imidazole based cations with simple substituent, like hydrogen, methyl, ethyl or propyl groups and any of the halides as counter-ions. For easy reference the force field developed in this work will be referred to as the "Imidazolium Ionic Liquid Force Field – (IILFF)".

One of the key aspects when developing or modifying a force field is the existence of structural data for the molecules to be modelled. These model compounds are usually referred to as training sets. Experimentally determined data are always preferred when developing a force field but when these are non-existent quantum mechanically calculated data are used.

In this study two sources were used to obtain the data, experimental data were obtained from the Cambridge Structural Database (CSD) (Allen and Kennard, 1993) while missing data were generated using *Gaussian98* (Frisch et al., 1998). Details of these two sets of data are given in sections 3.2 and 3.3 respectively.

In this work the "Program for the development of Empirical Force Fields" (PEFF) (Dillen, 1992), was used to model the imidazole based ionic liquids. Section 3.4 is devoted to the definition of the force field, including atom types, parameters used and how the interactions are defined in order to calculate the energy of the molecules.

In section 3.5 the details of the parameter optimisation are described and discussed and the results of the optimised parameters are given in section 3.6. The chapter is concluded by a discussion of the force field implementation and testing in section 3.7.

3.2. Structural data – experimental data

Experimental data were obtained from the Cambridge Structural Database (CSD) using the following three criteria for imidazole containing crystals. Firstly, the imidazole should contain a methyl group at position 1, hydrogen or methyl at position 2, methyl, ethyl or propyl at position 3 and hydrogen in positions 4 and 5 (see fig 3.1 for the numbering scheme). Secondly, the anion should be a halide and thirdly the crystal structure should be accurate, as indicated by a relatively low R-factor.

Five crystals satisfying the above-mentioned criteria were selected and full crystallographic details are given in Table 3.1.

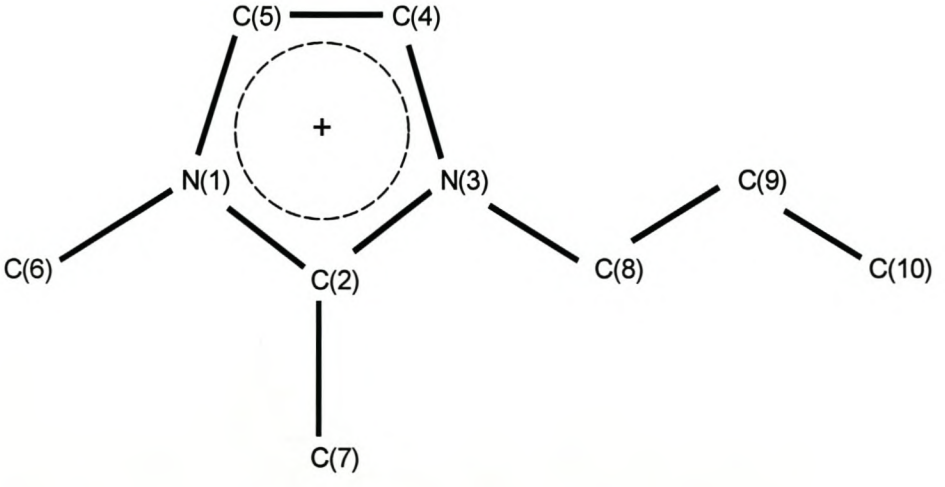

Fig 3.1 :- Numbering scheme used for imidazolium cation

Table 3.1 :- Details of crystals used in the training set

Structures	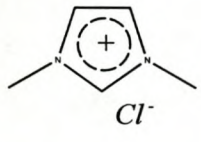 Cl^-	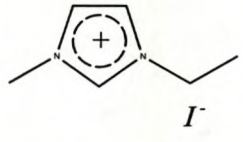 I^-	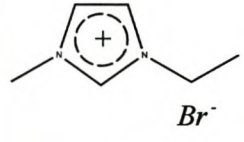 Br^-	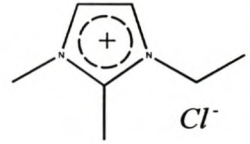 Cl^-	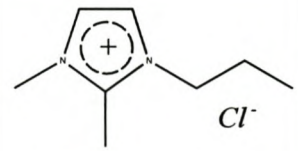 Cl^-
Formula	$[C_5H_9N_2][Cl]$	$[C_6H_{11}N_2][I]$	$[C_6H_{11}N_2][Br]$	$[C_7H_{13}N_2][Cl]$	$[C_8H_{15}N_2][Cl]$
Space group	$P2_1/c$	$P2_1/c$	$P2_1/c$	$P2_1/c$	$P2_1/c$
a (Å)	8.652(6)	8.789	8.749(1)	6.679(3)	6.981
b (Å)	7.858(6)	8.130(3)	7.999(1)	16.429(10)	12.068(1)
c (Å)	10.539(8)	13.364(3)	12.662(4)	8.239(4)	11.821
β	106.34(3)	107.33(2)	109.91(2)	105.16(4)	95.48
R-factor (%)	2.9	2.3	3.0	9.9	5.1
Temperature (K)	203	295	283 - 303	283 - 303	295
Density (g/cm^3)	1.281	1.734	1.523	1.223	1.17

3.3. Electronic structure calculations

Experimental structures obtained from the CSD were used as a basis for the models. Where necessary, the structures of cations were generated by modifying the experimental structures using Cerius^2 v 3.8. For example, the structure of the 1,2,3-trimethyl imidazolium cation was prepared by modifying the 1,3-dimethyl imidazolium cation.

There are several different ways of placing the double bonds within the five membered ring. For this work all bonds in the five membered ring were considered to be resonant.

3.3.1. Input for *Gaussian98* calculations

Only the isolated cations were taken for these calculations. In addition, several possible conformations of each cation were identified and were used as starting structures for *Gaussian98* calculations. The details of these conformations are given in Table 3.2 and Figure 3.2, where the different conformations of the same cation are indicated with a number.

3.3.2. *Gaussian98* Calculations

The *Gaussian98* calculations were performed at the Hartree-Fock (HF) level of theory with the 6-31G(d) basis set (Ditchfield, Hehre and Pople, 1971; Hehre, Ditchfield and Pople, 1972; Hariharan and Pople, 1973; Gordon, 1980; Hariharan and Pople, 1974) for geometry optimisations and frequency and partial atomic charge calculations. The size of the cations used is relatively large and all possible conformations of each the cation will be used as starting conformations for the calculation. Hence this level of theory is good considering the data required from the calculation and the amount of time spent.

Calculation of the vibrational frequencies is important for a number of different reasons. This includes predicting IR and Raman spectra of the molecules, identifying the nature of stationary points on the potential surface and computing zero point vibrations, etc. In this work, the calculated frequencies are used mainly to optimise the force-constant values in the force field being developed. In order to correctly determine the force-constant parameters,

vibrational frequencies calculated for optimised structures must be used. Hence it was necessary to do geometry optimisations prior to the frequency calculations.

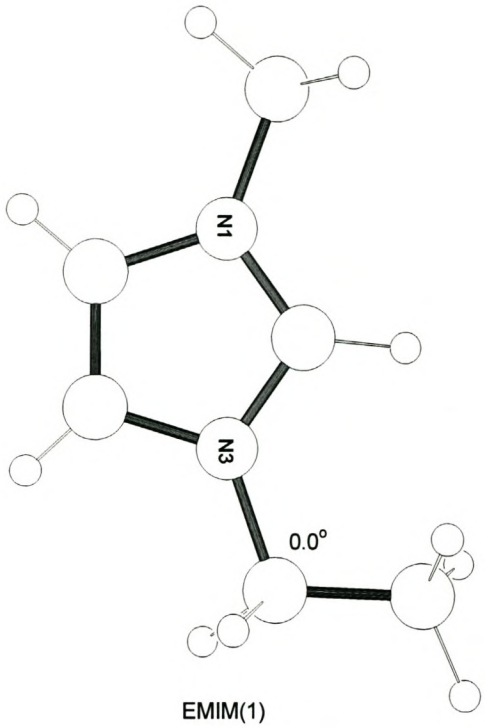

EMIM(1)

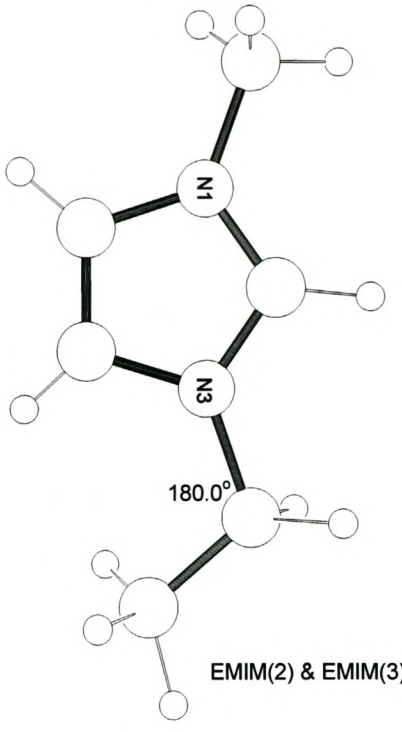

EMIM(2) & EMIM(3)

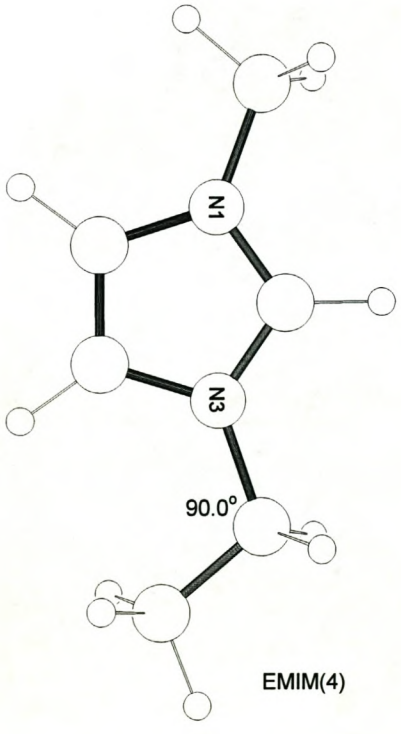

EMIM(4)

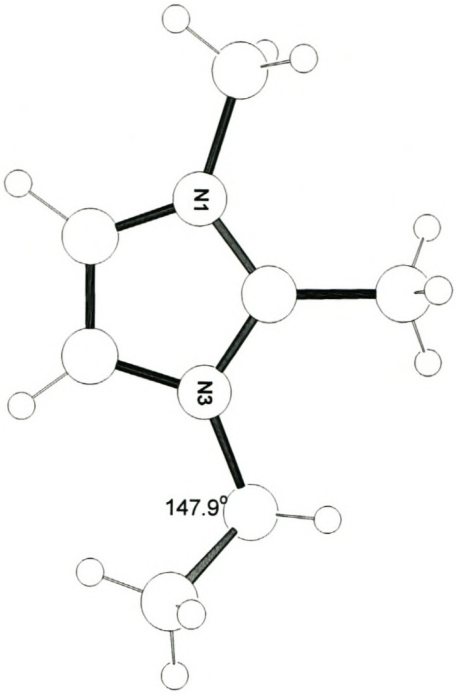

DMEIM(1)

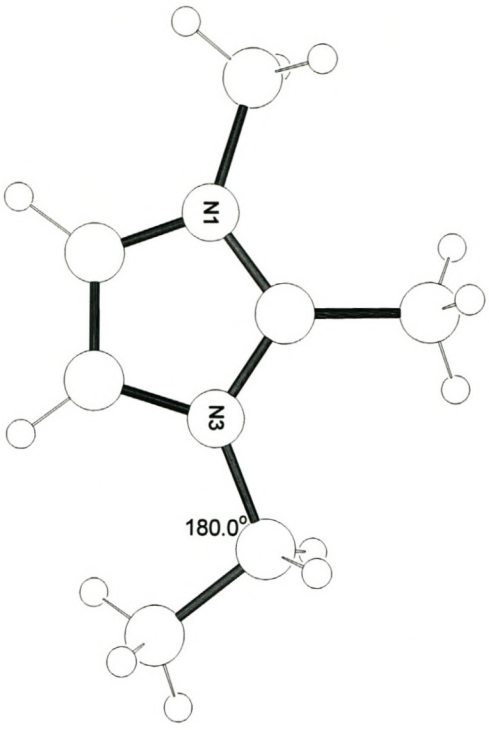

DMEIM(2)

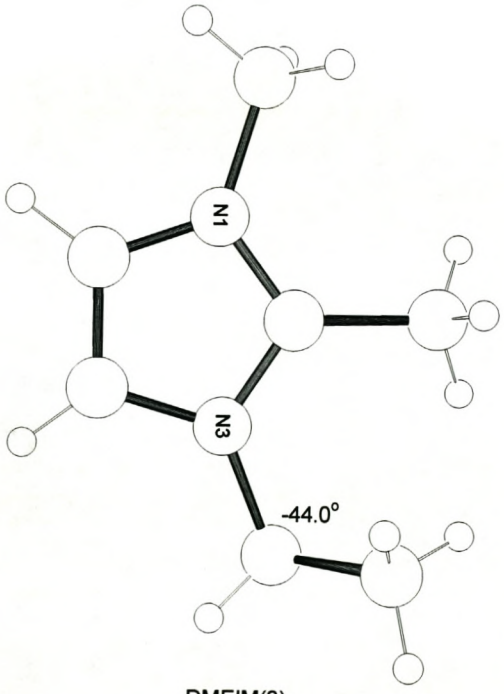

DMEIM(3)

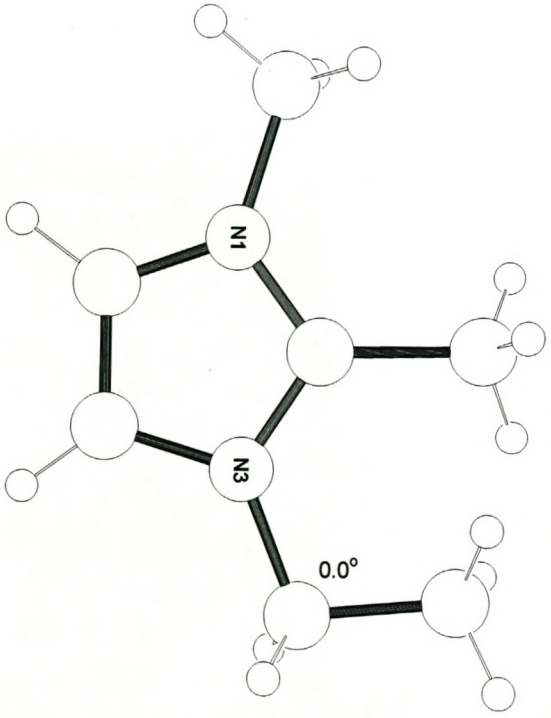

DMEIM(4)

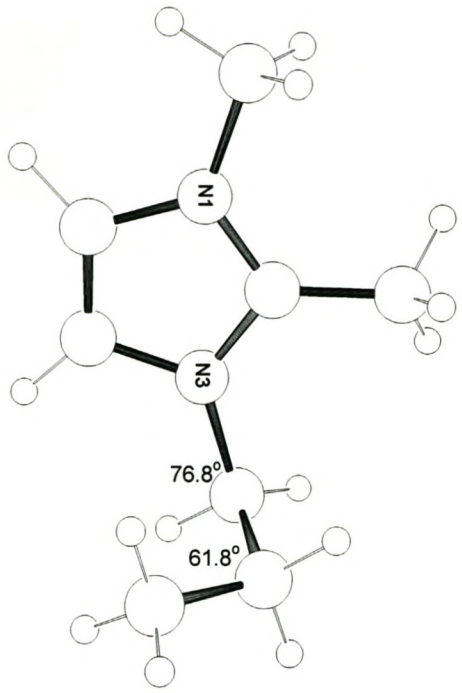

DMPIM(1)

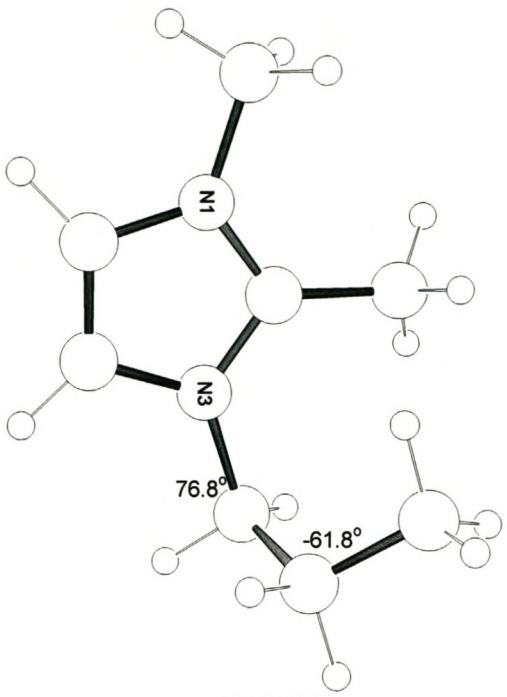

DMPIM(2)

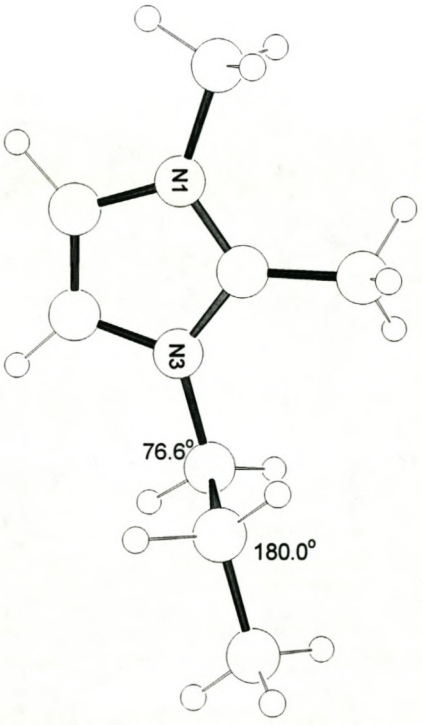

DMPIM(3)

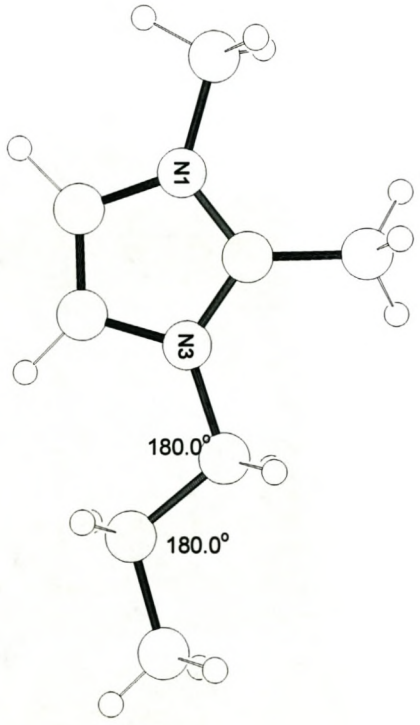

DMPIM(4)

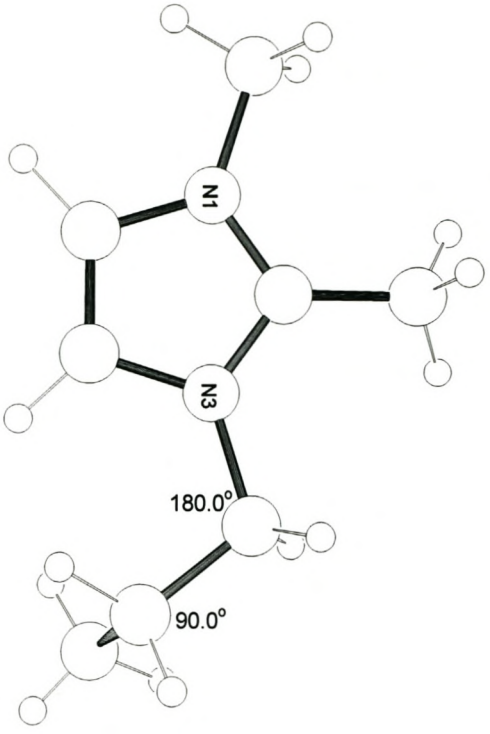

DMPIM(5)

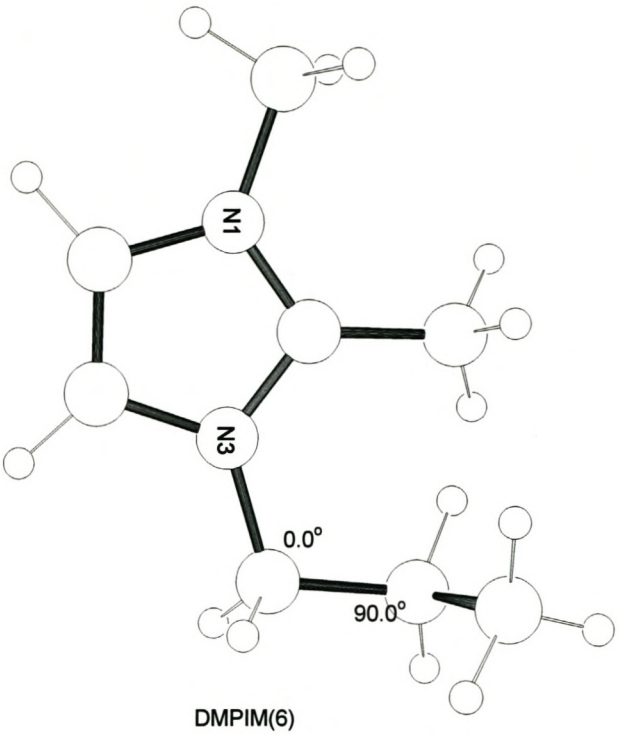

DMPIM(6)

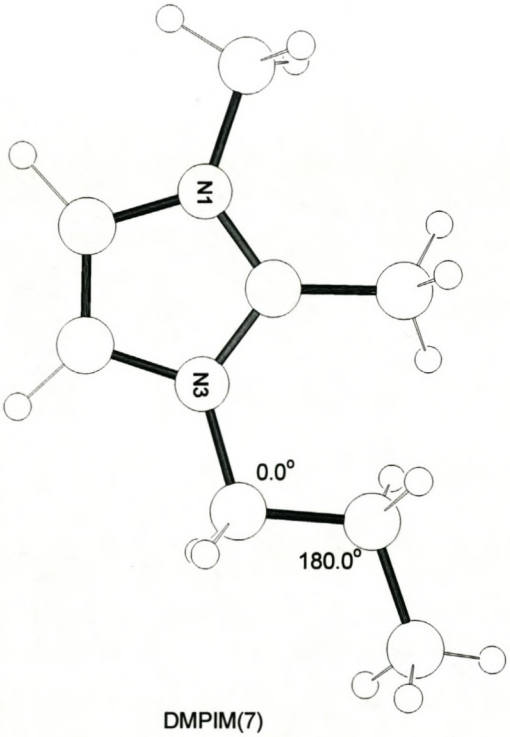

DMPIM(7)

Fig 3.2 :- Input conformations for Gaussian98 calculation – torsion angles around specific bonds are indicated.

3.3.3. Results of *Gaussian98* calculations

Three-dimensional representations of the final structures of the cations were viewed using *Gaussview2*.08 (Frisch et al., 1998) and *Molden* (Schaftenaar and Noordik, 2000), which allow animation of the calculated vibrational frequencies in order to identify their symmetry class.

The energies of the isolated cations calculated using the 6-31G(d) basis set are given in Table 3.2 in Hartrees (a.u). Also included in this *Gaussian98* output are the structural, vibrational and partial atomic charge data which were all used as observables when optimising the force field parameters.

Bond lengths, bond angles and torsion angles of the lowest energy conformations are tabulated in Addendum A and partial atomic charges of the imidazolium cations are given in Table 3.3.

In the following sections the results of these calculations will be discussed and compared with the experimental results.

3.3.3.1. Geometry optimisation

The variation in energy observed for different conformations of the same cation is mainly due to the orientation of the attached R groups (ethyl or propyl groups). Hence the initial torsion angle (T_i) and final torsion angle (T_f) of the substituted R groups are included in Table 3.2. For example, for conformations EMIM(1) to EMIM(4) and DMEIM(1) to DMEIM(4) the torsion angle specified by C(2)-N(3)-C(8)-C(9) is given for the substituted ethyl groups and for conformations DMPIM(1) to DMPIM(7) torsion angles of the substituted propyl group specified by C(2)-N(3)-C(8)-C(9) for T_{i1} and T_{f1} and N(3)-C(8)-C(9)-C(10) for T_{i2} and T_{f2} are given. The initial and final conformations of all structures mentioned in Table 3.2 are indicated in Fig 3.2 and 3.3 respectively and Fig 3.1 can be referred to for the numbering scheme. No input and output structures are given for the DMIM and TMIM cations as no significant change was observed in their structures.

As can be seen from Table 3.2 the same initial torsion angle was given for conformation EMIM(2) and EMIM(3). These two structures were obtained from two different experimental structures that had approximately the same conformations, but were nevertheless different enough to yield two different minima upon optimisation. This result was further confirmed by studying the progress of their optimisations using a three dimensional graphical visualiser, *Molden*, where it could be seen that the starting energies of these two conformations were at different points on the potential energy surface.

Convergence could not be attained for conformation DMEIM(4) and hence is represented by NC in Table 3.2. No other method to optimise the structure (such as a higher level of theory) was attempted as the aim of these calculations was mainly to collect data. The other three structures (DMEIM(1) to DMEIM(3)) were observed to converge to the same final conformation and energy.

For DMPIM cations, structures DMPIM(3), DMPIM(4) and DMPIM(7) led to the same lowest energy conformation and are indicated by an asterisk. It is interesting to note that these three conformations have initial torsion angles (T_{i2}) of 180°, which means that there is little interaction between the attached propyl group and the central five membered ring of the isolated cation. The final conformation of DMPIM(7) is a mirror image of conformations DMPIM(3) and DMPIM(4), as can easily be seen from Table 3.2 and Fig 3.3.

Bond lengths, bond angles and torsion angles of the minimum energy conformations are compared with the experimental measurements. At this level of theory, the bond lengths have an RMS deviation of 0.0228Å and a maximum deviation of 0.0720Å from the experimental value. Bond angles have a deviation of 1.29 degrees and a maximum deviation of 1.81 degrees.

Torsion angles were observed to deviate considerably from the experimental cation. This deviation is due to the substituted alkyl groups. This result is expected as we are dealing with a cation in a gas phase.

Table 3.2 :- Energy results of isolated imidazolium cations calculated with 6-31G(d) basis set

Conf.	Initial Torsion		Final Energy	Final Torsion	
	T_{i1}	T_{i2}	E (a.u.)	T_{f1}	T_{f2}
DMIM	-	-	-303.2738	-	-
TMIM	-	-	-342.3202	-	-
EMIM(1)	0.0	-	-342.3122	0.80	-
EMIM(2)*	180.0	-	-342.3134	105.0	-
EMIM(3)	180.0	-	-342.3098	180.0	-
EMIM(4)*	90.0	-	-342.3134	105.0	-
DMEIM(1)*	147.9	-	-381.3595	95.0	-
DMEIM(2)*	180.0	-	381.3595	95.9	-
DMEIM(3)*	-44.0	-	-381.3595	95.7	-
DMEIM(4)	0.00	-	NC	NC	-
DMPIM(1)	76.8	61.8	-420.3943	79.6	63.3
DMPIM(2)	76.8	-61.6	-420.3945	111.9	-64.3
DMPIM(3)*	76.6	180.0	-420.3954	95.5	178.9
DMPIM(4)*	180.0	180.0	-420.3954	95.5	178.9
DMPIM(5)	180.0	90.0	-420.3945	-111.9	64.3
DMPIM(6)	0.0	90.0	-420.3943	79.6	63.3
DMPIM(7)*	0.0	180.0	-420.3954	-95.5	-178.9

NC = not converged * = Conformations with minimum final energy

3.3.3.2. Vibrational frequency calculations and assignments

Molecular vibrational frequencies depend on the second derivative of the energy with respect to the nuclear positions. Frequency calculations can thus be used to determine the nature of the stationary point found by a geometry optimisation, which is done by counting the number of imaginary frequencies.

In this work, conformation EMIM(3) gave two negative frequencies, which shows that this conformation is at a saddle point. All other frequencies calculated were positive, which indicates a minimum energy conformation, that could be either a local minimum or a global minimum.

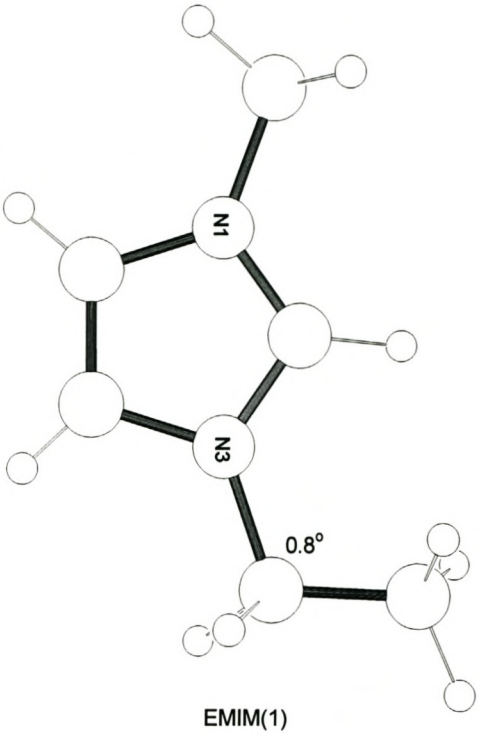

EMIM(1)

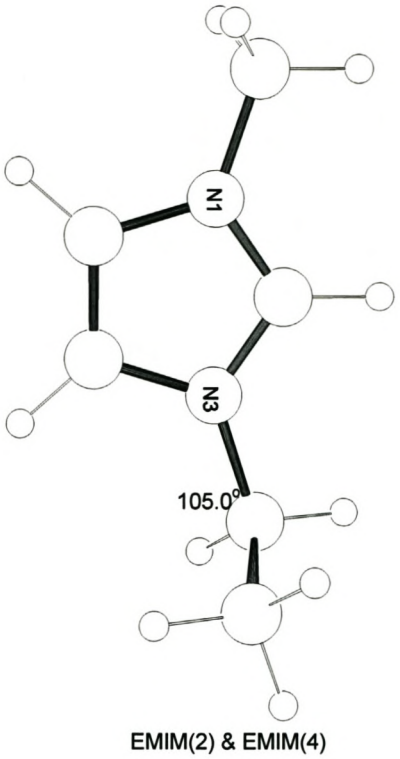

EMIM(2) & EMIM(4)

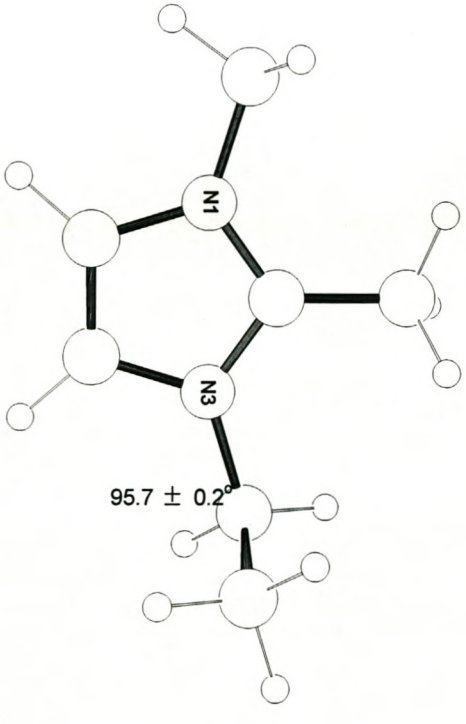

DMEIM(1), DMEIM(2) & DMEIM(3)

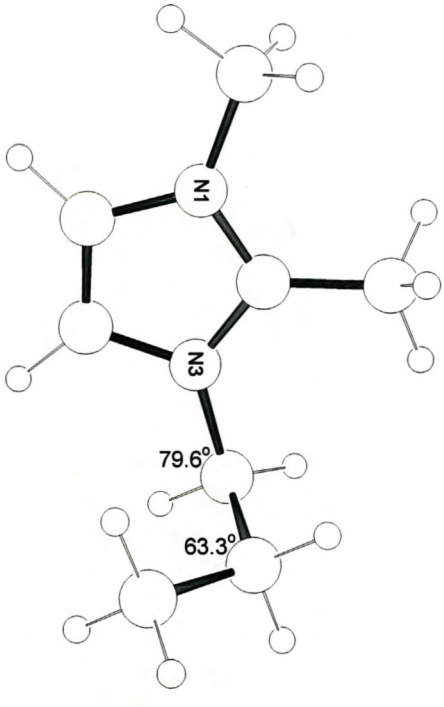

DMPIM(1) & DMPIM(6)

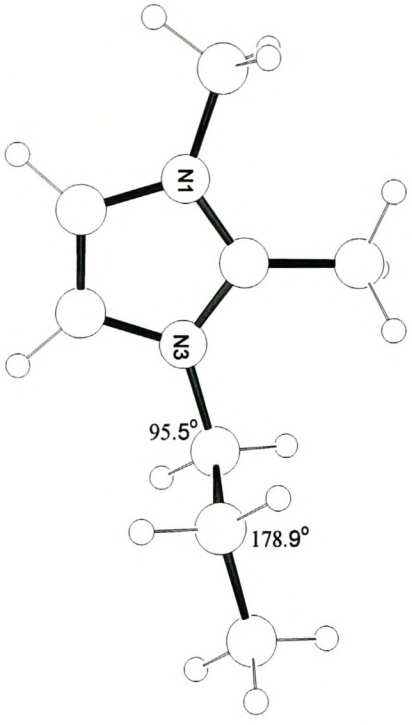

DMPIM(3), DMPIM(4) & DMPIM(7)

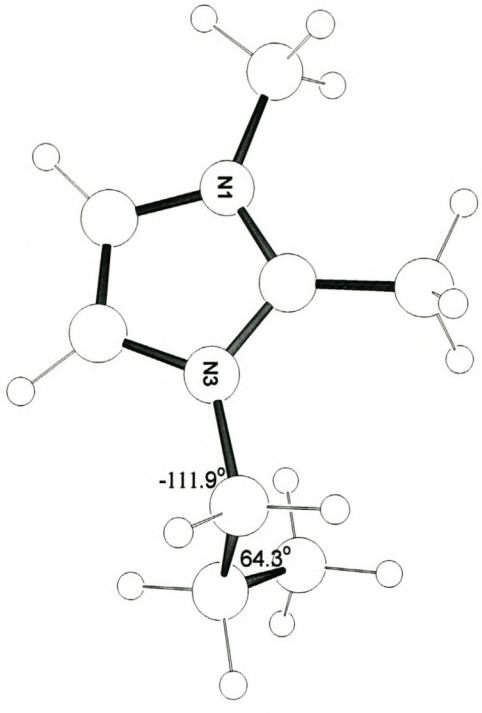

DMPIM(5)

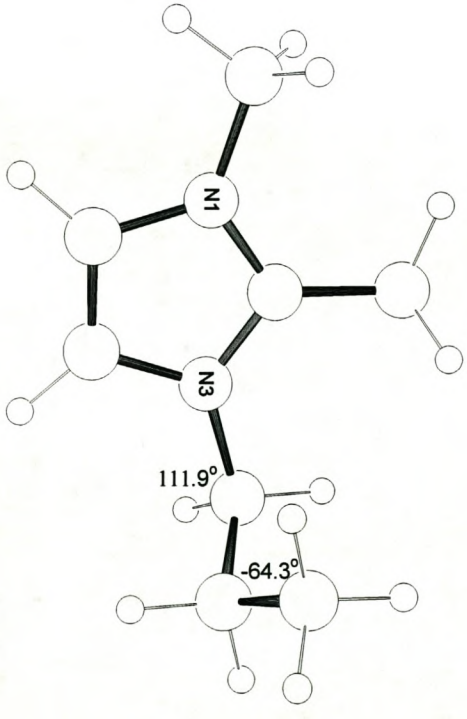

DMPIM(2)

Fig 3.3 :- Output conformations of Gaussian98 calculations – torsion angles around specific bonds are indicated.

As discussed in chapter two, section 2.3.1, frequencies computed using Hartree-Fock are known to give systematic errors due to the neglect of electron correlation (Foresman and Frisch, 1993). This results in an over-estimation of the frequency by about 10 – 12%, hence all the frequencies calculated were multiplied by a correction factor of 0.8929; which is the scaling factor for the Hartree-Fock/6-31G(d) level of theory. These vibrations were viewed using a vibrational viewing program, *Gaussview2.08*, in order to do a point group characterisation of the isolated imidazolium cations and a symmetry assignment of these calculated frequencies. The vibrational frequencies calculated at the optimised structures and their symmetry assignments are tabulated in Addendum C.

3.3.3.3. Partial atomic charge

Partial atomic charges calculated in *Gaussian98* are obtained using the Mulliken population analysis. This method partitions the total charge for the imidazole cation among the atoms of the molecule. This calculation shows a slight negative charge on the aromatic nitrogens (N(1) and N(3)) and the sp^3-hybridised carbons (C(6), C(7), C(8), C(9) and C(10)), while the balancing positive charges are divided between the aromatic carbons (C(2), C(4) and C(5)) and hydrogen atoms. Partial atomic charges calculated using the 6-31G(d) basis set are given in Table 3.3.

Partial atomic charges of the five membered ring

The results of this calculation show two types of partial atomic charge assignment on the five membered ring. Firstly, all imidazole based cations containing a hydrogen atom attached to C(2) show a similar assignment of the partial atomic charges on the aromatic carbons and aromatic nitrogens. Those cations containing an sp^3-hybridised carbon attached to C(2) show different charge assignments to those previously mentioned. This result is shown in Table 3.3.

Firstly, for those imidazolium cations containing a hydrogen attached to the C(2) partial atomic charge assignments of -0.586 ± 0.001 for nitrogen atoms and 0.419 ± 0.001 for aromatic carbons were obtained. These values were observed to shift to -0.635 ± 0.001 and 0.692 ± 0.002 respectively when the hydrogen in position C(2) was replaced by an sp^3-hybridised carbon. Similar changes in the assignment of charges were also observed for C(4)

and C(5). These results indicate the difference that exists between those imidazolium cations containing hydrogen in position C(2) and those imidazolium cations containing an sp^3-hybridised carbon.

Charge on sp^3 hybridised carbon

Methyl carbons attached to nitrogens of the ring (C(6) and C(8)) were all calculated to have a charge of -0.31 ± 0.01, while that attached to the aromatic carbon C(2) was calculated to have a higher negative charge, -0.56. When the methyl group attached to N(3) is replaced by an ethyl or propyl group the partial charge was found to drop substantially. For example, the charge on C(8) was observed to drop to -0.16 ± 0.01 when an ethyl group is used and -0.149 when a propyl group is attached (see Table 3.3).

3.4. Force field definitions

In this study a program called PEFF was used to develop the Imidazolium Ionic Liquid Force Field (IILFF). Initial parameters for this force field were taken from existing force fields and were optimised to fit the molecules of interest, where necessary additional interactions were added. Atom types were defined for all atoms in the molecules. In this program the steepest descent, diagonal and full matrix Newton-Raphson methods were used as minimisation algorithms (see to section 2.4).

PEFF requires an input that contains details of the atoms (atom types), the parameters defined and all the interactions. It also needs the Cartesian coordinates of the molecules used as training sets and the *Gaussian98* calculated results as observables. These include bond lengths, bond angles, torsion angles, vibrational frequencies, partial atomic charges etc.

The force field parameters are then optimised using the parameters and interactions specified and referring to the criteria and observables mentioned in the input file.

In the following section details of the atom types, interactions and parameters used when developing the force field will be discussed.

Table 3.3 :- Atomic charges of isolated imidazolium cations calculated with the 6-31G(d) basis set

Atom			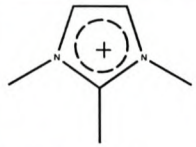	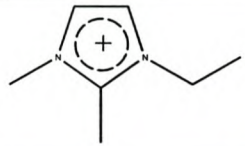	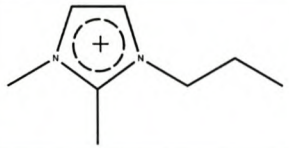
N(1)	-0.5868	-0.5873	-0.6359	-0.6346	-0.6426
N(3)	-0.5868	-0.5894	-0.6386	-0.6427	-0.6435
C(2)	0.4094	0.4104	0.6916	0.6941	0.6943
C(4)	0.0238	0.0247	0.0211	0.0219	0.0211
C(5)	0.0238	0.0219	0.0219	0.0200	0.0208
C(6)	-0.3148	-0.3144	-0.3189	-0.3191	-0.3189
C(7)	-	-	-0.5604	-0.5636	-0.5637
C(8)	-0.3148	-0.1604	-0.3171	-0.1651	-0.1490
C(9)	-	-0.4963	-	-0.4937	-0.3246
C(10)	-	-	-	-	-0.5026
H	0.3050	0.3100	0.2900	0.2900	0.2900
H *	0.2433	0.2225	0.2395	0.2282	0.2169

H = Charge of hydrogens attached to sp^2-hybridised carbon (average value)

H * = Charge of hydrogens attached to sp^3-hybridised carbon (average value)

3.4.1. Atom types

Just as the atomic numbers of the nuclei, geometry of the system, overall charge and spin multiplicity are important for quantum mechanical calculations, assigning atom types to each atom in the system is important when developing a force field.

"Atom type" is a term used to describe the force field type of the atom, which could be a letter code or a number. The atom type definition gives full details of the atoms used in the force field. This includes the atomic weight, van der Waals hardness, van der Waals radius, charge etc of each atom type. Full details of the force field atom types used in the development of the IILFF are tabulated in Table 3.4.

Atomic weights are used in the calculation of vibrational frequencies and thermodynamic properties. The van der Waals hardness and van der Waals radii are used in calculating non-bonded interactions. Flags are used to indicate whether an atom can be a terminal atom or a central atom for an out-of-plane interaction. For example, an "Oop" option is specified for nitrogen and aromatic carbons to indicate that these atoms could be a central atom for an out-of-plane interaction, while the "Terminal" option is specified for hydrogen to show that the atom will not be allowed to bond to more than one atom.

The van der Waals hardness and van der Waals radii for a methyl carbon, aromatic carbon and nitrogen were obtained from the Dreiding2.21 force field (Mayo et al., 1990), while the van der Waals hardness and van der Waals radii of hydrogen and the halides were optimised.

Atomic charge corrections for all halides used in the force field were given a value of –1. The atomic charge correction value for the aromatic carbon (Q_{C_R}) was optimised by the program, while that of nitrogen (Q_{N_R}) was calculated using the formula specified in equation 3.8. The atomic charge correction parameter mentioned here is defined as the partial atomic charge assigned to all atoms with in the five membered ring so as the total charge of the imidazolium cation will have a charge of +1.

Similar atoms are given the same atom type in the force field. Where similar atoms in different chemical environments are present it is important that a separate atom type is

specified for each. For example, depending on the chemical bonding involved it is necessary to distinguish between an sp^3-hybridised carbon atom and an sp^2-hybridised carbon atom. Since C(6) to C(10) are sp^3-hybridised carbons, they adopt a tetrahedral geometry and hence an atom type of C_3 is used to specify them in the force field.

The C_R atom type is assigned to those carbon atoms within the five membered ring, C(2), C(4) and C(5). These atoms adopt a trigonal-planar geometry leading to a reference angle near 120°. Nitrogen is given the atom type of N_R, where R in both cases is used to refer an aromatic carbon or nitrogen. For all other atoms used in the IILFF the chemical symbol of the atom followed by an underscore is used to specify their atom type.

3.4.2. Functional forms

As previously mentioned in section 2.3.2.2, the most important aspect when defining a force field is specifying the functional forms and the parameters to be used. In this section details of the individual functional forms used for defining the ionic liquid force field will be discussed. The total potential energy, E_{FF}, in a molecule or crystal is calculated by,

$$E_{FF} = \sum E_{str} + \sum E_{bend} + \sum E_{tors} + \sum E_{oop} + \sum E_{vdw} + \sum E_{coul}$$

where E_{FF} is a function of the positions of the atoms in the molecule or crystal. The various contributions to the potential energy function taken into account in the development of the IILFF are bond stretching (E_{Str}), angle bending (E_{bend}), torsion (E_{tors}), out of plane interaction (E_{oop}), van der Waals (E_{vdw}) and coulombic (E_{coul}) interactions. No cross term interactions were incorporated in this paper.

The various energy terms used are described in section 2.3.2.2, while specific aspects regarding their implementation are included below and summarised in Table 3.5. Also in this table, PEFF codes used to implement the formula in the program are given. The initial values of most of the parameters in the IILFF are taken from the Dreiding 2.21 force field (Mayo et al., 1990), when such parameters were missing an approximate starting value was assigned.

Table 3.4 :- Details of force field atom types used

No.	Element	Atom Type	Weight	Vdw_H ($kcal.mol^{-1}$)	Vdw_R (Å)	Charge (*coul*)	Flags
1	Aliphatic Carbon	C_3	12.0110	0.0951	1.950	-	-
2	Aromatic Carbon	C_R	12.0110	0.0951	1.950	Q_{C_R}	Oop
3	Nitrogen	N_R	14.0067	0.0774	1.837	Q_{N_R}	Oop
4	Hydrogen	H_	1.0079	$\varepsilon_{(H\_)}$	$r_{m(H\_)}$	-	Terminal
5	Fluorine	F_	18.9984	0.0725	1.736	-1	-
6	Chlorine	Cl_	35.3545	$\varepsilon_{(Cl\_)}$	$r_{m\,(Cl\_)}$	-1	-
7	Bromine	Br_	79.9040	$\varepsilon_{(Br\_)}$	$r_{m\,(Br\_)}$	-1	-
8	Iodine	I_	126.9045	$\varepsilon_{(I\_)}$	$r_{m\,(I\_)}$	-1	-

Vdw_H = van der Waals Hardness and Vdw_R = van der Waals radius

Q_{C_R} is taken to be a variable and Q_{N_R} is calculated using the formula mentioned in equation 3.8

a. Bond stretching interaction

There are many functional forms used to model the potential energy curve for a bond stretch. In this force field a simple harmonic expression, Hooke's Law, is used because it is a reasonable approximation of the shape of the potential energy curve near the equilibrium value and for a molecular mechanics calculation this is acceptable as the deviation from equilibrium value is very small. The other advantage of using this formula is that there are only two parameters to be optimised, these are the reference bond length, l_o and the force constant, k_l.

$$E_{str} = 0.5k_l[(l - l_o)^2] \qquad \text{--- 3.1}$$

b. Angle bending interaction

The deviation of an angle from its reference value is described using the harmonic potential given in equation 3.2, where k_θ is the bending force constant and θ_o is the strain-free bond angle. The parameters that will be optimised are the reference bond angle, θ_o and the bending force constant, k_θ.

$$E_{bend} = 0.5k_\theta[(\theta - \theta_o)^2] \qquad \text{--- 3.2}$$

c. Torsion interaction

When considering the torsion angle parameters in this force field all torsions containing the same central bond are assigned the same torsion angle. For example, all torsions in which the central bond is between two sp^3-hybridised carbon atoms are assigned the same torsional parameter.

In this force field the torsional potential is expressed as a cosine function (mentioned in equation 2.8), where the value of V_n gives a qualitative indication of the relative barrier to rotation. n in this equation is the multiplicity; its value gives the number of minimum points

in the function as the bond is rotated through 360°. In this force field n might take a value of $|\pm 2|, |\pm 3|, or |\pm 6|$. The value of s mentioned in the formula takes the sign of n, i.e., ± 1.

$$E_{tors} = 0.5V_n[1 + s\cos|n|\omega] \qquad \text{--- } 3.3$$

d. Out-of-plane interactions

The presence of an out-of-plane interaction in the IILFF is essential to ensure the planarity of the imidazole ring. *Gaussian98* results show that the geometry of the five membered ring and the heavy atoms attached directly to this ring (C(6), C(7) and C(8)) are planar (see section 3.3.3 and figure 3.3). In a molecular mechanics simulation, this structure can be achieved by introducing an out-of-plane interaction in the force field.

In this work, an out-of-plane interaction is incorporated by defining an angle, δ, between a bond from the central atom and the plane defined by the central atom and the other two atoms. Two atom types within the five membered ring, aromatic carbon and nitrogen, were assigned to be the centres for out-of-plane interactions. These two atoms are described by "Oop" in the flag column of the force field definition table, Table 3.4.

$$E_{oop} = k_{oop}[1 - \cos\delta] \qquad \text{--- } 3.4$$

e. Van der Waals interactions

In this force field the van der Waals interactions are incorporated by using the Lennard-Jones 12-6 (LJ-12-6) potential function given in equation 3.5. There are several advantages associated with this function. Firstly, this potential function contains only two adjustable parameters, r_m, the separation for which the energy is a minimum, and the well depth, ε. The other advantage associated with this formula is that for large systems the repulsive part that varies as r^{-12} can be evaluated easily by squaring the attractive part of the function r^{-6} without having to perform computationally intensive calculations.

$$E_{vdw}(r) = \varepsilon\left[\left(\frac{r_m}{r}\right)^{12} - 2\left(\frac{r_m}{r}\right)^{6}\right] \qquad \text{--- } 3.5$$

Experimentally, very short interactions were observed between hydrogens of the imidazole ring and the halide of the crystal, $H-X$. Hence it is necessary to incorporate such interactions in the force field explicitly. The same formula stated in equation 3.5 was used to calculate such an interaction. However, the two parameters were derived differently. That is, the van der Waals hardness, represented by $\varepsilon_{(X\_H\_)}$, is derived using the geometric mean of the previously optimised parameters for hydrogen and halides.

$$\varepsilon_{(X\_H\_)} = \sqrt{\varepsilon_{(H\_)} \cdot \varepsilon_{(X\_)}}$$

and for the van der Waals distance, which will be represented by $R_{m(X\_H\_)}$, a starting value was taken by adding the van der Waals radii of the previously optimised two parameters, $r_{m(H\_)}$ and $r_{m(X\_)}$.

$$R_{m(X\_H\_)} = r_{m(H\_)} + r_{m(X\_)}$$

where $X\_$ refers to any of the halides (Cl, Br or I).

f. Coulombic interaction

The simplest way to calculate electrostatic interactions is to assign a partial charge to every atom and to use Coulomb's law to calculate the interaction energy.

$$E_{coul} = (331.91)\left[\frac{Q_{AT1} \cdot Q_{AT2}}{r}\right] \qquad \text{--- 3.6}$$

Where Q_{AT1} and Q_{AT2} are charges of any two atoms in the crystal and r is the separation between the two atoms.

Since we are dealing with real crystals, the electrostatic interactions in a crystal can be calculated by using a different formula (mentioned in equation 3.7). The advantage that we get by introducing this function is that the summation involving the error function (erfc) converges very rapidly and beyond some cut-off distance its value can be considered negligible.

$$E_{coul} = (331.91)\left[\frac{Q_{AT1}.Q_{AT2}}{r}\right] erfc(w.r) \qquad \text{--- 3.7}$$

where *erfc* is the error function complement (Dillen, 2000).

$$erfc(x) = \frac{2}{\sqrt{\pi}} \int_{x}^{\infty} e^{-t^2} dt$$

and $w = \sqrt{\pi}.a$ where a in this equation is an Ewald summation constant which is given a value of 0.05 in the force field.

g. Bond increment

Assignment of partial atomic charges in this force field was done using bond increments. A bond increment is defined between any two connected non-identical atom types and it allows the assignment of atomic charges by assigning the negative value of the bond increment to the first atom type specified in the force field and an equal and positive value to the second atom type. Here the sequence in which the atom types are written is important.

This method has an obvious disadvantage in the IILFF as it gives a total charge of zero to the imidazolium cation, when it really contains a $+1$ charge. This problem was solved by introducing an atomic charge correction value that is assigned to each atom in the ring to correct the over-estimation or under-estimation of the partial atomic charge.

When introducing these parameters a $+1$ charge was assumed to be delocalised over the five membered ring and the atom correction value of the three aromatic carbons (C(2), C(4) and C(5)), represented by C_R, were assumed to be identical. Then an arbitrary atom correction value was assigned to the aromatic carbon which was later optimised in the force field. The atom correction value of the nitrogen (N_R) was calculated using equation 3.8:

$$Q_{(N\_R)} = 0.5 - 1.5Q_{(C\_R)} \qquad \text{--- 3.8}$$

Table 3.5 :- Interactions, equations and constants used in the force field

Interactions	Formula	Constants	PEFF Code
Bond stretch	$E_{str} = 0.5k_l(\Delta l)^2; \quad \Delta l = l - l_o$	l_o and k_l	101
Angle bending	$E_{bend} = 0.5k_\theta(\Delta\theta)^2; \quad \Delta\theta = \theta - \theta_o$	θ_o and k_θ	201
Torsion	$E_{tors} = 0.5V_n[1 + s\cos\lvert n\rvert\omega] \quad s = \pm 1$	n and V_n	301
Out of plane	$E_{oop} = k_{oop}[1 - \cos\delta]$	k_{oop} and δ	401
Van der Waals	$E_{vdw}(r) = \varepsilon\left[\left(\frac{r_m}{r}\right)^{12} - 2\left(\frac{r_m}{r}\right)^{6}\right]$	ε and r_m	512 / 2612
Explicit van der Waals	$E_{vdw}(r) = \varepsilon_{(x\_H\_)}\left[\left(\frac{R_m}{r}\right)^{12} - 2\left(\frac{R_m}{r}\right)^{6}\right]$	$\varepsilon_{(X\_H\_)}$ and $R_{m(x\_H\_)}$	506 / 2606
Coulombic interactions	$E_{coul} = (331.91)\left[\frac{Q_{AT1}\cdot Q_{AT2}}{r}\right]$	-	2305
Coulombic interactions for a crystal	$E_{coul} = (331.91)\left[\frac{Q_{AT1}\cdot Q_{AT2}}{r}\right]erfc(w.r)$	-	2705

3.4.3. Training set

Representative molecules were selected when developing the IILFF. A full description of these molecules and their full crystallographic data was given in section 3.2. Quantum mechanically calculated data obtained from isolated cations were also included in the training set (refer to section 3.3).

The information from the training set used in the force field development consists of the Cartesian coordinates of each experimental structure and the observables obtained from the quantum mechanical calculations. The observables include bond lengths, bond angles, selected torsion angles, partial atomic charges and corrected vibrational frequencies. For some cations the Cartesian coordinates of cations having different conformations are included in the data set, with the energy differences that exists between this conformation and the experimental structure added as observables to the data set.

All these data were used when optimising the reference bond lengths and bond angles, force constants and charge parameters. When optimising the non-bonded parameters like van der Waals radius and van der Waals hardness Cartesian coordinates of the full crystals were used, as well as other crystals with similar structures to those mentioned above were added. The crystals selected contain nitrogen, carbon and hydrogen atoms in their cation and any of the halides as an anion.

These crystals are histamine hydrobromide (Cole and Holt, 1986), 1,1',3,3'-tetramethyl-2,2'diimidazolium dibromide (Nagel, Bock and Eller, 2000), 4-methylpyridinium bromide (Andras, et al., 1993), 1,4-diethylquinoxalinium dioxide (Hausen et al., 1993), trimethyl (phenethyl) ammonium iodide (Barlow et al., 1989), dipyridinio-methane di-iodide (Brudgam, 1986), adenine dihydrochloride (Kistenmacher, 1974), histamine hydrochloride (Bonnet, 1975), pyrimidine hydrochloride (Furberg, 1975), 5-(2-Ammonioethyl)-1-methyl-imidazolium dichloride (Glowka, 1990).

Details of their crystallographic data are not important because only the fixed geometry of these crystals was used. Some nitrogen and carbon atoms in these newly added crystals were

observed to have chemically different environments. For these cases different atom types and interactions were defined and included in the force field definition.

3.5. Force field parameter optimisation

Most of the initial values are taken from existing force fields hence in the development of this force field it is necessary to optimise all these parameters to ensure accurate modelling of the molecules of interest.

PEFF offers the possibility of optimising such values in a force field by a least squares procedure, by referring to the quantum mechanically calculated observables given in the training set.

Optimisation of the parameters was done gradually because it is difficult to simultaneously modify a large number of parameters. This does not, however, mean that all parameters were refined in isolation. The refinement of the parameters is discussed in the following sections.

3.5.1. Optimisation of reference bond lengths and bond angles

The bond stretch and angle bend are highly coupled, i.e., a slight change in a bond length affects the corresponding angle and vice versa. Hence these two parameters were optimised together. When optimising these two sets of parameters bond lengths and bond angles obtained from quantum mechanical calculations of the isolated cations were taken as observables.

Furthermore a high degree of coupling was observed between the various bond angle parameters, therefore only selected reference bond angles were optimised, while the rest were calculated using basic geometrical principles. For example, the similarity between some internal angles of the five membered ring and the total internal angle of a five membered ring, 540°, were considered. A full list of these parameters is given in Table 3.7, where all the calculated values and the formulas used to calculate them are indicated.

In the optimisation of the reference bond lengths and bond angles of the imidazolium cation no significant change was observed when comparing the pre-optimised set of values to the optimised ones.

3.5.2. Optimisation of force constants

The corrected vibrational frequencies calculated using quantum mechanical methods were used as observables to optimise all the force constant parameters.

The optimisation process was commenced by adding all the initial sets of force constants to the force field and calculating the vibrational frequencies for each isolated cation in PEFF.

All the vibrations were animated using a vibrational viewing program, *Vibram* (Dillen, 2001) and the symmetry class of each of these vibrations was assigned. These vibrations were then correlated with those vibrations calculated at the Hartree-Fock level. In many cases it was observed that similar frequencies calculated using the Hartree-Fock and PEFF give different vibrations when viewed using the vibrational viewing programs and hence a visual tool was used to correlate the vibrations obtained from the two calculations.

The correlated PEFF frequencies were then added to the data set following their corresponding quantum mechanically calculated frequencies and used in the optimisation of the force constants in the force field.

After every optimisation the force field parameters were updated with the new values and the vibrational frequencies of the cations were recalculated. The frequency assignments were checked after every update and corrections were made to the previous correlation. This process was repeated, ideally, until no deviation in the order of vibrations was observed between the two vibrations.

3.5.3. Optimisation of charge parameters (bond increments and atomic charge corrections)

During optimisation of the charge parameters, the anion and cation in the crystal were seen as separate entities having a charge of –1 and +1 respectively. A charge of –1 was assigned to all the halides included in the ionic liquid force field. Assignment of partial atomic charges on the imidazolium cation was based on the bond increment and atomic charge correction parameters discussed in section 3.4.2.

The bond increment parameters were given a starting value of zero and the atomic charge correction parameter for the aromatic carbon (C_R) was assigned an arbitrary value. The quantum mechanically calculated partial atomic charges were then used as observables to optimise these two sets of parameters. The atomic charge correction value of the nitrogen (Q_{N_R}) was calculated using equation 3.8.

3.5.4. Optimisation of van der Waals parameters

All crystals mentioned in Table 3.1 were used when optimising the van der Waals hardness of hydrogen, whereas for the van der Waals hardness of the halides only those crystals containing that particular halide as an anion were included. For example, when optimising the van der Waals hardness of chloride only those crystals containing chloride as an anion were used. The van der Waals radius of hydrogen and the halides were combined and optimised together.

When dealing with the explicit van der Waals parameters, the optimised parameters were used as starting values for the optimisation of the explicit van der Waals distance parameters specified by $R_{m(X\_H)}$. During optimisation of these parameters fixed geometries of the crystals mentioned in Table 3.1 and those crystals mentioned in section 3.4.3 were used as observables.

While the explicit van der Waals hardness parameters were calculated from the previously optimised van der Waals hardness terms and they were used in the IILFF without further optimisation.

3.6. Results

3.6.1. Parameters

All parameters optimised are listed in Tables 3.6 to 3.15. As discussed in section 3.5.1 only selected angle parameters were optimised, while the rest were calculated using formulas mentioned following Table 3.7. The value of the $\theta_{(H\_C\_3H\_)}$ angle was taken directly from the literature and not optimised. For the sake of completeness, a full list of all the angle parameters is given in Table 3.7, where all the calculated parameters are indicated while the value taken from the literature is represented by a pound sign.

Table 3.6 :- Bond stretch force constants and reference bond lengths.

Parameters	l_o (Å)	k_l (k cal mol^{-1} Å^{-2})
C_3-N_R	1.436	624.0
C_3-C_R	1.526	609.2
C_3-C_3	1.509	514.6
C_R-C_R	1.359	840.2
C_3-H_	1.076	687.6
C_R-H_	1.061	756.3
C_R-N_R	1.332	768.2

Table 3.7 :- Angle bend force constants and reference bond angles.

Parameters	θ_o (deg)	k_θ (kcal mol^{-1} rad^{-2})
C_R-N_R-C_R	107.7	43.4
N_R-C_R-N_R	106.3 [a]	332.6
C_3-C_R-N_R	126.9 [b]	65.5
C_R-C_R-N_R	109.2	113.5
C_3-N_R-C_R	126.2 [c]	102.6
C_R-C_R-H_	130.0	45.3
N_R-C_R-H_	120.8 [d]	85.0
C_3-C_3-C_3	112.5	33.6
C_R-C_3-H_	113.4	88.3
H_-C_3-H_	109.5 [£]	72.7
N_R-C_3-H_	103.7	82.8
C_3-C_3-H_	108.5	77.1
C_3-C_3-N_R	113.2	252.9

[£] (Leach, 2001)

a = θ (N_R-C_R-N_R) = 540 – 2x θ (C_R-N_R-C_R) - 2x θ (N_R-C_R-C_R)

b = θ (C_3-C_R-N_R) = 180 – 0.5x θ (N_R-C_R-N_R)

c = θ (C_3-N_R-C_R) = 180 – 0.5x θ (C_R-N_R-C_R)

d = θ (N_R-C_R-H_) = 360 – θ (C_R-C_R-H_) - θ (C_R-C_R-N_R)

Table 3.8 :- Barrier height and multiplicity for torsions.

Parameters	V_n (kcal mol^{-1})	n
X_-C_R-N_R-X_	4.614	-2
X_-C_R-C_R-X_	2.710	-2
X_-C_3-N_R-X_	0.042	-6
X_-C_3-C_R-X_	0.167	-6
X_-C_3-C_3-X_	0.179	+3

Table 3.9 :- Optimised van der Waals hardness values for hydrogen and halides

Parameters	Vdw_H (kcal.mol^{-1})
$\varepsilon_{(H\_)}$	0.015
$\varepsilon_{(Cl\_)}$	0.283
$\varepsilon_{(Br\_)}$	0.370
$\varepsilon_{(I\_)}$	0.510

Table 3.10 :- Optimised van der Waals radii, r_m, for hydrogen and halides

Parameters	Vdw_r (Å)
$r_{m(H\_)}$	1.392
$r_{m(Cl\_)}$	1.816
$r_{m(Br\_)}$	1.586
$r_{m(I\_)}$	2.420

Table 3.11 :- Out-of-plane force constants

Parameters	k_{oop} (kcal.mol^{-1})
X-X-N_R-X	16.4
X-X-C_R-X	8.0

Table 3.12 :- Optimised van der Waals distance, R_m, for explicit interactions between halides and hydrogen.

Parameters	Vdw_R (Å)
$R_{m(Cl\_H\_)}$	2.934
$R_{m(Br\_H\_)}$	3.306
$R_{m(I\_H\_)}$	3.786

Table 3.13:- Atomic charge correction values for C_R, N_R and halides(e)

Parameters	Optimised Value
$Q_{(C\_R)}$	-0.0305
$Q_{(N\_R)}$	0.5457 *
$Q_{(Cl\_)}$	-1
$Q_{(I\_)}$	-1
$Q_{(Br\_)}$	-1

* calculated using equation 3.8

Table 3.14 :- Bond increments

Parameters	Optimised Value
INC(C_3-N_R)	-0.320
INC(C_3-C_R)	-0.078
INC(C_3_H_)	0.208
INC(C_R_H_)	0.328
INC(C_R_N_R)	-0.409

The fact that more energy is required to cause a bond to deviate significantly from its equilibrium value than is required to bend an angle or to twist around a bond is reflected in the magnitude of the force constants for bond stretching. That is, a higher value for bond stretching force constant as opposed to angle bending was obtained.

Comparing the stretch force constants listed in Table 3.6, the force constants of C_R-C_R and C_R-N_R are higher than the rest. This is because a higher energy is required to stretch or compress a double bond or resonant double bond, than that required for a single bond.

The reference bond lengths obtained can be compared with values from the MM2 force field. The values for the Imidazolium Ionic Liquid Force Field shows 1.96% deviation on C_R-C_3 bond, 0.91% deviation on C_3-C_3 bond and 1.66% deviation on C_R-C_R bond.

Comparing the out-of-plane bending force constants obtained in our optimisation, the value of nitrogen was observed to be higher than that of carbon. This indicates that aromatic carbon atoms are more sensitive to out-of-plane bending than nitrogen. That is, a higher out-of-plane energy is required to bend nitrogen in the ring than carbon. The reason for this is that, in all the molecules used in the training set nitrogen is always bonded to a methyl group while the aromatic carbons (especially those indicated by C(4) and C(5)) are bonded to lighter hydrogen atoms.

Higher torsional force constants are observed for bonds in which the central bond is C_R-N_R and C_R-C_R, which indicates that more energy is required to cause a rotation around those bonds. This is expected, because these two bonds are within the five membered ring and thus not easy to rotate.

3.6.2. Vibrational frequencies

All the optimised parameters were included in the force field definition file and the vibrational frequencies of the isolated cations were calculated. These vibrations were then compared with the *Gaussian98* calculated vibrations.

Results of these calculations are tabulated in Addendum C, along with the symmetry class and assignments. Also included in these tables are the absolute difference and percentage

deviation of the IILFF calculated vibrations from the *Gaussian98* calculated ones. In the tables the *Gaussian98* calculated frequencies are indicated by "Obs" and those calculated using the force field are indicated by "Calc".

Using this force field containing only the diagonal terms it is possible to calculate the vibrational frequencies to a maximum RMS deviation of 15% which was typically observed in the low frequency vibrations.

The high frequency vibrations calculated using this force field show a reasonable agreement with the *Gaussian98* calculated frequencies. Most of the large deviations are observed in the low frequencies; typically the methyl rocking frequencies were consistently calculated high by the IILFF. Also, those containing a combination of two or more vibrations were observed to give a deviated result. This is because no cross terms are included in the IILFF. Hence frequency fitting could be improved by including cross terms in the force field.

3.7. Force field implementation

The optimised parameters were implemented in Cerius^2, which contains a module for dynamics simulation using molecular mechanics. The performance of the force field was checked and the results were compared with the structures minimised using the Universal force field (UFF) (Rappe et al., 1992).

The calculation of partial charges in the crystals using the IILFF was done separately using the optimised bond increments and atomic charge correction value for the aromatic carbons, nitrogens and halides. The results are reported in section 3.7.2. The crystals with calculated partial charges were also optimised using the IILFF and compared with the experimental and UFF results in section 3.7.3.

3.7.1. Geometry of isolated cations

An isolated cation was prepared from each of the crystals used in the training set. The IILFF was used to assign the atom type of all the atoms in the cation, while the partial atomic charges on all the atoms were assigned using a script. Finally the isolated cations were

minimised using the IILFF. The same procedure was repeated but using UFF. The minimised structures obtained from these two force fields were compared with the quantum mechanically minimised structures.

An RMS deviation of the minimised isolated cations from the quantum mechanically calculated structures are tabulated in Table 3.15. Also a full list of these results is given in Addendum A, while selected bond lengths, bond angles and torsion angles are tabulated in Tables 3.16 to 3.19. The numbering in the headings columns in these tables indicate as follows 1 = Hartree-Fock 6-31(G)d results, 2 = IILFF results, 3 = UFF results.

Table 3.15 :- RMS deviation of distances and angles from the Gaussian98 calculated structures for isolated molecules measured using the IILFF and UFF

	RMS of distances (Å)		**RMS of angles (deg)**	
	IILFF	UFF	IILFF	UFF
DMIM	0.014	0.025	0.56	1.61
EMIM	0.018	0.024	0.86	2.12
DMEIM	0.020	0.022	0.81	1.73
DMPIM	0.024	0.022	1.11	1.65

As can be seen from the RMS deviation in Table 3.15 the IILFF showed better results especially in angle measurements than those of UFF. This improvement is observed to reduce as we go down the list from DMIM to DMPIM cations.

In all the cations the imidazole ring was observed to retain the geometry obtained from the experimental crystal structures. Results of the IILFF and Hartree-Fock calculations for the isolated DMIM cation showed a symmetrical molecule with C_{2v} symmetry, while the structure calculated using UFF showed a deviation from this symmetry. This is a good indication of the improvements of the IILFF from the UFF.

Except for a slight rotation the torsion angle showing the conformation of the methyl substituent was also observed to show a good fit. However a considerable deviation was observed when the methyl constituent was replaced by an ethyl or propyl group.

Using the IILFF which contains only the stretch, bend, torsion, out-of-plane and non-bonded interactions, a much better result was obtained. The deviation observed in the measurements could be further improved by introducing cross terms, like the bend-bend, bend-stretch etc. However this requires extra parameters to be optimised and was not included in this work.

Table 3.16 :- Selected bond lengths, bond angles and torsion angles of the 1,3-dimethylimidazolum cation calculated using Gaussian98 (1), IILFF (2) and UFF (3) and the difference of the last two from the Gaussian98 value (in Å and deg).

	1	2	3	1-2	1-3
N(1)-C(2)	1.315	1.324	1.348	-0.009	-0.033
N(1)-C(5)	1.378	1.361	1.349	0.017	0.029
N(3)-C(8)	1.467	1.469	1.459	-0.002	0.008
C(4)-C(5)	1.341	1.355	1.381	-0.014	-0.040
C(2)-N(1)-C(5)	108.0	107.8	106.4	0.2	1.6
N(1)-C(2)-N(3)	109.8	108.9	111.1	0.9	-1.3
N(3)-C(4)-C(5)	107.1	108.2	108.3	-1.1	-1.2
C(6)-N(1)-C(5)-C(4)	180.0	180.0	180.0	0.0	0.0

Table 3.17 :- Selected bond lengths, bond angles and torsion angles of the 1-ethyl-3-methylimidazolum cation calculated using Gaussian98 (1), IILFF (2) and UFF (3) and the difference of the last two from the Gaussian98 value (in Å and deg).

	1	2	3	1-2	1-3
N(1)-C(5)	1.378	1.362	1.349	0.02	0.03
N(1)-C(2)	1.314	1.327	1.350	-0.01	-0.04
N(1)-C(6)	1.477	1.451	1.460	0.03	0.02
N(3)-C(8)	1.466	1.468	1.461	0.00	0.00
C(5)-C(4)	1.342	1.355	1.380	-0.01	-0.04
C(5)-N(1)-C(2)	107.9	108.0	106.1	-0.1	1.8
C(2)-N(3)-C(4)	108.0	107.8	106.2	0.2	1.8
N(1)-C(2)-N(3)	109.9	108.0	111.1	1.9	-1.2
N(3)-C(4)-C(5)	107.0	108.1	108.3	-1.1	-1.3
C(2)-N(1)-C(5)-C(4)	0.1	0.9	0.3	-0.8	-0.2
C(6)-N(1)-C(5)-C(4)	178.9	179.7	179.0	-0.8	-0.1
C(2)-N(1)-C(8)-C(9)	104.9	67.2	67.9	37.7	37.0

Table 3.18 :- Selected bond lengths, bond angles and torsion angles of the 1,2-dimethyl-3-ethylimidazolum cation calculated using Gaussian98 (1), IILFF (2) and UFF (3) and the difference of the last two from the Gaussian98 value (in Å and deg).

	1	2	3	1-2	1-3
N(1)-C(2)	1.323	1.346	1.355	-0.023	-0.032
N(1)-C(5)	1.380	1.340	1.357	0.04	0.023
N(1)-C(6)	1.475	1.456	1.467	0.019	0.008
N(3)-C(8)	1.466	1.477	1.463	-0.011	0.003
C(4)-C(5)	1.336	1.352	1.380	-0.016	-0.044
C(2)-C(7)	1.495	1.502	1.504	-0.007	-0.009
C(5)-N(1)-C(2)	108.7	108.1	105.7	0.6	3.0
C(2)-N(3)-C(4)	108.7	107.8	106.0	0.9	2.7
N(1)-C(2)-N(3)	108.4	108.0	108.9	0.4	-0.5
N(3)-C(4)-C(5)	107.0	108.1	108.4	-1.1	-1.4
N(3)-C(8)-C(9)	112.2	111.2	110.6	1	1.6
C(5)-N(1)-C(2)-N(3)	-0.4	0.9	0.2	-1.3	-0.6
C(2)-N(3)-C(8)-C(9)	95.7	93.5	111.5	2.2	-15.8
C(6)-N(1)-C(2)-C(7)	2.1	0.4	0.9	1.7	1.2

Table 3.19 :- Selected bond lengths, bond angles and torsion angles of the 1,2-dimethyl-3-propylimidazolum cation calculated using Gaussian98 (1), IILFF (2) and UFF (3) and the difference of the last two from the Gaussian98 value (in Å and deg).

	1	2	3	1-2	1-3
N(1)-C(6)	1.475	1.464	1.467	0.011	0.008
N(1)-C(2)	1.323	1.345	1.356	-0.022	-0.033
N(1)-C(5)	1.380	1.339	1.35	0.041	0.030
N(3)-C(8)	1.466	1.477	1.463	-0.011	0.003
C(5)-C(4)	1.336	1.352	1.379	-0.016	-0.043
C(2)-C(7)	1.495	1.501	1.505	-0.006	-0.010
C(5)-N(1)-C(2)	108.7	108.2	105.7	0.5	3.0
C(2)-N(3)-C(4)	108.7	107.7	106.0	1.0	2.7
N(1)-C(2)-N(3)	108.4	108.0	111.2	0.4	-2.8
N(3)-C(4)-C(5)	107.0	108.1	108.4	-1.1	-1.4
N(1)-C(8)-C(9)	112.4	112.9	111.5	-0.5	0.9
C(10)-C(9)-C(8)	111.3	115.2	112.2	-3.9	-0.9
C(10)-C(9)-C(8)-N(3)	178.9	80.6	54.1	98.3	124.8
C(2)-N(3)-C(5)-C(4)	-0.1	0.0	-0.1	-0.1	0.0
C(9)-C(8)-N(3)-C(2)	95.5	93.3	81.3	2.2	14.2

3.7.2. Partial charges

Results of the calculation of partial atomic charges on the atoms in the isolated cations are tabulated in Table 3.19 along with those partial charges calculated using *Gaussian98*.

The partial atomic charges on nitrogen (N(1) and N(3)) calculated for imidazolium structures containing hydrogen attached to C(2) show good agreement with the results obtained from *Gaussian98,* a maximum deviation of ± 0.005 being observed. A deviation of about ± 0.04, was observed for those cations containing a methyl group at position C(2). A deviation from the *Gaussian98* calculated partial atomic charges was also observed for C(8). This deviation was observed to diminish as a longer chain such as a propyl group, was used.

This deviation is because, unlike the Mulliken charge assignment, the force field charge assignment is based on bond increments and hence they are completely dependant on the types of atoms attached to that particular atom. For example, in all the cations the partial charge of nitrogen could not be expected to change greatly because the types of atoms attached to it are the same for all cases.

A higher partial atomic charge assignment was observed for the C(2) than the other two sp^2-hybridised carbon atoms, which indicates high localisation of charge. The partial atomic charge assignment of C(7) was also observed to differ from the other sp^3-hybridised carbons of the cation.

Partial atomic charges on hydrogen attached to the sp^2-hybridised carbons (C(4) and C(5)) were calculated to be 0.3279, while those attached to the sp^3-hybridised carbons (C(6) to C(10)) gave values of 0.2082. This is because charge assignment in IILFF is done based on bond increments and atomic charge correction values and the difference observed in this context is expected as the two hydrogen atoms are bonded to two different atom types.

The same partial atomic charge assignment of the nitrogen atoms of the ring was observed, while those calculated using *Gaussian98* were observed to give two types of partial atomic charge assignment for the two sets of imidazolium cations (those containing hydrogen attached to C(2) and those containing sp^3-hybridised carbon atoms) (see Table 3.20). Also a

higher partial atomic charge was calculated for the sp^3-hybridised carbon atoms (C(2), C(4) and C(5)) using the IILFF.

This deviation could be improved by assigning a different atom type to the aromatic carbon indicated by C(2) in Fig 3.1, because in this force field the same atom type was given to all the carbon atoms in the aromatic ring. Further improvement could also be attained by modifying the assumption taken when formulating the atomic charge correction parameters (refer subsection g of section 3.4.2). That is, the atomic charge correction parameter of the C(2) should be considered different from the C(4) and C(5).

Table 3.20 :- Comparison of charges in isolated imidazolium cations calculated with IILFF and with the Hartree-Fock 6-31G(d) basis set

Atom			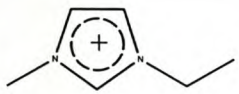		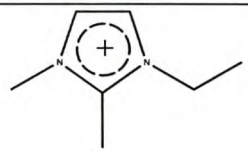		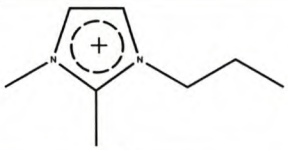	
	Q (IILFF)	**Q (HF)**	**Q (IILFF)**	**Q (HF)**	**Q (IILFF)**	**Q (HF)**	**Q (IILFF)**	**Q (HF)**
N(1)	-0.5916	-0.5868	-0.5916	-0.5873	-0.5916	-0.6346	-0.5916	-0.6426
N(3)	-0.5916	-0.5868	-0.5916	-0.5894	-0.5916	-0.6427	-0.5916	-0.6435
C(2)	0.4586	0.4094	0.4586	0.4104	0.7090	0.6941	0.7090	0.6943
C(4)	0.0501	0.0238	0.0501	0.0247	0.0501	0.0219	0.0501	0.0211
C(5)	0.0501	0.0238	0.0501	0.0219	0.0501	0.0200	0.0501	0.0208
C(6)	-0.3042	-0.3148	0.3042	-0.3144	-0.3042	-0.3191	-0.3042	-0.3189
C(7)	-	-	-	-	-0.5471	-0.5636	-0.5471	-0.5637
C(8)	-0.3042	-0.3148	-0.0960	-0.1604	-0.0960	-0.1651	-0.0960	-0.1490
C(9)	-	-	-0.6246	-0.4963	-0.6246	-0.4937	-0.4164	-0.3246
C(10)	-	-	-	-	-	-	-0.6246	-0.5026
H	0.3279	0.3050	0.3279	0.3100	0.3279	0.2900	0.3279	0.2900
H*	0.2082	0.2433	0.2082	0.2225	0.2082	0.2282	0.2082	0.2169

H = Charge of hydrogen attached to sp^2-hybridised carbon (average value)

H* = Charge of hydrogen attached to sp^3-hybridised carbon (average value)

IILFF = Imidazolium Ionic Liquid Force Field

HF = Hartree-Fock 6-31G(d) basis set

3.7.3. Geometry of crystals

Using the partial atomic charges assigned as described in section 3.7.2, a unit cell of each of the crystals mentioned in section 3.2 was minimised systematically using the IILFF. First the light atoms of the crystal were minimised, keeping all the heavy atoms and the cell parameters constant. This was followed by minimising all the atoms of the crystal keeping the cell parameters constant. Finally, the whole crystal was minimised together.

The RMS deviations of the minimised crystals from the experimental crystals were compared with the crystals minimised using the same procedure but with UFF. The results are tabulated in Table 3.21.

Table 3.21 :- RMS deviation of atomic coordinates of crystals minimised using the IILFF and UFF from the experimental crystals.

	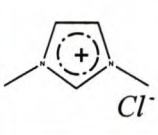	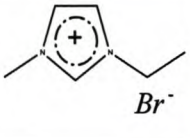	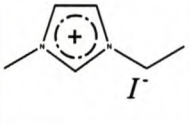	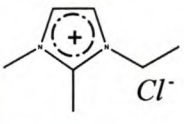	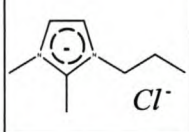
IILFF	0.4877	0.6755	0.5841	1.2210	1.567
UFF	1.4620	2.2614	0.8275	0.7987	1.073

As can be seen from the RMS deviation, the IILFF shows an improvement over UFF for 1,3-dimethylimidazolium chloride, 1-ethyl-3-methylimidazolium bromide and 1-ethyl-3-methylimidazolium iodide. However, the RMS deviation indicates that UFF gave better results for 1,2-dimethyl-3-ethylimidazolium chloride and 1,2-dimethyl-3-propylimidazolium chloride.

A closer look shows that those crystals with imidazole based cations containing hydrogen attached to C(2) give good results, but where this hydrogen is replaced by a methyl group the RMS value indicates that the structures deviate considerably from the experimental structure.

Details of the unit cell parameters obtained from CSD, optimised using IILFF and UFF are tabulated in Table 3.22.

A better result was obtained for 1,3-dimethylimidazolium chloride and 1-ethyl-3-methylimidazolium bromide when the IILFF was used. Both force fields, IILFF and UFF were observed to give an acceptable result for 1-ethyl-3-methylimidazolium iodide. Results of the UFF for optimisation of 1,2-dimethy-3-ethylimidazolium chloride gave a much better result than those of the IILFF minimised structure.

Table 3.22 : Cell parameters of the crystal unit cell from CSD, minimised using the IILFF force field and UFF

	 Cl^-			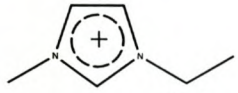 Br^-			 I^-			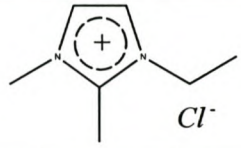 Cl^-		
	CSD	**IILFF**	**UFF**	**CSD**	**IILFF**	**UFF**	**CSD**	**IILFF**	**UFF**	**CSD**	**IILFF**	**UFF**
A	8.652	8.785	10.845	8.749	8.600	8.294	8.789	8.565	9.720	6.213	6.679	6.143
B	7.858	8.049	8.359	7.999	8.636	7.261	8.130	8.012	8.425	19.421	16.429	18.139
C	10.539	10.195	10.836	12.662	12.750	14.465	13.364	13.532	13.130	8.903	8.239	8.875
α	90	90	90	90.0	90.0	90.0	90.0	90.0	90.0	90.0	90.0	90.0
β	106.3	108.8	126.8	109.9	109.0	114.0	107.3	113.7	106.3	124.6	105.2	121.6
γ	90	90	90	90.0	90.0	90.0	90.0	90.0	90.0	90.0	90.0	90.0

Chapter 4 :- Molecular Dynamics Simulation

4.1. Introduction

In this chapter the IILFF is used to study the molecular dynamics simulation of the melting process of ionic liquids. General principles used when simulating the melting process of imidazole based ionic liquids are given. In the actual computational experiment only the dynamics simulation of 1,3-dimethylimidazolium chloride is performed and the results are given and discussed.

Details of the crystal preparation for dynamics simulation are discussed in section 4.2. In this section two main concepts are discussed. These are the size of the simulated crystal and number of molecules used for the dynamics simulation and the implementation of the IILFF in the Cerius^2 v 3.8. In section 4.3 the time integration algorithms used by the program, Cerius^2 are introduced. Running a dynamics simulation is discussed in section 4.4, where the detailed experimental procedure used when performing the two types of dynamics simulations is given and their results are discussed. Simulating a defective crystal is discussed in section 4.5, where a crystal with five cations less is simulated. The results of the dynamics simulation is discussed and concluded.

4.2. Crystal preparation for dynamics simulation

4.2.1. Building the crystal

The crystal structure of 1,3-dimethylimidazolium chloride was determined at 203 K by Arduengo, (1992). This unit cell of this crystal shows that it contains four 1,3-dimethylimidazolium cations and 4 chloride anions. The unit cell parameters, R-factor and density are mentioned in Table 3.1.

There are several important concepts that should be considered before any simulation is performed. First is the source of the initial configuration (structure) of the system to be used. This starting structure must have a reasonable conformation and be energy minimum. In this dynamics simulation the above mentioned crystal structure obtained from the CSD was used.

The second important step is to decide on the number of particles (or molecules) that should be included in the simulation box. Other dynamics simulations summarised in chapter two were found to use 192 molecules in their model cell. Typical examples of these are the work of Gavezzotti (1999) and Hank, Price and Cynden-Bell (2001), that both used 192 molecules in their model cells.

For this work, it was thus decided to start with 192 imidazolium cations and 192 halide anions. This was done by adding unit cells together until the required number of molecules in the crystal was reached.

A crystal super-lattice containing this number of molecules was constructed for 1,3-dimethylimidazolium chloride by a 4 x 4 x 3 repetition of the unit cell. The cell parameters for the crystal super lattice were found to be much larger than those previously described in the literature, thus performing a dynamics simulation experiment with such a large crystal cell would be expensive computationally. Hence an alternative crystal super lattice was prepared, which consists of a smaller number of molecules. Another dynamics simulation performed by Kung, Books, Freeman et al., (1996) used a cell consisting of 32 benzene molecules. Thus a crystal consisting of 32 imidazolium cations and 32 chloride anion was constructed by a 2 x 2 x 2 repetition of the unit cell. These two crystal cells are illustrated in Fig 4.1.

Cell parameters of the crystal supper lattice in a dynamics simulation were checked so that the smallest side of the model cell is greater than the longest non-bonded interactions observed in the unit cell. If this was not taken into account the long non-bonded interactions would not be included in the calculation.

Periodic boundary conditions were applied to ensure that the molecules near the borders of the original box experience similar interactions to the molecules in the centre. This also allows the calculation of all properties using a relatively small number of particles.

4.2.2. Adaptation of the force field

The IILFF was implemented in Cerius^2. Using this force field the atom types of all the atoms used in the molecules of the crystal were calculated and partial atomic charges were also assigned. This force field was then used to calculate the intra-molecular and inter-molecular interactions during the dynamics simulation.

Before the dynamics simulation commenced, the IILFF was used to minimise the crystal structure, using a stepwise minimisation technique discussed in section 3.7.3.

The first step, the pre-minimisation of the crystal, is an important step because it ensures that the initial configuration does not contain any high-energy interactions, which can cause instability in the simulation.

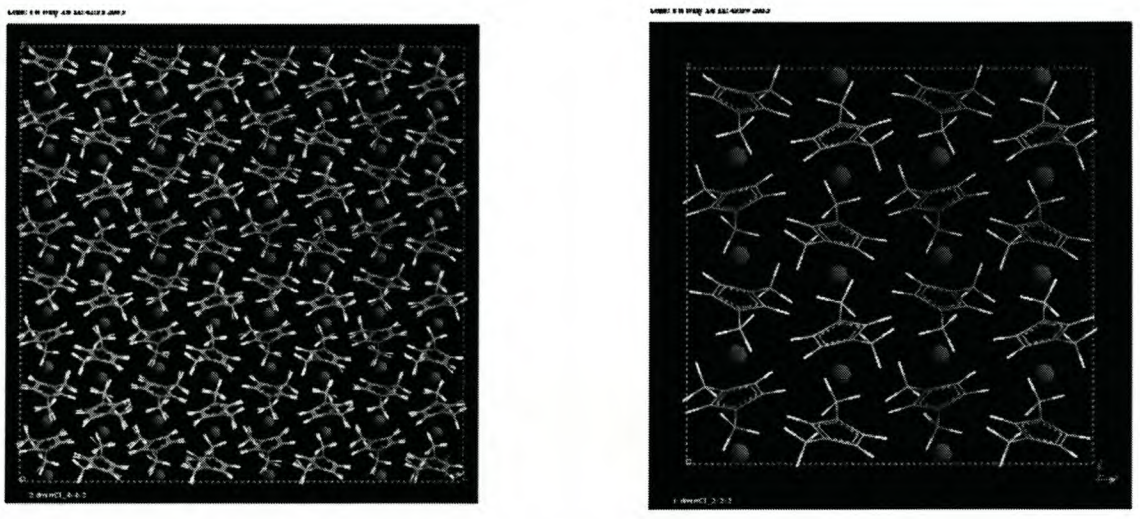

Fig 4.1 :- (a) 4 x 4 x 3 crystal structure (b) 2 x 2 x 2 crystal structure of 1,3-dimethylimidazolium chloride

4.3. Dynamics time step

In Cerius^2 the velocity Verlet algorithm and the leap-frog algorithm discussed in chapter 2 were used to update the atom coordinates, r, and velocities, v. For the first step of the dynamics simulation the program uses a single point velocity Verlet algorithm and for the subsequent steps the leap-frog formula was used.

The equations to determine the positions and velocities are equations 2.22 and 2.23 for the velocity Verlet algorithm and equations 2.26 and 2.27 for the leap-frog algorithm. In those equations δt is the time step (in ps), which is given in the input. In the dynamics experiment this value was taken to be 0.001ps.

4.4. Running the dynamics simulation

When simulating the mechanism by which solids and liquids inter-convert, the melting part is computationally inexpensive because it can easily be attained by moderate overheating of the system. The time scale of crystallisation, on the other hand, is almost prohibitive even with modern computational resources. Hence in this work the focus is on the melting.

The temperature of the system was increased gradually until the temperature of the ensemble passed the experimental melting temperature of the ionic liquid. For example, the experimental melting temperature of 1,3-dimethylimidazolium chloride is 398 K (Fennin, 1984) or 397.5 K (Wilkes, 1982), however it is difficult to reproduce the experimental melting temperature in a computational simulation for a number of reasons. A typical problem is the adequacy of the potential used to simulate the interactions. Hence the system was heated beyond the experimental melting temperature.

There are several possible dynamics methods available in Cerius^2, which were briefly described in chapter 2, section 2.5.4. An NPT ensemble was used in this work to simulate the melting process of the 1,3-dimethylimidazolium chloride.

In Cerius^2, the temperature of the system is handled in three different ways. Of these, the T_Damp method of Berendsen (Berendsen et al., 1984) was chosen (default selection). This method is very similar to the other two methods, Nose (Nose, 1984) and Hoover (Hoover, 1985), which are available in Cerius^2. This method performs constant temperature dynamics through weak coupling to a thermal bath via the damping time constant "Relaxation time". Relaxation time was referred to in chapter 2 as the coupling constant. This gives an indication of how strongly the system is coupled with the heat bath.

The T_Damp method controls the temperature of the system (increases or decreases the temperature) by multiplying the existing velocities of the systems by a constant, λ (refer to equation 2.28). This constant, λ, is calculated from the current temperature of the system at time t, the target temperature and coupling parameters, τ.

In this simulation the pressure of the system is also constrained to 1 atm by coupling to an external pressure bath.

In this work the temperature of the crystal was increased in two ways. Firstly the temperature of the system was increased step-wise with the aid of a script and the second method uses the generic annealing dynamics method for only one cycle to increase the temperature of the system. The advantages and disadvantages of these two methods are discussed below.

4.4.1. Running the dynamics simulation from a script

In this method an ordered 4 x 4 x 3 crystal box minimised using the IILFF was used as starting point. The temperature of the system was increased in different temperature increments.

First a dynamics simulation was carried out starting from an un-equilibrated system. A script that can sequentially increase the temperature of the system from 300 K to 500 K in 50 K increments was used. The temperature versus dynamics time profile showed a sudden jump in the temperature of the system from 300 K to 500 K in the first dynamics step despite the fact that only a 50 K increment is given. This problem was also observed in the subsequent increments. That is, the required change in temperature, ΔT, could not be attained. A plot of temperature versus time-step results of this dynamics simulation is given in Fig 4.2.

A possible reason for this behaviour is that we started from an un-equilibrated system. Hence in the second experiment, the system was equilibrated initially, at an equilibration temperature of 300 K. Then the temperature of the system was increased from 300 K to 500 K in 50 K increments.

Unfortunately, the problem persisted. It thus appears that the main reason for these deviations is the re-initialisation of the velocity every time the temperature of the system is incremented, which could not be avoided by using this method. Therefore, it was decided that we perform generic annealing dynamics and see if we can simulate the required increment in the temperature of the system.

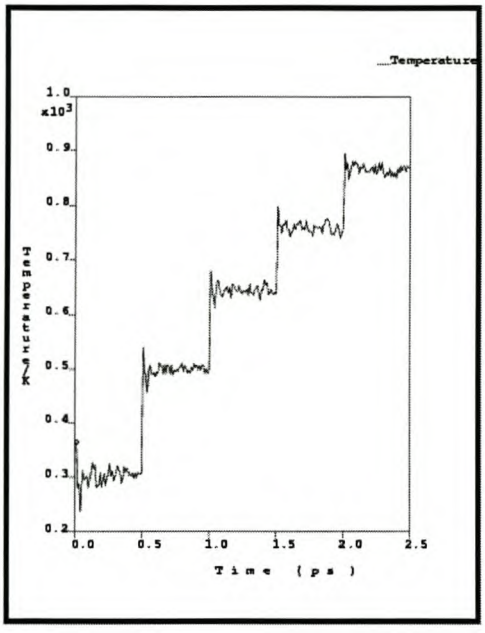

Fig 4.2 :- Temperature increment of an NPT dynamics for a 4 x 4 x 3 crystal heated from 300K to 500K in 50K increment.

4.4.2. One cycle of generic annealing dynamics

Annealing dynamics simulations work by incrementing the temperature of the crystal to the mid-cycle temperature and then decrementing to the initial temperature. This cycle can be repeated as required, but for this work only one cycle was considered, since we are not interested in the real annealing dynamics but are using it to increase the temperature of the system. In particular, attention was paid to the first part of this cycle, i.e., the melting process. This is primarily because we are interested in the melting process of the crystal, but also because the time-scale of crystallisation is almost prohibitive. An obvious disadvantage of this method is that only half of the data thus obtained will be used.

In annealing dynamics, the temperature of the system is changed by adjusting the kinetic energy of the atoms, i.e., by scaling the velocities of the atoms. At the end of each

temperature step, the lowest energy structure of that step is taken and saved in a trajectory. The dynamics then continues using the structure and velocity from the previous step.

Annealing dynamics were performed on a 4 x 4 x 3 crystal and a 2 x 2 x 2 crystal. In the annealing dynamics experiment the number of cycles, initial temperature, mid-cycle temperature, temperature increment and steps of dynamics per increment need to be specified. In this work, several annealing experiments were done and the details of these are given in Table 4.1.

In this study we did not start with a very large crystal and very long dynamics time. Instead the 4 x 4 x 3 starting crystal mentioned previously and small time step were selected to get a rough idea of how computationally intensive the simulation will be. Thus in the first dynamics simulation we started with a small number of dynamics cycles per increment, which was increased in later experiments.

Generally the initial temperature and mid cycle temperature of the system were taken to be 300 K and 500 K respectively. A full description of the different one cycle annealing dynamics simulations is given in Table 4.1 while the details are discussed below.

Table 4.1 : Annealing dynamics experiments

	Exp 1	**Exp 2**	**Exp 3**	**Exp 4**	**Exp 5**	**Exp 6**
Cell	4 x 4 x 3	4 x 4 x 3	4 x 4 x 3	2 x 2 x 2	2 x 2 x 2	4 x 4 x 3
Initial temperature (K)	300	300	270	300	250	300
Mid cycle temperature (K)	500	500	320	500	400	500
Temperature increment (K)	50	50	10	20	20	20
Steps of Dynamics/increment	100	500	500	5000	5000	5000

4.4.2.1. Trial one cycle annealing dynamics simulations

To see if the required increase in the dynamics temperature could be attained using this method, we simulated a 4 x 4 x 3 crystal which was heated from 300 K to 500 K in 50 K increments.

The result of this simulation showed a continuous increase of the dynamics temperature from 300 K to 500 K and then back to the starting temperature. The temperature versus time step profile is given in Fig 4.3. The dynamics time step given is very small so that the system could not stabilise during these temperature steps. It is very important for a dynamics simulation that the molecules have enough time to equilibrate at each temperature increment to attain the lowest energy possible at those specific temperatures.

This experiment, however, proved that annealing dynamics can reproduce the temperature increments specified in the input.

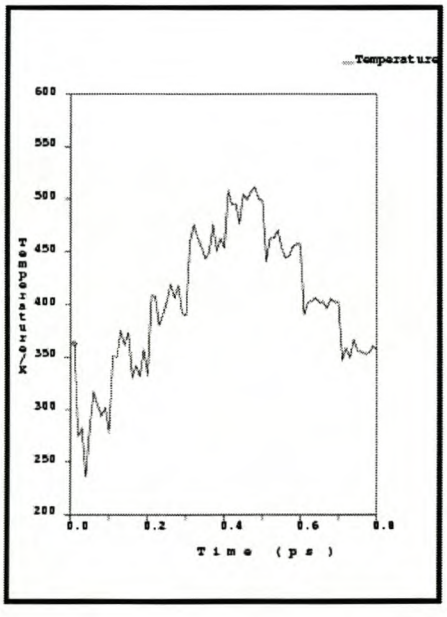

Fig 4.3 : An annealing dynamics run for a 4 x 4 x 3 crystal structure with parameters as indicated in Exp 1 in Table 4.1

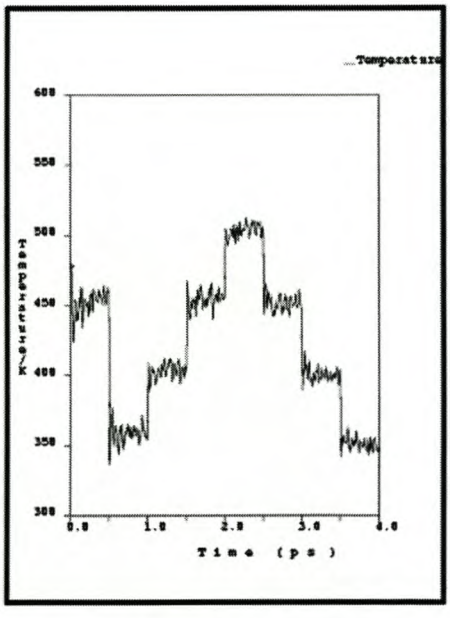

Fig 4.4 : An annealing dynamics run for a 4 x 4 x 3 crystal structure with parameters as indicated in Exp 2 in Table 4.1

In the second experiment (Exp 2), which is similar to Exp 1, more dynamics time per increment of 500 ps were considered. The results of this dynamics simulation shown in Fig 4.4 show a jump of the simulation temperature from 300 K to 450 K directly after the dynamics started. In order to study this effect more closely another dynamics simulation given by Exp 3 in Table 4.1 was performed. In this case we lowered the initial temperature and decreased the temperature increment to 10 K. However the jump in the temperature of the system as observed in Exp 2 occurred again.

The 500 dynamics steps per increment specified in Exp 2 is equivalent to 4 ps which is very small for a dynamics simulation. Hence we simulated a dynamics simulation with a higher dynamics time step per increment, in which case we used a smaller crystal cell, a 2 x 2 x 2 crystal, so that we could see how intensive the simulation will be.

4.4.2.2. 2 x 2 x 2 dynamics simulation with 100 ps run time

Most of the dynamics simulations reviewed in the literature use a minimum run time of 100 ps. Based on this we decided to simulate an experiment with a run time of 100 ps (50 ps for melting and 50 ps for crystallisation) on a 2 x 2 x 2 crystal. The simulation temperature was warmed up from 300 K to 500 K in steps of 20 K.

Fig 4.5 shows the time evolution of temperature for the whole dynamics simulation. The output temperature was observed to correspond, with about 5-6% fluctuation, to the temperature imposed in the input, except in the range of 2 ps to 13 ps, where the temperature of the system jumped suddenly to a temperature of 400 K and then dropped back to 375 K and stayed at this temperature for some time.

This sharp increase in temperature observed in Exp 4 happened at an early stage of the dynamics simulation. This deviation could be due to starting from an un-equilibrated system. To check if this jump is correct we simulated an identical dynamics simulation with a lower starting and mid-cycle temperature. The details of this dynamics simulation is given by Exp 5 in Table 4.1.

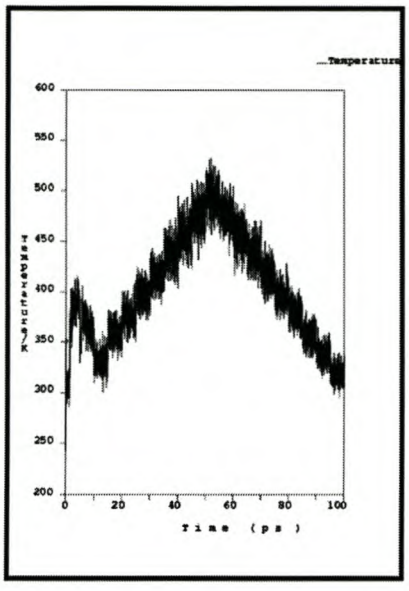

Fig 4.5 : Temperature vs time step profile for an annealing dynamics run of a 2 x 2 x 2 crystal structure explained in Exp 4 of Table 4.1. The warm up rate is about 4K/ps.

Since we are dealing with an identical crystal and we are using the same experimental details, it was expected that we would see a jump in temperature at the same range observed in Exp 4 above. But this jump was observed to occur at the beginning of the dynamics simulation, which convinced us that the sharp increase in temperature observed in Exp 4 is an artefact and not a true melting.

The reason for this could be the size of the crystal used for the dynamics simulation. Hence we did a separate dynamics simulation with the 4 x 4 x 3 crystal size.

4.4.2.3. 4 x 4 x 3 dynamics simulation with 100 ps run time

In an attempt to obtain a better result by increasing the number of molecules included in the crystal box to 192 molecules, a 4 x 4 x 3 repetition of the unit cell was constructed. Other than the simulation cell parameters (number of molecules included in the unit cell) all other details are identical to that of the 2 x 2 x 2 simulation given in Exp 4, section 4.4.2.2. Details of this dynamics experiment are given by Exp 6 in Table 4.1. The total temperature change in the annealing dynamics run performed in this experiment is 400 K (200 K for melting and 200 K

for crystallisation) in 100 ps, which corresponds to a 4 K increase in the simulation temperature at each time step (1 ps). The results of this dynamics simulation are given and discussed below.

Temperature

The temperature profile given in Fig 4.6 shows a deviation at the beginning of the dynamics simulation but this is ignored as we started from an un-equilibrated crystal structure. An interesting result was observed at 15 ps, where a sharp increase in the dynamics temperature from 340 K to 380 K was observed. This result can be seen well from Fig 4.6(b) where a block average of the temperature versus time is given for the first 25 ps only. After 15 ps the system should have increased 60 K above the starting temperature, 360 K, while for the rest of the simulation the temperature observed agrees with the value imposed.

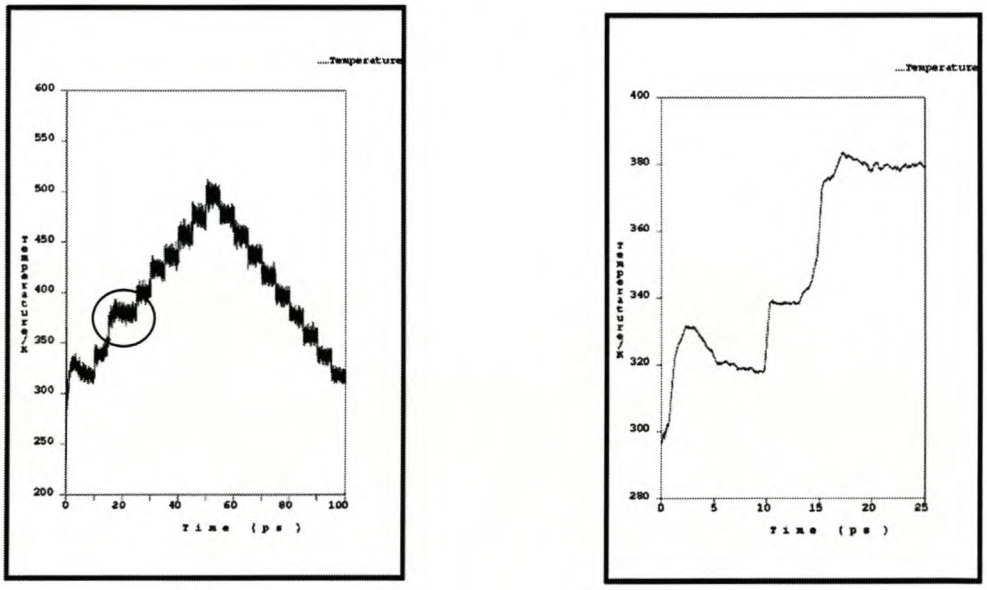

(a) (b)

Fig 4.6 : (a) temperature profile of an annealing dynamics simulation for a 4 x 4 x 3 crystal with a 100 ps run (b) block average of temperature versus time for the first 25ps (warm up rate of the system is about 4K/ps).

Density and volume

The volume and density profiles of the dynamics simulation are shown in Fig 4.7. The results are as expected, because there is an inverse relationship between these two terms and for a

crystal melting an increase in the volume and decrease in density is expected. An important point here is the sharp increase in the volume (or decrease in density) of the system observed in the vicinity of 10 ps to 15 ps, which coincides with the increase in temperature observed above.

The increase in the volume of the crystal structure during the warm up process did not correspond to a uniform increase in the parameters of the crystal cell. For example, the a and b axes were observed to increase by 2.6 % and 11.4 % respectively, while c decreased by 7.1 % when the system attained a temperature of 385 K. The large change observed along the b axis is due to the reduction in hydrogen bonding that exists between a ring hydrogen and the chloride anion, where the chloride anion is displaced along the b direction. The chloride-hydrogen interaction along the a direction is minimal compared to the other two directions and hence we don't expect a large displacement of atoms to occur along this direction. A slight deviation was also observed in the α angle. Cell parameters for the whole dynamics simulation are given in Fig 4.8.

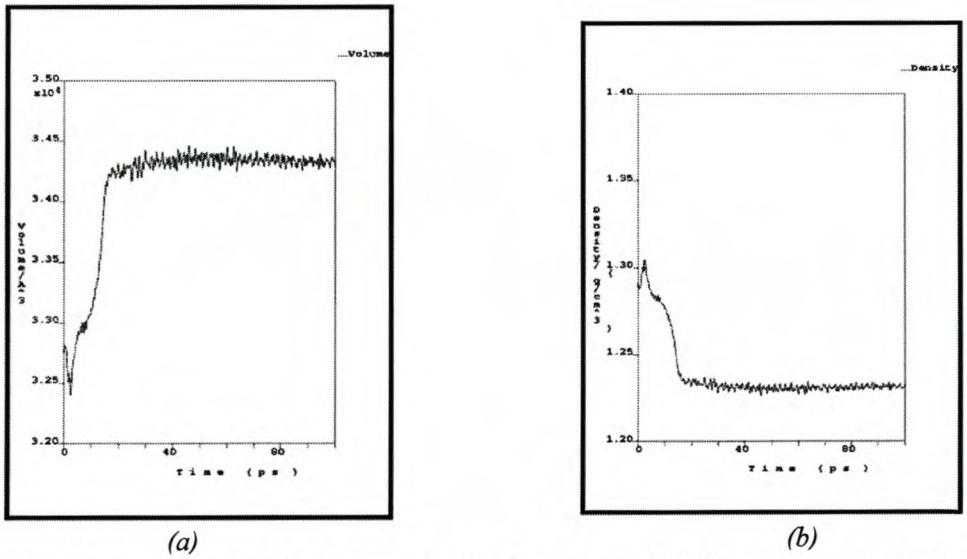

(a) (b)

Fig 4.7 : (a) volume and (b) density profiles for an annealing dynamics simulation for a 4 x 4 x 3 crystal.

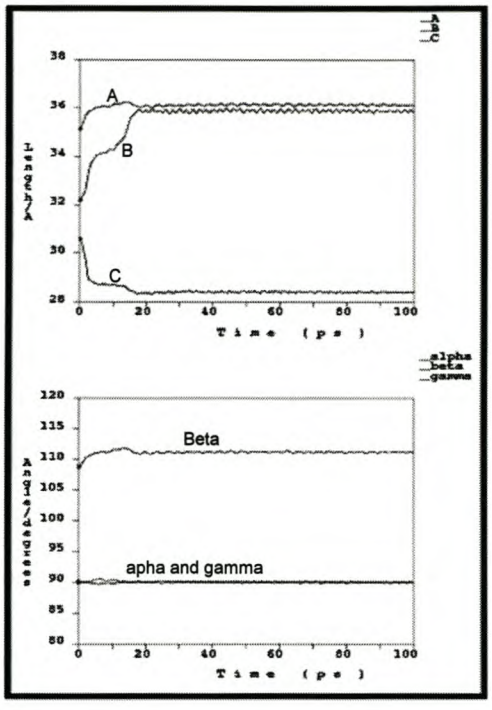

Fig 4.8 : Cell parameters for the whole annealing dynamics simulation for a 4 x 4 x 3 crystal.

Bond lengths, angles and torsion angles

The radial distribution function (RDF) of bond lengths between different atom types was calculated. Fig 4.9(a) shows the distances between sp^2-hybridised carbons in the imidazolium cation (indicated by C(2), C(4) and C(5) in Fig 3.1). The RDF of this parameter gives just two intense peaks during the whole dynamics simulation. The first one, which appears at 1.4 Å, corresponds to the bonded aromatic carbon atoms (C(4)-C(5) distance) while the second peak, which appears at 2.1 Å, is for the bonds between C(2)-C(4) and C(2)-C(5). In the crystal structure minimised using the IILFF the distance between C(4) and C(5) was observed to be 1.33 Å and that of C(2)-C(4) and C(2)-C(5) is 2.1 Å.

The major peak observed in Fig 4.9(b) indicates a bond between an aromatic nitrogen and sp^3-hybridised carbon, which are represented by N(1)-C(6) or N(3)-C(8), while the second small peak could be for distances between N(1)-C(8) or N(3)-C(6). Fig 4.9(c) also shows an intense peak which corresponds to a distance between an aromatic nitrogen and an aromatic carbon, which are represented by N(1)-C(2), N(1)-C(5), N(3)-C(2) and N(3)-C(4).

From these results one can conclude that the bond lengths in the imidazole based ionic liquids are insensitive to temperature, because in the full dynamics simulation no significant change was observed.

Analysis of bond bending and torsional motions indicates that the 1,3-dimethylimidazolium residue maintains a rigid structure. As becomes evident from some selected angles summarised in Table 4.2 and 4.3, no significant deformation of the intra-molecular bond angles was observed throughout the simulation. The attached methyl groups were observed to remain in an undistorted tetrahedral arrangement.

Table 4.2 : selected angles of the imidazolium cation and their variation during the simulation

Angles	Bond Angle (deg)
N(1)-C(2)-N(3)	108.79 ± 0.09
C(2)-N(3)-C(4)	108.22 ± 0.09
N(3)-C(4)-C(5)	107.66 ± 0.09
C(4)-C(5)-N(1)	106.96 ± 0.09
C(5)-N(1)-C(2)	107.63 ± 0.09
Total internal angles	**539.26**

Table 4.3 : selected torsion angles of the imidazolium cation and their variation during the simulation

Torsions	Torsion Angle (deg)
C(6)-N(1)-C(2)-N(3)	176.9 ± 0.3
C(8)-N(3)-C(4)-C(5)	175.6 ± 0.3

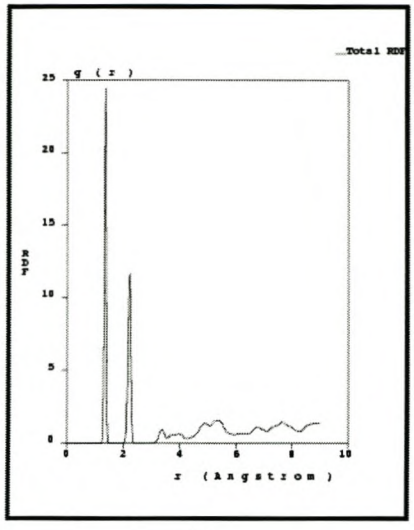

(a)

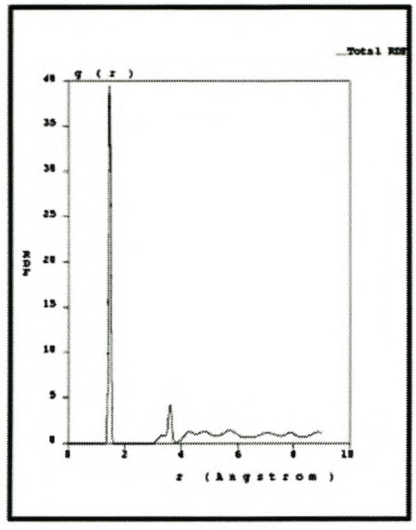

(b)

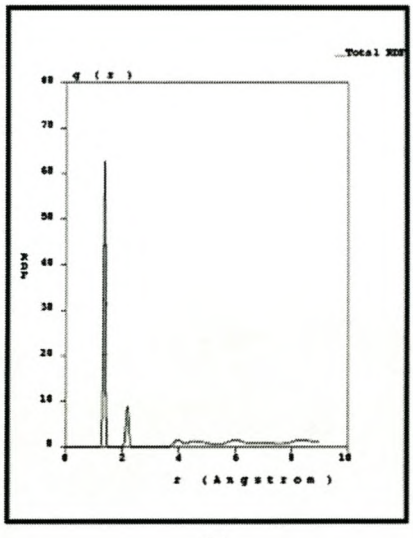

(c)

Fig 4.9 : RDF vs distance in Å for bond lengths during the annealing dynamics experiment on a 4 x 4 x 3 crystal structure given by Exp 4 in Table 4.1. Distance between (a) sp^2-hybridised carbons (b) nitrogen and sp^3-hybridised carbons (c) nitrogen and sp^2-hybridised carbons.

Hydrogen bonding

In order to extract information about the hydrogen bonding in the crystal structure throughout the dynamics simulation we calculated the radial distribution function (RDF) for a distance between chloride anion and hydrogen atom of the cation. Except for a change in the intensity

of the peak no significant shifting in the distance between these two atoms was observed. This tells us that the breaking of hydrogen bonds did not occur during the dynamics simulation.

This phenomenon is very important when studying the melting process of crystals. That is, we were expecting hydrogen bond breaking and hence a shift towards a longer distance between the hydrogen atom of the cation and chloride anion, which did not happen at all.

4.5. Defective crystal

To see if a defective crystal gives good results, a 4 x 4 x 3 crystal box was prepared by removal of five imidazolium cations chosen at random. The position of all other 187 imidazolium cations and 192 chlorides were left unchanged. The system was then warmed up from 300 K to 480 K in steps of 20 K, running at 5000 steps at each temperature increment.

The effect of the removing the five cations on the structural evolution of the system was seen quickly. The density of the system was observed to decrease suddenly right after the start of the simulation at 5 ps and ends quickly. The other parameters like potential energy and kinetic energy and intra molecular measurements gave similar results to those of the ordered crystal. No variation in the hydrogen bonding distance was observed in this simulation.

A comparison of the frames at 15 ps for the perfect and defective crystals confirms that the disorder of the defective crystal starts earlier than that of the perfect crystal. Some molecules are even observed to move out of the crystal cell.

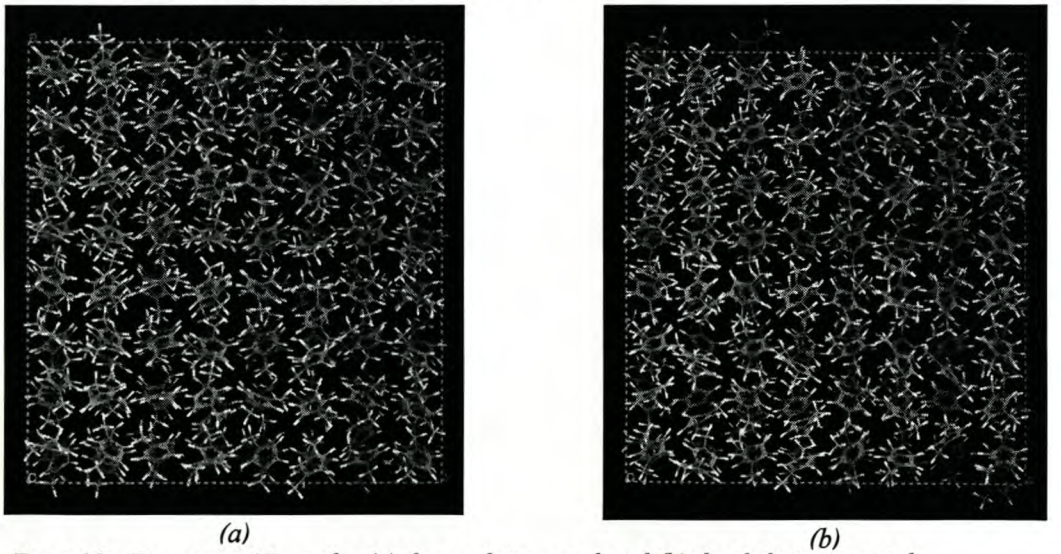

(a) (b)

Fig 4.10 : Frames at 15 ps for (a) the perfect crystal and (b) the defective crystal

The crystal disorder observed in both the perfect and defective crystals even at the highest temperature of the system is not enough to confirm the occurrence of melting. In particular, the shifting of the chloride anion of the crystal was minimal and can be ignored.

There are several reasons associated to this, some of which are: the time step considered could be too short, the lowest temperature increment (ΔT) considered is 20 K, which could be too large, and the efficiency of the force field parameters in simulating the non-bonded interactions is not good enough.

With the limited time available a dynamics simulation using a large time step was not possible. The other option that could be tried is optimisation of the force field parameters which would require more experimental data.

Chapter 5 : Conclusion

Important results obtained during development of the imidazolium ionic liquid force field can be summarised as follows.

- Reviewing the literature on modelling the imidazololium based ionic liquids revealed the importance of using accurate intermolecular interaction parameters. Those force fields developed for dynamics simulation were observed to use simple potential energy functions, because they need to be evaluated a large number of times during the simulation. Also all the literature reviewed on dynamics simulation of ionic liquids were observed to use molecular mechanics force fields due to the computational effort required to simulate such liquids quantum mechanically.

- Results from the calculation of partial atomic charges using *Gaussian98* can be summarised as follows: All imidazolium cations containing hydrogen atoms attached to C(2) show similar partial atomic charge assignments and those cations containing an sp^3-hybridised carbon attached to C(2) show a different set of charge assignment. This result indicates the difference that exists between these two sets of imidazolium cations. Partial atomic charge assignments of the sp^3-hybridised carbon atom attached to C(2) were observed to deviate from carbon atoms attached to nitrogen (N(1) and N(3)).

- The Imidazolium Ionic Liquid Force Field (IILFF) was developed by optimising the parameters of the force field based on the structural, vibrational and partial atomic charge data calculated using *Gaussian98* and the force field was successfully tested against the experimental structures.

- Optimisation of the force constant parameters was observed to give stretch force constants with higher values than those of the bend and torsion constants. Furthermore, the stretch force constants of the resonant double bonds, i.e., C_R-C_R and C_R-N_R are larger than for others. Referring the MM2 force field (Allinger, 1977) for stretching and bending force constants the IILFF stretch force constants for an sp^3-hybridised carbon atoms and sp^2-hybridised carbon atoms was observed to give an acceptable fit. But that between the sp^2-hybridised carbon atoms was observed to deviate slightly. Also a good agreement was

observed for angle bending force constant of C_R-C_3-C_3. A good fit with MM2 was also observed for reference bond lengths.

- The fitting of the vibrational frequencies calculated using IILFF was accurate for the higher frequencies. However, those vibrations that combine more than one frequency, especially the lower vibrations, were observed to deviate slightly from the *Gaussian98* calculated vibrations. This could be improved by introducing some cross terms in the force field.

- The RMS deviation of the structural measurements of the isolated imidazolium cations calculated using IILFF showed a good improvement over those calculated using UFF, particularly in the RMS deviation of angle measurements. The structure of the five membered ring of the imidazolium cation minimised using the IILFF gave the correct planar structure.

- Partial atomic charge calculations for the imidazolium cations containing hydrogen attached to C(2) using the IILFF show a good agreement with the *Gaussian98* calculated results. A small deviation on some atoms was observed for those containing an sp^3-hybridised carbon atom attached to C(2). The deviation observed could be improved by introducing a different atom type to the sp^2-hybridised carbon indicated by C(2) and by modifying the assumption taken when formulating the atomic charge correction parameters. That is, by considering only the two sp^2-hybridised carbon atoms o f the ring (C(4) and C(5)) as equivalent.

- Crystals minimised using IILFF showed an improvement over those calculated with UFF for those crystal structures containing hydrogen attached to the C(2) of the imidazolium ring. However, once this hydrogen is replaced by an sp^3-hybridised carbon the RMS value indicates that the structure deviates considerably from the experimental structure.

- Unit cell parameters of the crystals containing imidazolium cations with a hydrogen attached to C(2) were found to be close to the experimental crystals when the IILFF was used, while those containing imidazolium cations with a methyl attached to C(2) were observed to deviate.

A dynamics simulation study of the melting process of 1,3-dimethylimidazolium chloride was performed and the results of this simulation can be summarised as follows:

- Increasing the temperature of the system during modelling with Cerius^2 using a script could not be accomplished as required. However, with one cycle of annealing dynamics the imposed change in temperature could be attained.

- During the dynamics simulation no significant change in the bond lengths in the imidazolium cation was observed, while the expected decrease in the calculated density was obtained for the system. However, no hydrogen bond breaking was observed for either a perfect crystal or a defective crystal and the crystal disorder observed was not large enough to conclude that melting had occurred.

The performance of this force field can be further improved by assigning a different atom type to the sp^2-hybridised carbon atom indicated by C(2) and by adding cross-term interactions to the force field.

The scope of the force field can also be increased to model any imidazole based cations with any alkyl group attached to the five atoms within the ring and a variety of anions, such as BF_4^{-1} , $AlCl_4^{-1}$ etc.

With respect to the dynamics simulations the next investigation should be to run a dynamics simulation using a longer time, say 100 ps, in each temperature increment. It would also help to further optimise the van der Waals parameters of the cations used, like in the case of 1,3-dimethylimidazolium chloride the chloride anion since the expected deviation from its original position was not observed during dynamics simulation.

Reference

Allinger N. L. (1977) *J. Am. Chem. Soc.*, **99**, 8127.

Allen, H. H. and Kennard, O. (1993) *Chemical Design Automation News*, **8**, 31

Andrade, J.; Böes, E. S. and Stassen, H. (2002) *J. Phys. Chem. B,* **106**, 3546 – 3548.

Andras, M. T.; Hepp, A. F.; Fanwick, P. E.; Martuch, R. A.; Duraj, S. A. (1993) *Acta Crystallogr., Sect. C: Cryst. Struct. Commun.,* **49**, 548.

Arduengo, A. J.; Dias, H. V. R.; Harlow, R. L. and Kline, M. (1992) *J. Am. Chem. Soc.*, **114**, 5530.

Atkins, P. W. (1994) *Physical Chemistry*, Fifth Edition, Oxford University Press, Oxford, UK.

Barlow, R. B.; Johnson, O.; Howard, J. A. K.; Walton, D. C.; Koeliner, G. (1989) *Acta Crystallogr., Sect. B: Struct. Sci*, **45**, 396.

Berendsen, H. J. C.; Postma, . P. M.; van Gunsteren, W. F.; DiNola, A. and Haak, J.R. (1984) *J. Chem. Phys.* **81(8)**, 3684.

Bonnet, J. J.; Yeannin Y. and Laaouini, M. (1975) *Bull. Soc. Fr. Miner. Crist.*, **98**, 208.

Boulaire, V. L. and Grée, R. (2000) *Chem. Commun.*, 2195.

Berendsen, H. J.; Postman, J. P. O.; Van Gunsteren, W. I,; DiNicola, A. and Haak, J. R. (1984) *J. Chem. Phys*, **81**, 3684.

Brudgam, I. and Hartl, H. (1986) *Acta Crystallogr., Sect. C: Cryst. Struct. Commun*, **42**, 866.

Carmichael, A. J.; Hardacre, C.; Holbrey, J. D.; Seddon K. R.; and Nieuwenhuizen M. *Electrochem. Soc. Proceedings*, **99-41**, 209.

Cerius^2 (1998) Software Environment for Chemical Computing, Molecular Simulations Inc., San Diego.

Chariclea, S.; Kerry, D. R. and Kenneth A. B. (1993) *J. Crystallogr. Spectrosc. Res.*, **23(7)**, 601.

Cole, L. B. and Holt, E. M. (1986) *J. Chem. Soc., Perkin Trans.* 1, 151.

Comba, P. and Hambley, T. W. (1995) *Molecular Modelling of Inorganic Compounds*, VCH Publishers Inc., New York.

Cotton, F. A. (1990) *Chemical Applications of Group Theory,* John Wiley & Sons, U.S.A.

Dillen, J. L. M. (1992) *J. Comput. Chem.,* **13**, 257.

Dillen, J. L. M. (1995) *J. Comput. Chem.,* **16(5)**, 610.

Dillen, J. L. M. (1995) *J. Comput. Chem.*, **16(5)**, 595.

Dillen, J. L. M. (2000) unpublished notes.

Dillen, J. L. M. (2001) *Vibram, Vibrational Animation of Molecules*, Version 2.0, Department of Chemistry, Stellenbosch University.

Dupont, J.; Suarez, P. A. Z.; De Souza, R. F.; Burron, R. A. and J.-P. Kintzinger (2000) *Chem. Eur. J.*, **6(13)**, 2377.

Elaiwi, A.; Hitchcock, P. B.; Seddon, K. R.; Srinivasan, N.; Tan, Y.; Welton, T. and Zora, J. A. (1995) *J. Chem. Soc. Dalton Trans.* 3467.

Ercolessi, F. (1997) *A Molecular Dynamics Primer*, Spring College in Computational Physics, Italy.

Fannin (1984) *J. Phys. Chem.*, **88**, 2614.

Foresman, J. B. and Frisch, A. (1993) *Exploring Chemistry with Electronic Structure Methods*, 2nd, Gaussian, Inc., U.S.A.

Fuberg, S. and Aas, B. J. (1975) *Acta Chem Scand. Ser. A.*, **29**, 713.

Fuller, J.; Carlin, R. T.; De Long, H. C. and Haworth, D. (1994) *J. Chem. Soc., Chem. Commun.,* 299.

Furniss, B. S.; Hannaford, A. J.; Smith, P. W. G. and Tatchell, A. R. (1989) *Vogel's Textbook of Practical Organic Chemistry*, 5th ed., Longman Scientific and Technical, Essex.

Gaussian98, Frisch, M. J.; Trucks, G. W.; Schelgel, H. B.; Scuseria, G. E.; Robb, M. A.; Cheeseman, J. R.; Zakrzewski, V. G.; Montgomery, J. A.; Stratmann, Jr., R. E.; Burant, J. C.; Dapprich, S.; Millam, J. M.; Daniels, A. D.; Kudin, K. N.; Strain, M. C.; Farkas, O.; Tomasi, J.; Barone, V.; Cossi, M.; Cammi, R.; Mennucci, B.; Pomelli, C.; Adamo, C.; Clifford, S.; Ochterski, J.; Petersson, G. A.; Ayala, P. Y.; Cui, Q.; Morokuma, K.; Salvador, P.; Dannenberg, J. J.; Malick, D. K.; Rabuck, A. D.; Raghavachari, K.; Foresman, J. B.; Cioslowski, J.; Ortiz, J. V.; Baboul, A. G.; Stefanov, B. B.; Liu, G.; Liashenko, A.; Piskorz, P.; Komaromi, I.; Gomperts, R.; Martin, R. L.; Fox, D.J.; Keith, T.; Al-Lahma, M. A.; Peng, C. Y.; Nanayakkara, A.; Challacombe, M.; Gill, P. M. W.; Johnson, B.; Chen, W.; Wong, M. W.; Andres, J. L.; Gonzalez, C.; Head-Gordon, M.; Replogle E. S. and Pople, J. A. Gaussian, Inc., Pittsburgh, PA (1998).

Gavezzotti, A. (1999) *J. Mol. Struct.,* 485.

Glowka, M. L.; Galdecki, Z. and Iwanicka, I. (1990) *Acta Crystallogr., Sect. C: Cryst. Struct. Commun.,* **46**, 1025.

Goodman, J. M. (1998) *Chemical Applications of Molecular Modelling*, Royal Society of Chemistry, UK.

Hanke, C. G.; Price, S. L. and Lynen-Bell, R. M. (2001) *Mol. Phys.*, **99**, 801.

Hausen, H. D.; Kaim, W.; Schulz, A.; Moscherosch, M.; Jordanov, J. (1993) *Z. Naturforsch., Teil B.* **48**,1181.

Hinchliffe, A. (1996) *Modelling Molecular Structures*, John Wiley and Sons, England.

Hinchliffe, A. (1999) *Chemical Modelling from Liquids to Liquids*, John Wiley and Sons, Ltd, England.

Hinchliffe, A. (2000) *Modelling Molecular Structures*, 2nd, John Wiley and Sons Ltd, England.

Hinchliffe, A. (2002) *Chemical Modelling applications and Theory*, Royal Society of Chemistry.

Hockney, W. G. (1985) *Methods in Computational Physics, Plasma Physics,* **9**, 136.

Hoover, W. H. (1985) *Phys. Rev. A.*, **31**, 1695.

Jensen, F. (1999) *Introduction to Computational Chemistry*, John Wiley and Sons, England.

Kistenmacher, T. J. and Shigematsu, T. (1974) *Acta Crystallogr., Sect. B,* **30**, 1528

Kung, P. W. C.; Books, J. T.; Freeman, C. M.; Levine, S. M.; Vessal, B.; Newsam, J. M. and Klein, M. L. (1996) *Mat. Res. Soc. Symp. Proc.*, **408**, 327

Larsen A. S.; Holbrey, J. D.; Tham, F. S. and Reed, C. A. (2000) *J. Am. Chem. Soc.*, **122**, 7264.

Leach, A. R. (2002) *Molecular Modelling Principles and Application*, 2nd, Pearson Education, England.

Lipkowitz, K. B. and Boyd, D. B. (2000) *Reviews in Computational Chemistry*, Wiley-VCH, **14**, 399 - 439.

Machida, K. (1999) *Principles of Molecular Mechanics*, Akodansha Ltd, Japan and Wiley and Sons, Inc, USA.

Nagel, N.; Bock, H. and Eller, P. (2000) *Z. Kristallogr.*, **39**, 215.

Nose, S. (1984) *J. Chem. Phys.*, **91**, 511.

Nose, S. (1984) *Mol. Phys.*, **52**, 255.

Ornstein, R. L. and Zheng, Y. (1997) *J. Biomol. Struct. Dyn.*, **14,** 657.

Ortwerth, M. F.; Wyzlic, M. J. and Baughman, R. G. (1998) *Acta Cryst.* **54**, 1594.

Pavia, D. L.; Lampman, G. M. and Kriz, G. S. (2000) *Introduction to spectroscopy, a guide for students of organic chemistry*, 3rd edition, Hardcourt college publishers, U.S.A.

Rappé, A. K. and Casewit, C. J. (1997) *Molecular Mechanics across Chemistry,* University Science Books, U.S.A.

Rooney, D. W. and Seddon, K. R. (2001) *Handbook of solvents*, ChemTec Publishing Inc.

Schaftenaar, G. and Noordik, J. H., (2000) *J. Comput.-Aided Mol. Design,* **14**, 123

Shah, J. K.; Brennecke, J. F. and Maginn, E. J. (2002) *Green Chem.*, **4**, 112.

Stenzel, O.; Raubenheimer, H. G. and Esterhuysen, C. (2002) *J. Chem. Soc. Dalton Trans.*, 1132.

Stewart, J. J. P. (1989) *J. Comput. Chem.*, **10**, 209

Swope, W. C.; Anderson, H. C.; Berens, P. H. and Wilson, K. R. (1982) *J. Chem. Phys.*, **76**, 637.

Verlet, L. (1967) *Phys. Rev.*, **159**, 98.

Wasserscheid, P. and Keim, W. (2000) *Angew. Chem. Int. Ed.*, **39,** 3772.

Welten (1999) *T. Chem. Rev.*, **99**, 2071.

Wilkes (1982) *Inorg. Chem.*, **21**, 1263.

Wypch, G. (2001) *Handbook of Solvents*, ChemTec Publishing Inc.

Young, D. (2001) *Computational Chemistry, A practical Guide for Applying Techniques to Real World Problems*, John Wiley & Sons, Inc., Canada.

Addendum A :- Comparison of measurements of isolated cations calculated using HF , IILFF and UFF

Table 3.1 : Geometric parameters of the isolated 1,3-dimethylimidazolium cation

	Definition	1	2	3	1 - 2	1 - 3
Stretch interactions	N(1)-C(2)	1.315	1.324	1.348	-0.009	-0.033
	N(1)-C(5)	1.378	1.361	1.349	0.017	0.029
	N(1)-C(6)	1.467	1.469	1.46	-0.002	0.007
	N(3)-C(2)	1.315	1.324	1.349	-0.009	-0.034
	N(3)-C(4)	1.378	1.341	1.35	0.037	0.028
	N(3)-C(8)	1.467	1.469	1.459	-0.002	0.008
	C(2)-H	1.069	1.069	1.085	0.000	-0.016
	C(4)-C(5)	1.341	1.355	1.381	-0.014	-0.040
	C(4)-H	1.068	1.068	1.083	0.000	-0.015
	C(5)-H	1.068	1.068	1.085	0.000	-0.017
	C(6)-H*	1.079	1.082	1.111	-0.003	-0.032
	C(8)-H*	1.079	1.082	1.111	-0.003	-0.032
Bending interactions	C(2)-N(1)-C(5)	108.0	107.8	106.4	0.2	1.6
	C(2)-N(1)-C(6)	126.4	126.6	126.6	-0.2	-0.2
	C(2)-N(3)-C(4)	108.0	107.9	106.1	0.1	1.9
	C(2)-N(3)-C(8)	126.4	126.5	127.3	-0.1	-0.9
	N(1)-C(2)-N(3)	109.8	108.9	111.1	0.9	-1.3
	N(3)-C(2)-H	125.1	126.1	124.3	-1	0.8
	N(3)-C(4)-C(5)	107.1	108.2	108.3	-1.1	-1.2
	N(3)-C(4)-H	122.0	122.4	125.3	-0.4	-3.3
	N(1)-C(5)-C(4)	107.1	108.2	108.1	-1.1	-1
	N(1)-C(5)-H	122.0	122.5	125.2	-0.5	-3.2
	N(1)-C(6)-H*	109.2	109.1	110.3	0.1	-1.1
	H-C(6)-H*	109.8	109.9	108.8	-0.1	1
	N(3)-C(8)-H*	109.2	109.0	110.3	0.2	-1.1
	H-C(8)-H*	109.8	109.9	108.9	-0.1	0.9
Torsions	C(8)-N(3)-C(2)-H	0	0	0	2.6	2.6
	C(6)-N(1)-C(5)-C(4)	180	180	180	-0.9	-0.9
	C(8)-N(3)-C(4)-H	0	0	0	176.8	176.8
	C(2)-N(3)-C(4)-C(5)	0	-0.2	0	0.0	-0.2

Table 3.2. Geometric parameters of the isolated 1-ethyl-3-methylimidazolium cation

	Definition	1	2	3	1 - 2	1 - 3
Stretch interactions	N(1)-C(2)	1.378	1.362	1.349	0.02	0.03
	N(1)-C(2)	1.314	1.327	1.350	-0.01	-0.04
	N(1)-C(6)	1.477	1.451	1.46	0.03	0.02
	N(3)-C(2)	1.315	1.354	1.349	-0.04	-0.03
	N(3)-C(4)	1.378	1.361	1.348	0.02	0.03
	N(3)-C(8)	1.466	1.468	1.461	0.00	0.00
	C(5)-C(4)	1.342	1.355	1.380	-0.01	-0.04
	C(5)-H	1.068	1.068	1.083	0.00	-0.01
	C(2)-H	1.069	1.069	1.084	0.00	-0.02
	C(4)-H	1.068	1.068	1.083	0.00	-0.01
	C(8)-H*	1.079	1.081	1.112	0.00	-0.03
	C(8)-C(9)	1.522	1.515	1.526	0.01	0.00
	C(6)-H*	1.081	1.087	1.116	-0.01	-0.04
	C9(8)-H*	1.084	1.078	1.111	0.01	-0.03
Bending Interactions	C(5)-N(1)-C(2)	107.9	108	106.1	-0.1	1.8
	C(5)-N(1)-C(6)	125.9	126.1	126.8	-0.2	-0.9
	C(2)-N(3)-C(4)	108	107.8	106.2	0.2	1.8
	C(2)-N(3)-C(8)	126.4	127.5	127.4	-1.1	-1
	N(1)-C(5)-H	122.1	122.6	125.3	-0.5	-3.2
	C(4)-C(5)-H	130.7	129.3	126.4	1.4	4.3
	N(1)-C(2)-N(3)	109.9	108	111.1	1.9	-1.2
	N(1)-C(2)-H	125.1	125.9	124.4	-0.8	0.7
	N(3)-C(4)-C(5)	107	108.1	108.3	-1.1	-1.3
	N(3)-C(4)-H	122	122.4	125.1	-0.4	-3.1
	H-C(8)-H*	109.8	109.9	108.7	-0.1	1.1
	N(3)-C(8)-C(9)	112.1	111.5	109.5	0.6	2.6
	C(8)-C(9)-H*	110.2	110.4	110.3	-0.2	-0.1
	H-C(9)-H*	108.3	108.5	108.7	-0.2	-0.4
Torsions	C(2)-N(1)-C(5)-C(4)	0.1	0.9	0.3	-1.1	-0.3
	C(2)-N(1)-C(5)-H	179.7	178.9	179.7	-1.3	-2.1
	C(6)-N(1)-C(5)-C(4)	178.9	179.7	179	-179.1	-178.3
	C(2)-N(3)-C(8)-C(9)	104.9	67.2	67.9	16	-21.7

Table 3.3. Geometric parameters of the isolated 1,2-dimethyl-3-ethylimidazolium cation

	Definition	1	2	3	1 - 2	1 - 3
Stretch interactions	N(1)-C(2)	1.323	1.346	1.355	-0.023	-0.032
	N(1)-C(5)	1.38	1.34	1.357	0.04	0.023
	N(1)-C(6)	1.475	1.456	1.467	0.019	0.008
	N(3)-C(8)	1.466	1.477	1.463	-0.011	0.003
	N(3)-C(2)	1.325	1.353	1.354	-0.028	-0.029
	N(3)-C(4)	1.381	1.341	1.348	0.04	0.033
	C(8)-H*	1.079	1.081	1.111	-0.002	-0.032
	C(2)-C(7)	1.495	1.502	1.504	-0.007	-0.009
	C(7)-H*	1.082	1.071	1.11	0.011	-0.028
	C(4)-C(5)	1.336	1.352	1.38	-0.016	-0.044
	C(4)-H	1.068	1.069	1.085	-0.001	-0.017
	C(5)-H	1.068	1.069	1.083	-0.001	-0.015
	C(8)-C(9)	1.523	1.513	1.526	0.01	-0.003
	C(6)-H*	1.08	1.086	1.111	-0.006	-0.031
	C(9)-H*	1.084	1.078	1.111	0.006	-0.027
Bending Interactions	C(2)-N(1)-C(5)	108.7	108.1	105.7	0.6	3
	C(2)-N(1)-C(6)	127	127.7	128.3	-0.7	-1.3
	C(8)-N(3)-C(2)	126.5	128.2	128.1	-1.7	-1.6
	C(2)-N(3)-C(4)	108.7	107.8	106	0.9	2.7
	N(3)-C(8)-H*	109.5	109	110.4	0.5	-0.9
	H-C(8)-H*	109.5	109.9	108.7	-0.4	0.8
	N(1)-C(2)-N(3)	108.4	108	108.9	0.4	-0.5
	N(1)-C(2)-C(7)	125.8	125.8	124.3	0	1.5
	C(2)-C(7)-H*	110.5	110.6	110.3	-0.1	0.2
	N(3)-C(4)-C(5)	107	108.1	108.4	-1.1	-1.4
	N(1)-C(5)-C(4)	107.1	108	108.6	-0.9	-1.5

	N(3)-C(8)-C(9)	112.2	111.2	110.6	1	1.6
	N(1)-C(6)-H*	107.1	108.2	110.2	-1.1	-3.1
	C(8)-C(9)-H*	110.7	110.4	110.1	0.3	0.6
	H-C(9)-H*	108.2	108.5	108.8	-0.3	-0.6
Torsions	C(5)-N(1)-C(2)-N(3)	-0.4	0.9	0.2	-0.6	0.7
	C(5)-N(1)-C(2)-C(7)	-179.3	-179.2	-179.7	0	0.1
	C(6)-N(1)-C(2)-C(7)	2.1	0.4	0.9	2.4	0.7
	C(2)-N(3)-C(8)-C(9)	95.7	93.5	111.5	25.1	22.9
	C(8)-N(3)-C(2)-N(1)	-179.5	-179.6	-179.9	-0.4	-0.5

Table 3.4 :- Geometric parameters of the isolated 1,2-dimethyl-3-propylimidazolium cation

	Definition	1	2	3	1 – 2	1 - 3
Stretch Interactions	N(1)-C(6)	1.475	1.464	1.467	0.011	0.008
	N(1)-C(2)	1.323	1.345	1.356	-0.022	-0.033
	N(1)-C(5)	1.38	1.339	1.35	0.041	0.03
	C(10)-C(9)	1.529	1.534	1.528	-0.005	0.001
	C(10)-H*	1.084	1.08	1.111	0.004	-0.027
	C(9)-C(8)	1.527	1.464	1.535	0.063	-0.008
	C(8)-H*	1.086	1.084	1.11	0.002	-0.024
	C(6)-H*	1.081	1.084	1.112	-0.003	-0.031
	C(2)-C(7)	1.495	1.501	1.505	-0.006	-0.01
	C(2)-N(3)	1.325	1.353	1.354	-0.028	-0.029
	C(7)-H*	1.082	1.07	1.109	0.012	-0.027
	N(3)-C(8)	1.466	1.477	1.463	-0.011	0.003
	N(3)-C(4)	1.381	1.341	1.348	0.04	0.033
	C(8)-H*	1.079	1.081	1.111	-0.002	-0.032
	C(4)-C(5)	1.336	1.352	1.379	-0.016	-0.043
	C(4)-H	1.068	1.069	1.083	-0.001	-0.015
	C(5)-H	1.068	1.068	1.085	0	-0.017
Bending Interactions	C(2)-N(1)-C(5)	108.7	108.2	105.7	0.5	3
	C(9)-C(10)-H*	111.1	110.8	110.2	0.3	0.9
	H-C(10)-H*	107.8	108.1	108.7	-0.3	-0.9
	C(10)-C(9)-C(8)	111.3	115.2	112.2	-3.9	-0.9
	H-C(8)-H	106.7	106.8	107.5	-0.1	-0.8
	N(3)-C(8)-C(9)	112.4	112.9	111.5	-0.5	0.9
	N(1)-C(6)-H*	107.1	108.2	109.9	-1.1	-2.8
	H-C(6)-H*	107.2	107	106.7	0.2	0.5
	N(1)-C(2)-N(3)	108.4	108	111.2	0.4	-2.8
	C(2)-C(7)-H*	110.5	110.5	110.5	0	0
	H-C(7)-H*	108.4	108.5	108.5	-0.1	-0.1
	C(2)-N(3)-C(5)	108.7	107.7	106	1	2.7

	N(3)-C(8)-H*	109.5	109.3	110.2	0.2	-0.7
	H-C(8)-H*	109.5	110.2	108.7	-0.7	0.8
	N(1)-C(5)-C(4)	107.1	108	108.6	-0.9	-1.5
	N(3)-C(4)-C(5)	107	108.1	108.4	-1.1	-1.4
Torsions	C(6)-N(1)-C(5)-C(4)	178.9	179.8	178.5	-3.5	-2.6
	C(10)-C(9)-C(8)-N(3)	178.9	80.6	54.1	-18.8	-117.1
	C(7)-C(2)-N(3)-C(8)	-0.6	-0.4	-1.6	-1.9	-1.7
	C(2)-N(3)-C(4)-C(5)	-0.1	0.0	-0.1	-0.2	-0.1
	C(8)-N(3)-C(4)-C(5)	179.7	179.9	179.4	-0.9	-0.7
	C(9)-C(8)-N(3)-C(2)	95.5	93.3	81.3	-16.7	-18.9

Addendum B :- Point group characterization of cations

1,3-Dimethyl Imidazolium Cation

- Point group = C_{2v}
- Number of atoms = 16
- Degree of freedom = 3N = 48
- Symmetry elements = E, C2, $\delta(xy)$, $\delta(yz)$

C_{2v}	E	C2	$\delta(xy)$	$\delta(yz)$
	48	-2	12	2

$\Gamma_{xyz} = 15A_1 + 8A_2 + 15B_1 + 10B_2$

$\Gamma_{trans} = A_1 + B_1 + B_2$

$\Gamma_{rota} = A_2 + B_1 + B_2$

$\Gamma_{vib} = 14A_1 + 7A_2 + 13B_1 + 8B_2$

Other Imidazolium Cations used

- Point group = C_1

Cation used	EMIM	DMEIM	TMIM
▪ Number of atoms	19	22	19
▪ Degree of freedom = 3N	57	66	57
▪ Vibrations	$\Gamma_{vib} = 51A$	$\Gamma_{vib} = 60A$	$\Gamma_{vib} = 51A$

Addendum C :- Vibrational Analysis

Table 1. Vibrations of the dimethyl imidazolium cation [DMIM]$^+$

Sym	Assignment	Obs	Calc	Obs – Calc	%
A1	Sym C(6)-N-CR bending	262.0	268.0	6.0	2.3
A1	N-CR-N bending	569.8	517.0	52.8	9.3
A1	Sym breathing	983.6	873.0	110.6	11.2
A1	CR-H scissoring + CH_3 rocking	1,074.9	1,007.0	67.9	6.3
A1	CR-H scissoring	1,098.6	1,095.0	3.6	0.3
A1	Ring breathing	1,302.7	1,171.0	131.7	10.1
A1	Sym N-CR stretching	1,406.6	1,460.0	53.4	3.8
A1	Sym C(6)-H bending	1,440.2	1,477.0	36.8	2.6
A1	H-C(6)-H bending	1,472.9	1,428.0	44.9	3.0
A1	H-C(8)-H bending	1,473.1	1,423.0	50.1	3.4
A1	CR-CR stretching	1,584.0	1,622.0	38.0	2.4
A1	Sym C(8)-H stretching	2,911.8	2,878.0	33.8	1.2
A1	CR(2)-H stretching	3,108.9	3,118.0	9.1	0.3
A1	Sym CR-H stretching	3,122.7	3,120.0	2.7	0.1
A2	CH_3 Rocking	82.7	143.0	60.3	72.9
A2	Asym CH_3 wagging	253.5	316.0	62.5	24.7
A2	CR-H twisting	613.5	562.0	51.5	8.4
A2	CR-H twisting	903.7	1,134.0	230.3	25.5
A2	CH_3 twisting	1,123.3	1,134.0	10.7	1.0
A2	Asym C(8)-H bending	1,448.9	1,442.0	6.9	0.5
A2	asym C(8)-H stretching	2,995.5	3,001.0	5.5	0.2
B1	asym C(6)-N-CR bending	397.4	502.0	104.6	26.3
B1	CR-H twisting	678.2	610.0	68.2	10.1
B1	CR-H rocking	999.5	1,022.0	22.5	2.3
B1	CR-H rocking	1,065.0	1,098.0	33.0	3.1
B1	CR-H in plane bending	1,150.9	-	-	-
B1	CR-H in plane bending	1,276.0	1,320.0	44.0	3.4
B1	Asym N-CR stretching	1,359.3	1,485.0	125.7	9.2
B1	Sym C(6)-H bending	1,423.3	1,467.0	43.7	3.1
B1	Asym CR-N stretching	1,584.4	1,659.0	74.6	4.7
B1	Sym C(6)-H stretching	2,911.7	2,878.0	33.7	1.2
B1	asym C(6)-H stretching	3,001.3	3,000.0	1.3	0.0
B1	asym C(6)-H stretching	3,001.5	2,999.0	2.5	0.1
B1	Asym CR-H stretching	3,105.0	3,105.0	0.0	0.0
B2	CH3 twisting	84.8	140.0	55.2	65.1
B2	sym CH_3 wagging	181.0	156.0	25.0	13.8
B2	CR-H oop bending	611.9	596.0	15.9	2.6
B2	CR-H wagging	770.5	923.0	152.5	19.8
B2	CR(2)-H oop bending	904.4	991.0	86.6	9.6
B2	CH_3-H rocking	1,129.6	1,095.0	34.6	3.1
B2	Sym C(8)-H bending	1,450.1	1,442.0	8.1	0.6
B2	asym C(8)-H stretching	2,995.5	3,002.0	6.5	0.2

Table 2. Vibrations of the trimethyl imidazolium cation $[TMIM]^+$

Assignment	Obs	Calc.	Diff	% Diff
CH_3 rocking	16.4	-	-	-
CH_3 rocking	72.7	51.0	21.7	29.8
CH_3 rocking	86.6	210.0	123.4	142.5
CH_3 wagging	140.7	122.0	18.7	13.3
CH_3 twisting	256.6	255.0	1.6	0.6
CH_3 wagging	261.1	344.0	82.9	31.8
CH_3 scissoring	278.0	313.0	35.0	12.6
CH_3 scissoring	284.8	332.0	47.3	16.6
CH_3 rocking	464.4	496.0	31.6	6.8
N-CR-N bending	547.4	540.0	7.4	1.4
CR-H twisting	608.7	564.0	44.7	7.3
CR-H wagging	664.0	693.0	29.0	4.4
Sym Ring breathing	683.3	600.0	83.3	12.2
Asym ring breathing	702.3	645.0	57.3	8.2
CR-H wagging	763.3	878.0	114.8	15.0
CR-H twisting	895.3	1,137.0	241.7	27.0
H- rocking	949.8	923.0	26.8	2.8
CH_3-H rocking	1,013.2	959.0	54.2	5.3
CH_3-H rocking	1,040.6	1,018.0	22.6	2.2
C(7)-H rocking	1,045.0	1,083.0	38.0	3.6
CR-H scissoring	1,086.8	1,045.0	41.8	3.8
CH_3-H rocking	1,102.8	1,018.0	84.8	7.7
CH_3 wagging	1,121.0	1,007.0	114.0	10.2
CH_3 wagging	1,126.4	1,027.0	99.4	8.8
CH_3 rocking + CR-H scissoring	1,196.6	1,124.0	72.6	6.1
CR-H rocking	1,239.1	1,191.0	48.1	3.9
C(6)-N stretching	1,321.4	1,196.0	125.4	9.5
CR-N stretching (asym)	1,332.2	1,411.0	78.8	5.9
H-C(7)-CR bending	1,398.6	1,476.0	77.5	5.5
H-C(7)-CR bending	1,417.9	1,543.0	125.1	8.8
H-C(7)-CR bending	1,435.7	1,430.0	5.7	0.4
Scissoring	1,439.0	1,445.0	6.0	0.4
Scissoring	1,448.9	1,473.0	24.1	1.7
Asym bending	1,458.8	1,439.0	19.8	1.4
Asym bending	1,459.9	1,435.0	24.9	1.7
Sym bending	1,467.5	1,430.0	37.5	2.6
Scissoring	1,470.2	1,441.0	29.2	2.0
CR-CR stretching	1,516.4	1,663.0	146.6	9.7
CR-N stretching	1,539.3	1,411.0	128.3	8.3
CR-CR stretc + CR-N stretc	1,594.5	1,591.0	3.5	0.2
Sym C(6)-H stretching	2,884.5	2,888.0	3.5	0.1
Sym C(6)-H stretching	2,910.3	2,879.0	31.3	1.1
Sym C(6)-H stretching	2,911.3	2,880.0	31.3	1.1
Asym C(7)-H stretching	2,954.3	2,995.0	40.8	1.4
Asym C(7)-H stretching	2,982.6	2,994.0	11.4	0.4
Asym C(8)-H stretching	2,988.4	2,999.0	10.6	0.4

Asym C(6)-H stretching	2,989.6	2,999.0	9.4	0.3
Asym C(8)-H stretching	3,006.0	3,002.0	4.0	0.1
Asym C(6)-H stretching	3,006.6	3,002.0	4.6	0.2
Asym CR-H stretching	3,108.1	3,104.0	4.1	0.1
Asym CR-H stretching	3,126.4	3,119.0	7.4	0.2

Table 3. Vibrations of the ethyl methyl imidazolium cation [EMIM]$^+$

Assignment	Obs.	Calc.	Diff	% Diff
Ethyl rocking	45.5	74.0	28.5	62.5
Methyl rocking	83.0	-	-	-
Ethyl wagging	130.4	113.0	17.4	13.3
C(9)-H rocking	199.4	244.0	44.6	22.4
Methyl wagging	222.4	252.0	29.6	13.3
Ethyl and methyl wagging	277.7	314.0	36.3	13.1
Ethyl wagging	360.6	349.0	11.6	3.2
Ethyl and methyl wagging	406.4	499.0	92.6	22.8
C(9)-C(8)-N bending	564.5	537.0	27.5	4.9
CR-H wagging	612.7	600.0	12.7	2.1
N oop bending	637.7	692.0	54.3	8.5
Methyl wagging	664.4	558.0	106.4	16.0
CR-H wagging & C(8)-H twisting	767.6	796.0	28.4	3.7
CR-H wagging	771.6	857.0	85.4	11.1
CR-H oop bending	903.0	1,140.0	237.0	26.2
CR(2)-H oop bending	905.9	997.0	91.1	10.1
C(8)-C(9)-H bending	921.0	944.0	23.0	2.5
Ring breathing	987.1	892.0	95.1	9.6
CR-H rocking	1,003.7	1,022.0	18.3	1.8
C(6)-H rocking	1,067.4	1,008.0	59.4	5.6
C(9)-H rocking	1,074.0	1,096.0	22.0	2.1
CR-H scissoring	1,092.7	1,082.0	10.7	1.0
CR-CR stret and ethyl bending	1,110.1	1,140.0	30.0	2.7
C(6)H3 wagging	1,126.7	1,125.0	1.7	0.1
CR-H rocking	1,147.0	1,176.0	29.0	2.5
C(8)-H and C(9)-H twisting	1,237.7	-	-	-
CR-H bending	1,281.9	1,318.0	36.1	2.8
C(8)-N stretching	1,305.3	1,179.0	126.3	9.7
C(8)-H rocking	1,354.5	1,400.0	45.5	3.4
Asym CR-H stretching	1,372.9	1,488.0	115.1	8.4
Sym H-C(9)-H bending	1,406.9	1,400.0	6.9	0.5
CR-CR and CR-N stretching	1,415.9	1,452.0	36.1	2.6
Sym H-C(6)-H bending	1,431.2	1,464.0	32.8	2.3
Asym H-C(6)-H bending	1,449.7	1,440.0	9.7	0.7
Asym H-C(9)-H bending	1,456.0	1,436.0	20.0	1.4
H-C(9)-H and H-C(8)-H bending	1,457.5	1,434.0	23.5	1.6
H-C(9)-H, H-C(8)-H and H-C(6)-H bend	1,473.3	1,431.0	42.3	2.9
H-C(9)-H, H-C(8)-H and H-C(6)-H bend	1,473.3	1,509.0	35.7	2.4
Asym CR-N stretching	1,576.2	1,666.0	89.8	5.7
CR-CR stretching	1,582.3	1,621.0	38.7	2.4
Sym C(9)-H stretching	2,880.5	2,884.0	3.5	0.1
Sym C(6)-H stretching	2,911.1	2,878.0	33.1	1.1
Sym C(8)-H stretching	2,924.4	2,928.0	3.6	0.1
Asym C(9)-H stretching	2,942.5	3,000.0	57.5	2.0

Asym C(9)-H stretching	2,953.1	2,996.0	42.9	1.5
Asym C(8)-H stretching	2,975.6	2,996.0	20.4	0.7
Asym C(6)-H stretching	2,994.1	3,002.0	7.9	0.3
Asym C(6)-H stretching	3,000.7	2,999.0	1.7	0.1
Asym CR-H stretching	3,106.0	3,105.0	1.0	0.0
CR(2)-H stretching	3,107.8	3,118.0	10.2	0.3
Sym CR-H stretching	3,123.9	3,120.0	3.9	0.1

Table 4. Vibrations of the ethyl methyl imidazolium cation $[DMEIM]^+$

Assignment	Obs.	Calc.	Diff	% Diff
R group rocking	45.0	64.0	19.0	42.2
R group rocking	63.3	-	-	-
C(6) methyl rocking	98.8	-	-	-
Sym methyl and ethyl wagging	103.3	105.0	1.7	1.6
Sym methyl and ethyl twisting	200.0	231.0	31.0	15.5
C(9)-H rocking	204.2	238.0	33.8	16.6
C(6) & C(7) methyl wagging	262.2	375.0	112.8	43.0
C(6) & C(7) methyl wagging	289.0	304.0	15.0	5.2
C(8)-H and C(9)-H rocking	300.8	347.0	46.2	15.4
Ethyl wagging	376.9	375.0	1.9	0.5
Methyl wagging	462.3	-	-	-
N-CR-N bending	545.7	536.0	9.7	1.8
CR-H twisting	619.9	567.0	52.9	8.5
C(2) oop bending	672.5	630.0	42.5	6.3
C(2) oop bending	674.9	733.0	58.1	8.6
Asym N-CR-CR bending	689.1	666.0	23.1	3.4
CR-H wagging	765.8	-	-	-
C(9)-H and C(8)-H twisting	771.0	799.0	28.0	3.6
CR-H twisting	896.7	1,134.0	237.3	26.5
C(9)-C(8) stretching	921.7	940.0	18.3	2.0
C(7)-H twisting	953.5	1,005.0	51.5	5.4
Sym N-CR stretching	1,020.5	1,110.0	89.5	8.8
C(7)-H twisting	955.8	1015.0	59.2	6.2
C(7)-H and C(8)-H twisting	1,052.2	1,033.0	19.2	1.8
C(7)-H wagging	1,073.9	1,070.0	3.9	0.4
CR-H scissoring	1,089.3	1,052.0	37.3	3.4
C(7)-H twisting	1,108.8	-	-	-
C(6)-H wagging	1,123.7	1,110.0	13.7	1.2
C(9)-H twisting & C(8)-H rocking	1,181.8	1,033.0	148.8	12.6
CR-H rocking	1,225.5	1,170.0	55.5	4.5
C(8)-H twisting	1,274.3	1,197.0	77.3	6.1
Sym CR-N stretching	1,314.4	1,218.0	96.4	7.3
Asym CR-N stretching	1,349.7	1,376.0	26.3	1.9
C(8)-H wagging	1,360.0	1,423.0	63.0	4.6
Sym bending C(7)	1,400.3	1,444.0	43.7	3.1
C(7)-H scissoring & Sym bending C(6)	1,406.6	1,435.0	28.4	2.0
Sym H-C(6)-H sym bending & asym H-C(7)-	1,423.4	1,448.0	24.6	1.7
H-C(7)H scissoring & sym H-C(6)-H	1,441.8	1,451.0	9.2	0.6
Asym H-C(6)-H bending	1,447.5	1,454.0	6.5	0.4
H-C(9)-H bending	1,455.7	-	-	-
Asym H-C(9)-H & H-C(6)-H bending	1,459.5	1,486.0	26.5	1.8
H-C(7)-H, Asym H-C(9)-H & H-C(6)-H	1,462.4	1,499.0	36.6	2.5
Asym H-C(6)-H bend & C(7)-H scissoring	1,470.2	1477.0	7.2	0.4
C(8)-H scissoring	1,478.0	-	-	-

Sym CR-CR stretching & CR-N stretching	1,514.5	1,663.0	148.5	9.8
Asym CR-N stretching	1,535.4	1,547.0	11.6	0.8
CR-CR stretching	1,594.8	1,592.0	2.8	0.2
Sym C(9)-H stretching	2,878.6	2,884.0	5.4	0.2
Sym C(7)-H stretching	2,887.9	2,888.0	0.1	0.0
Sym C(6)-H stretching	2,911.3	2,879.0	32.3	1.1
Sym C(8)-H stretching	2,930.9	2,930.0	0.9	0.0
Asym C(9)-H stretching	2,940.1	3,000.0	59.9	2.0
Asym C(9)-H stretching & sym C(8)-H str	2,951.8	3,000.0	48.2	1.6
Asym C(7)-H stretching	2,955.9	2,997.0	41.1	1.4
Asym C(8)-H stretching	2,980.4	2,997.0	16.6	0.6
Asym C(7)-H & C(8)-H stretching	2,986.3	2,997.0	10.7	0.4
Asym C(6)-H stretching	2,989.3	3,002.0	12.7	0.4
Asym C(6)-H stretching	3,005.9	3,002.0	3.9	0.1
Asym CR-H stretching	3,106.3	3,105.0	1.3	0.0
Sym CR-H stretching	3,125.0	3,120.0	5.0	0.2